Transition Metal Complexes of 3,7-Diazabicyclo[3.3.1]nonane Derivatives:

Complex Stabilities and Oxidation Reactivity of Cobalt (II) and Vanadium (IV)

Inaugural-Dissertation

zur

Erlangung der Doktorwürde

der

Naturwissenschaftlich-Mathematischen Gesamtfakultät

der

Ruprecht-Karls-Universität Heidelberg

vorgelegt von

Shigemasa Kuwata

aus Hyogo, Japan

2005

Abbreviations

s	second(s)
h	hour(s)
min	minute(s)
CT	charge transfer
IR	infrared spectroscopy
NMR	nuclear magnetic resonance
UV-Vis	ultraviolet -visible
XRD	X-ray diffraction
CV	cyclic voltammetry
EPR	electron paramagnetic resonance
IC	inhibitory concentration
MeOH	methanol
EtOH	ethanol
THF	tetrahydrofuran
ε	extinction coefficient
FAB	fast atom bombardment
ESI	electrospray ionization
ls	low spin
hs	high spin
sod	superoxide dismutase
eq	equivalent
acac	acetylacetonato

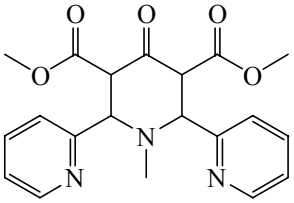

NPy2 [1]

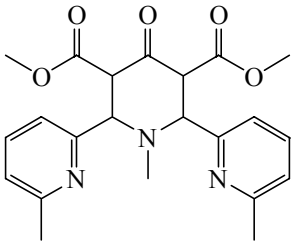

6Me-NPy2 [1]

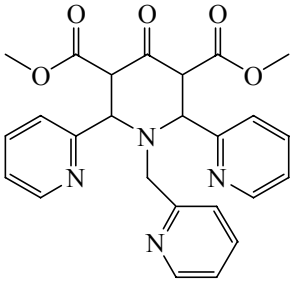

Npy3 [2]

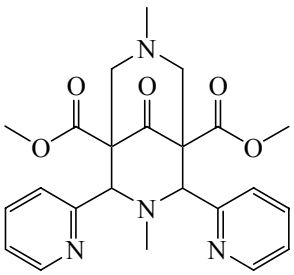

N2Py2 [1]

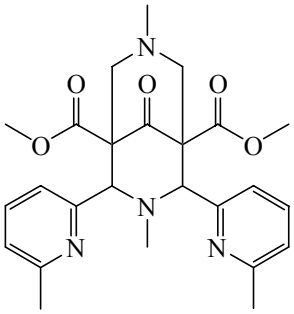

6Me-N2Py2 [1]

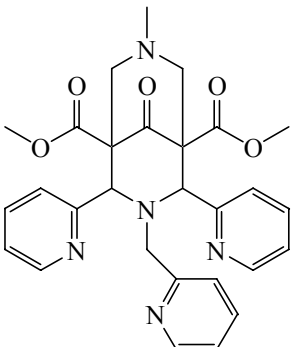

N2Py3u [3]

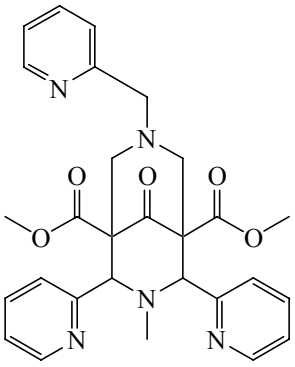

N2Py3o [4]

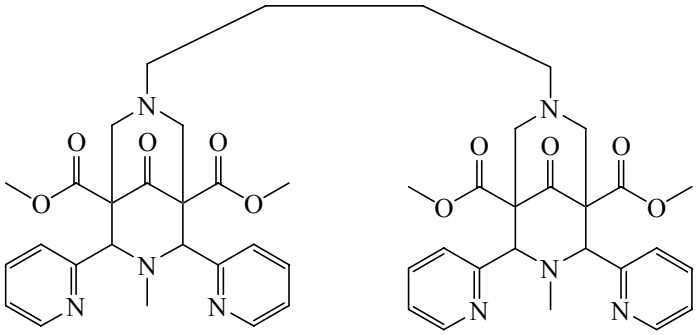

PY4AEa[4]

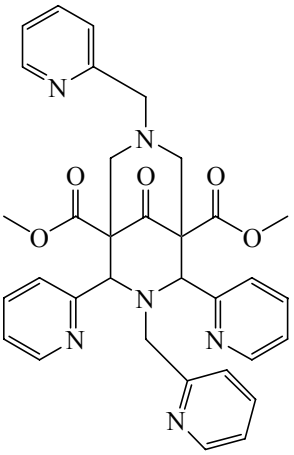

N2Py4 [4]

References

[1] U. Holzgrabe, E. Ericyas, *Arch. Pharm.*,1992, *325*, 657.

[2] A. Lienke, Doctor dissertation, Ruprecht-Karls-Universität, 1998.

[3] M. Merz, Doctor dissertation, Ruprecht-Karls-Universität, 2002.

[4] H. Brörzel, Doctor dissertation, Ruprecht-Karls-Universität, 2000.

Index

Abstract

In Chapter 2, it is reported that the syntheses and properties of a variety of tetra-, penta- and hexadentate bispidine-based ligands, which have a very rigid backbone, were prepared by two times of Mannich condensation with the corresponding aldehydes and amine.

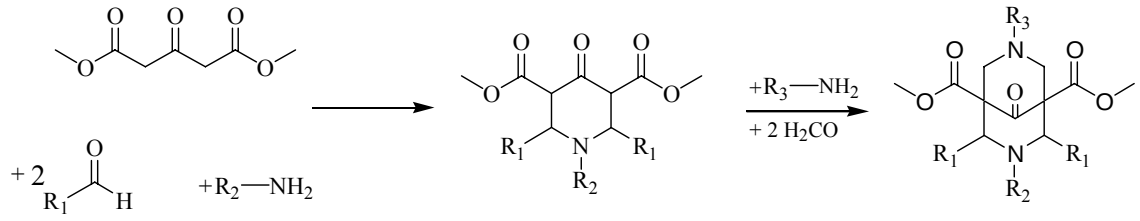

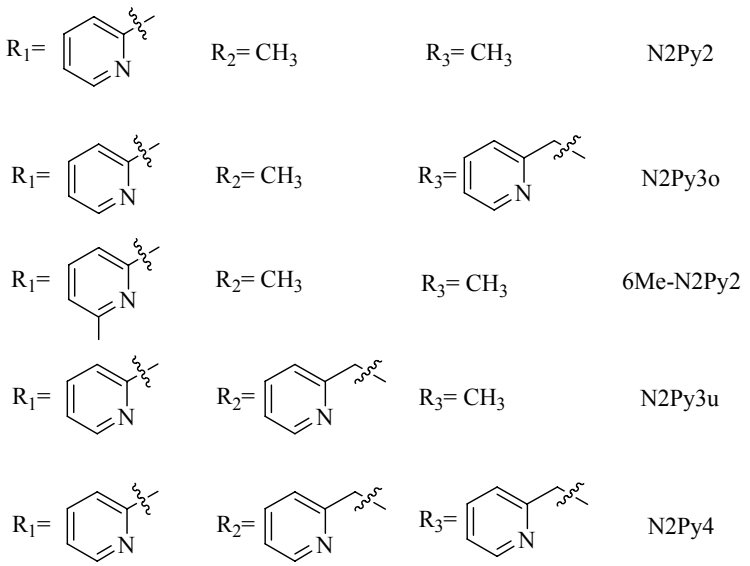

Fig. 1 Syntheses of substituted 3,7-diazabicyclo[3.3.1]nonanes

In Chapter 3, the selectivity and stabilization of bispidine complexes are discussed. This is confirmed by potentiometric measurement of stability constants, which indicated stabilities comparable to those with macrocyclic ligands. An interesting feature is that the usual Irving-Williams series behavior is not observed, and the stabilities (K_{ML}) follow the order Zn(II)>Cu(II)>>Co(II)>Ni(II). This is also predicted by force field calculations, which indicate that short metal donor distances lead to a build-up of strain in the ligand and that there is no size-match selectivity for large metal ions.

Stability constants	Co^{2+}	Ni^{2+}	Cu^{2+}	Zn^{2+}	Hg^{2+}	Pb^{2+}	Li^{+}
$\mathbf{M^n + L + 2H^+ \rightleftarrows [MLH2]^{n+2}}$	23.8	24.4	-	-	-	-	24.8
$\mathbf{M^n + L + H^+ \rightleftarrows [MLH]^{n+1}}$	20.8	20.4	22.9	24.7	20.3	18.9	20.4
$\mathbf{M^n + L \rightleftarrows [ML]^n}$	**15.0**	**14.1**	**19.8**	**21.5**	**15.8**	**14.0**	**13.2**
$\mathbf{M^n + L + OH^- \rightleftarrows [ML(OH)]^{n-1}}$	5.0	6.2	9.2	10.8	7.2	4.4	3.2
$\mathbf{M^n + L + 2OH^- \rightleftarrows [ML(OH)_2]^{n-2}}$	-	-4.0	-	-	-	-	-

Table 1 Potentiometrically determined stability constants (logK values) of N2Py4 (H_2O, T=25°C, μ =0.1M (KCl)

Protonation constants of 5 types of bispidine ligands were also determined, and the 'proton sponge' effect was observed. The first $logK_a$ values of all ligands were found in the range of 11.2 to 12.2. These can be divided into two groups: to the first one belong N2Py2, N2Py3u and 6Me-N2Py2, which contain a methyl substituent at N7; in the second category fall N2Py3o and N2Py4 which have a picolyl group attached to the bispidine backbone at N7.

Table 2 Potentiometrically determined protonation constants of a variety of bispidine ligands

	N2Py2 (H_2O/Dioxane=3:2)	N2Py3u (H_2O/Dioxane=3:2)	N2Py3o (H_2O/Dioxane=3:2)	6Me-N2Py2 (H_2O/Dioxane=3:2)	N2Py4 (H_2O/Dioxane=3:2)	N2Py4 (H_2O)
$L+H^+ = [LH]^+$	11.2	11.3	12.2	11.3	12	11.8
$L + 2H^+ = [LH_2]^{2+}$	8.8	8.2	7.1	8.4	6.7	6.9
$L + 3H^+ = [LH_3]^{3+}$	2.3	4	2.8	2	4.1	5.1
$L + 4H^+ = [LH_4]^{4+}$	≥2	≥2	2.4	≥2	2.2	2.2
$L + 5H^+ = [LH_5]^{5+}$	-	≥2	≥2	-	≥2	≥2
$L + 6H^+ = [LH_6]^{6+}$	-	-	-	-	≥2	≥2

In Chapter 4, the oxidation of Co(II) bispidine complexes is reported. Their crystal structures show an octahedral coordination geometry, when the Co(III)N2Py2 complex was formed by oxidation with H_2O_2, the methyl group at N7 of was removed but this was not observed for other Co(III) complexes, such as N2Py3u and N2Py3o. This reactivity is supposed to be an intramolecular effect of the cobalt center.

The oxidation of Co(II) bispidine complexes (distances of Co(II)-N : 2.13-2.21Å) leads to a decreasing of the Co-N distances (Co(III)-N : 1.93 -2.05Å).

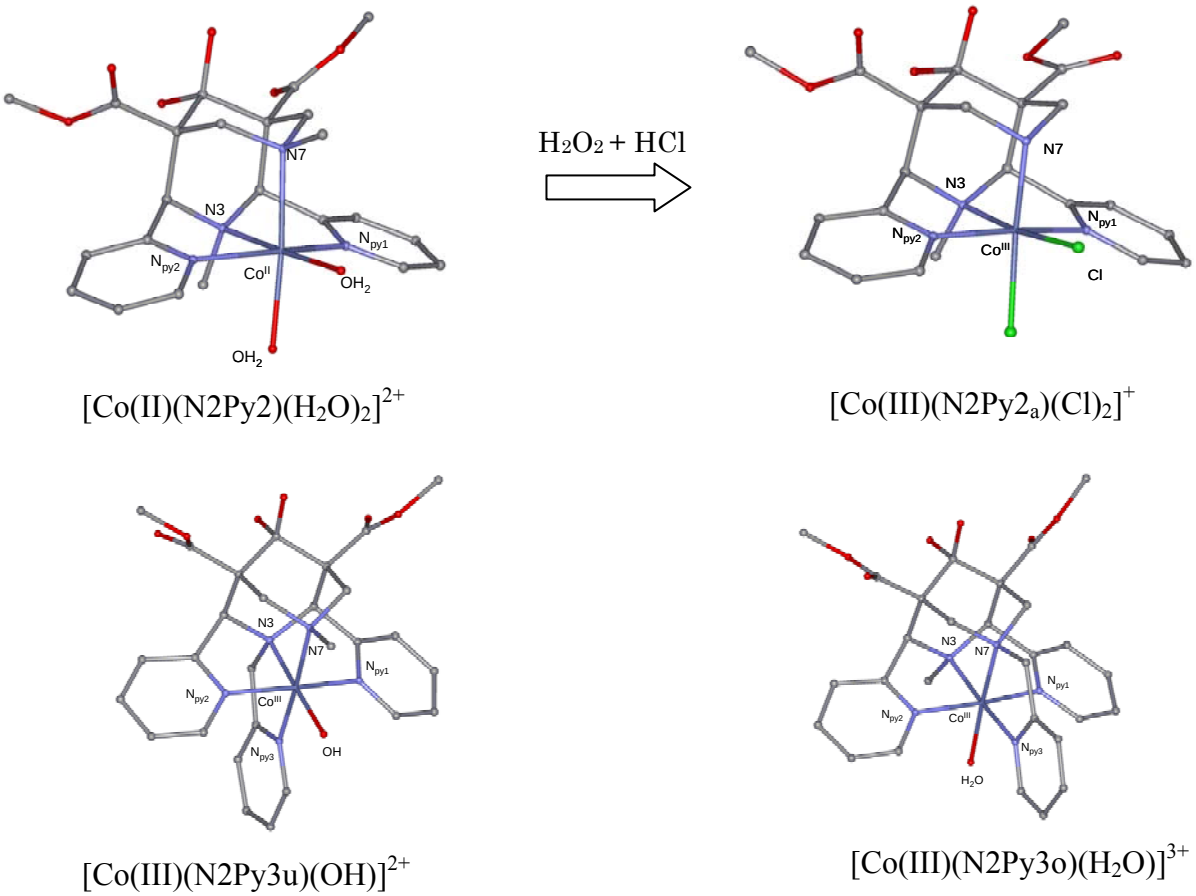

$[Co(II)(N2Py2)(H_2O)_2]^{2+}$ $[Co(III)(N2Py2_a)(Cl)_2]^{+}$

$[Co(III)(N2Py3u)(OH)]^{2+}$ $[Co(III)(N2Py3o)(H_2O)]^{3+}$

Fig. 2 Crystal structures of cobalt complexes with 3,7-diazabicyclo[3.3.1]nonane derivatives

The oxidation of Co(II) complexes with H_2O_2 was followed spectrophotometrically, the spectra clearly indicated the formation of the Co(III) complexes. The reaction is pseudo first order.

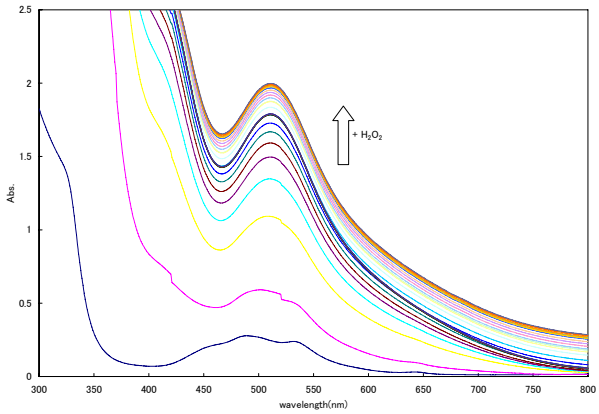

Fig. 3 UV-Vis spectra of the oxidation from Co(II) to Co(III)(N2Py2 complex)

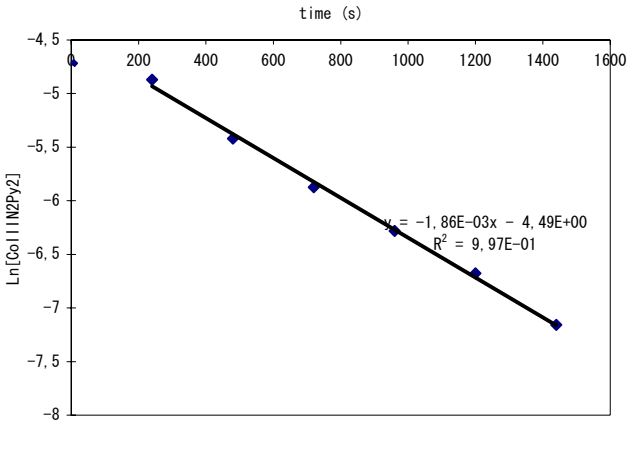

Fig. 4 Half logarithmic plot (ln[Co(II)N2Py2] vs. time) for the determination of rate constant for the oxidation of the Co(II)N2Py2 complex

In Chapter 5, the syntheses of V(IV) complexes with a pentadentate bispidine-based ligand (N2Py3o) and its oxidation are reported. It was observed that the vanadium (V) complex an contains η^2-side-on peroxo unit, coordinated to vanadium, the third pyridine donor of the picolyl arm is not coordinated to the vanadium center.

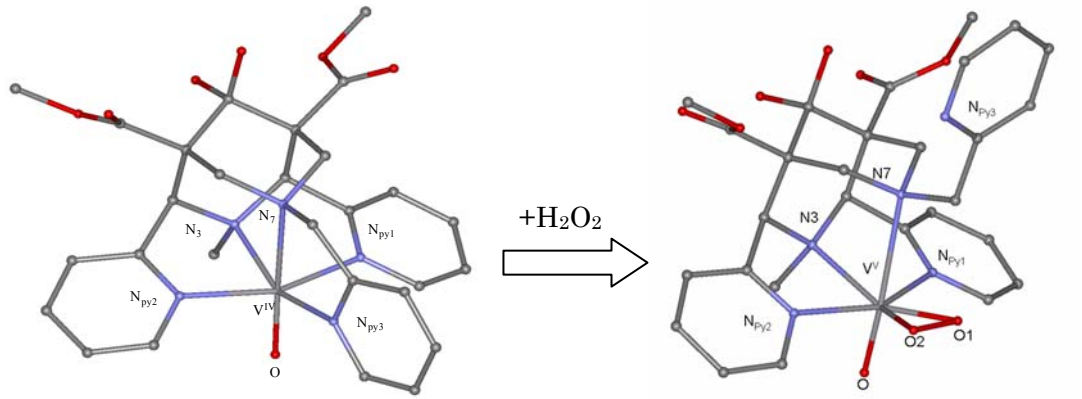

[V(IV)O(N2Py3o)](ClO$_4$)$_2$ [V(V)=O(O$_2$)(N2Py3o)]ClO$_4$

Fig. 5 Crystal structure of vanadium complexes with 3,7-diazabicyclo[3.3.1]nonane

The oxidation from vanadium (IV) to vanadium (V) was successfully carried out by using hydrogen peroxide and was studied spectrophotometrically.

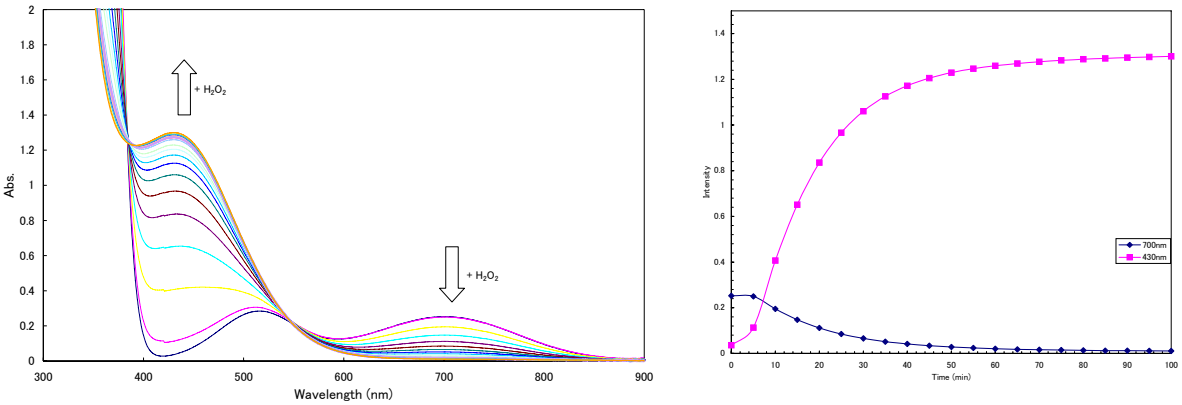

Fig. 6 Oxidation reaction of $[V(IV)=O(N2Py3o)]^{2+}$ in methanol with H_2O_2

Zusammenfassung

In Kapitel 2 wird über die Synthese und die Eigenschaften von verschiedenen vier-, fünf- und sechszähnigen Bispidinliganden berichtet, welche eine rigide Struktur besitzen und durch zweifache Mannich-Kondensation aus den entsprechenden Aldehyden und Aminen dargestellt wurden.

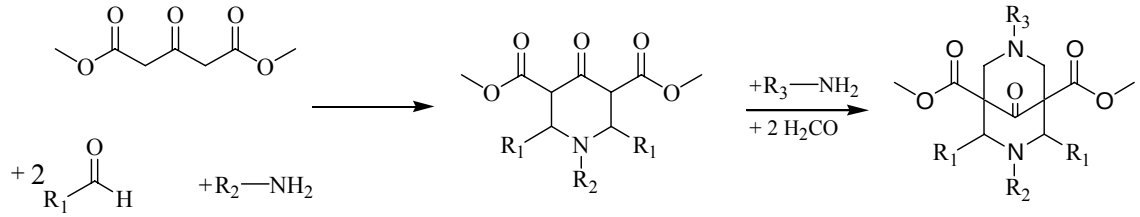

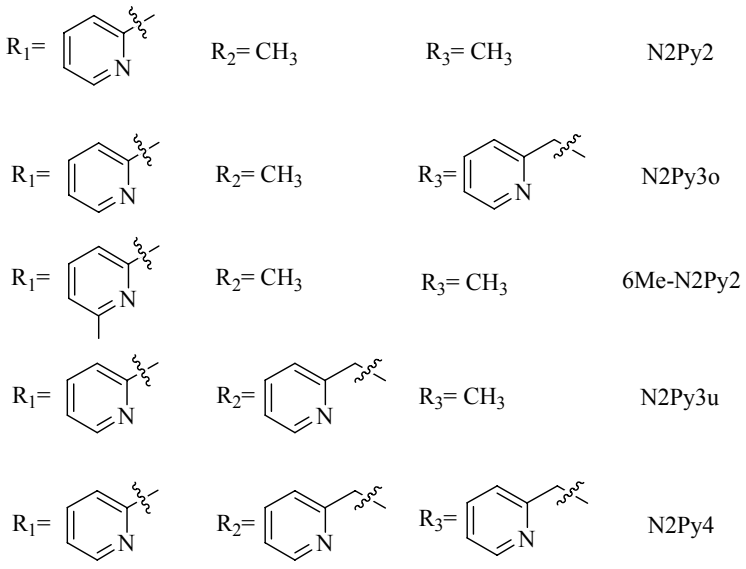

Abb. 1 Synthese von substituierten 3,7-Diazabicyclo[3.3.1]nonane

In Kapitel 3 wird über die Selektivität und Stabilität von Bispidinkomplexen diskutiert. Durch potentiometrische Messungen der Stabilitätskonstanten wurden mit makrocyclischen Liganden vergleichbare Stabilitäten erhalten. Interessant hierbei ist, dass ein Verhalten gemäß der Irving-Williams Reihe nicht auftritt, sondern die Stabilitäten (K_{ML}) die Reihenfolge Zn(II)>Cu(II)>>Co(II)>Ni(II) befolgen. Dies wird auch durch Kraftfeldrechnungen vorausgesagt, welche zeigen, dass kurze Metall-Donor-Abstände zu Spannung im Liganden führen und dass es keine Größenselektivitäten für große Metallionen gibt.

Tabelle 1 Potentiometrisch bestimmte Stabilitätskonstanten (logK-werte) von (H_2O, T=25°C, μ =0.1M KCl)

Stabilitätskonstanten	Co^{2+}	Ni^{2+}	Cu^{2+}	Zn^{2+}	Hg^{2+}	Pb^{2+}	Li^{+}
$\mathbf{M^n + L + 2H^+ \rightleftarrows [MLH2]^{n+2}}$	23.8	24.4	-	-	-	-	24.8
$\mathbf{M^n + L + H^+ \rightleftarrows [MLH]^{n+1}}$	20.8	20.4	22.9	24.7	20.3	18.9	20.4
$\mathbf{M^n + L \rightleftarrows [ML]^n}$	**15.0**	**14.1**	**19.8**	**21.5**	**15.8**	**14.0**	**13.2**
$\mathbf{M^n + L + OH^- \rightleftarrows [ML(OH)]^{n-1}}$	5.0	6.2	9.2	10.8	7.2	4.4	3.2
$\mathbf{M^n + L + 2OH^- \rightleftarrows [ML(OH)_2]^{n-2}}$	-	-4.0	-	-	-	-	-

Weiterhin wurden pKs-Werte von 5 Arten von Bispidinliganden bestimmt, wobei der “proton sponge“ Effekt beobachtet werden konnte. Der erste logKs-Wert aller Liganden wurde im Bereich 11,2 bis 12,2 gefunden. Die Liganden können in zwei Gruppen eingeteilt werden. Zur ersten Gruppe gehören N2Py2, N2Py3, N2Py3u und 6Me-N2Py2, welche einen Methylsubstituten am N7 haben; in die zwei Kategorie fallen N2Py3o und N2Py4, welche mit einer Picolylgruppe am N7verbunden sind.

Tabelle 2 Potentiometrisch bestimmte pKs-werte von verschiedenen Bispidinliganden

	N2Py2 (H_2O/Dioxane=3:2)	N2Py3u (H_2O/Dioxane=3:2)	N2Py3o (H_2O/Dioxane=3:2)	6Me-N2Py2 (H_2O/Dioxane=3:2)	N2Py4 (H_2O/Dioxane=3:2)	N2Py4 (H_2O)
$L+H^+ = [LH]^+$	11.2	11.3	12.2	11.3	12	11.8
$L + 2H^+ = [LH_2]^{2+}$	8.8	8.2	7.1	8.4	6.7	6.9
$L + 3H^+ = [LH_3]^{3+}$	2.3	4	2.8	2	4.1	5.1
$L + 4H^+ = [LH_4]^{4+}$	≥2	≥2	2.4	≥2	2.2	2.2
$L + 5H^+ = [LH_5]^{5+}$	-	≥2	≥2	-	≥2	≥2
$L + 6H^+ = [LH_6]^{6+}$	-	-	-	-	≥2	≥2

In Kapitel 4 wird über die Oxidation von Bispidinkomplexen berichtet. Ihre Kristallstrukturen zeigen eine oktaedrische Koordinationsgeometrie. Wird der Co(III) N2Py2-Komplex durch Oxidation mit H_2O_2 dargestellt, verschwindet die Methylgruppe. Dies wird jedoch nicht bei anderen Co(III)-Komplexen beobachtet, wie z.B., N2Py3u und N2Py3o. Diese Reaktivität ist vermutlich ein intramolekularer Effekt des Kobaltzentrums.

Die Oxidation von Co(II) Bispidinkomplexen (Bindungsabstände von Co(II)-N: 2,13-2,21Å) führt zu einer Verkürzung der Co-N Abstände(Co(III)-N: 1,93-2,05Å)

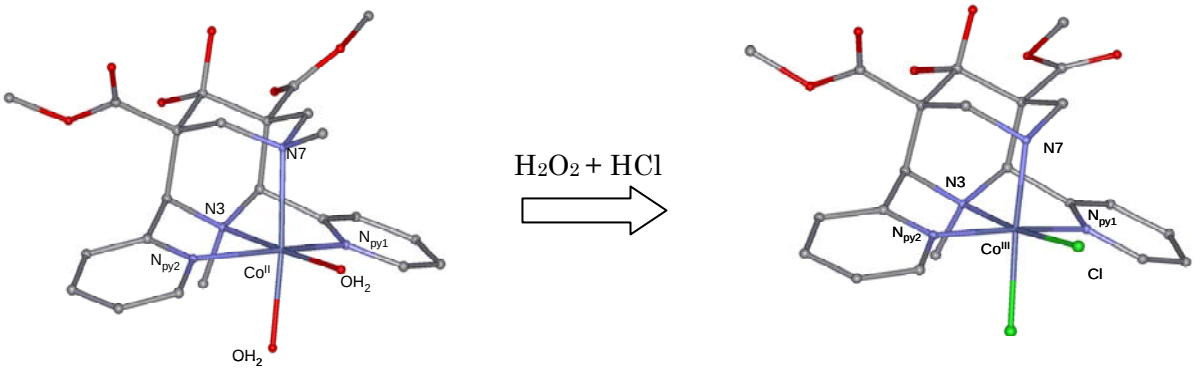

$[Co(II)(N2Py2)(H_2O)_2]^{2+}$ $[Co(III)(N2Py2_a)(Cl)_2]^{+}$

$[Co(III)(N2Py3u)(OH)]^{2+}$ $[Co(III)(N2Py3o)(H_2O)]^{3+}$

Abb. 2 Kristallstrukturen von Kobaltkomplexen mit 3,7-Diazabicyclo[3.3.1]nonan-Derivaten

Die Oxidation of Co(II) Bispidinkomplexen mit H_2O_2 wurde spektrometrisch verfolgt. Das Spektrum zeigt eindeutig die Bildung von Co(III)-Komplexen an. Die Reaktion ist pseudo-erster Ordnung.

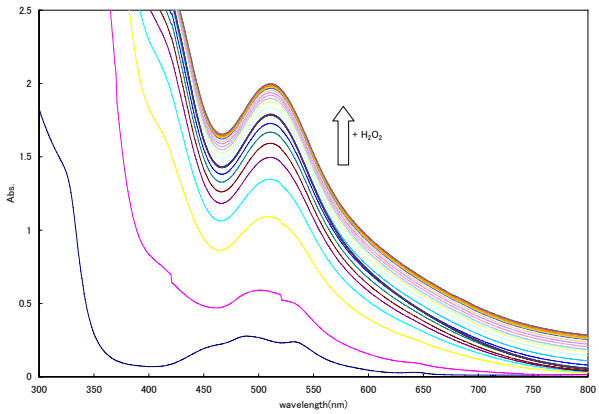

Abb. 3 UV-Vis Spektrum von der Oxidation von Co(II) zu Co(III) (N2Py2 Komplex)

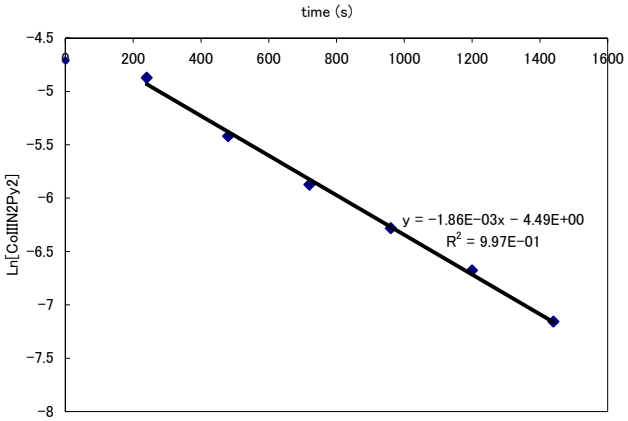

Abb. 4 Halb-logarithmische Darstellung (ln [Co(II) N2Py2] vs. Zeit) zur Bestimmung der Geschwindigkeitskonstante der Oxidation des Co(II)N2Py2-Komplexes

In Kapitel 5 wird über die Synthese von V(IV) Komplexen mit einem fünfzähnigen Bispidinliganden (N2Py3o) und dessen Oxidation bereichtet. Der Vanadium (V) Komplex besitzt eine η^2-side-on Peroxo-Einheit. Der dritte Pyridindonor des Picolylarms ist nicht koordiniert.

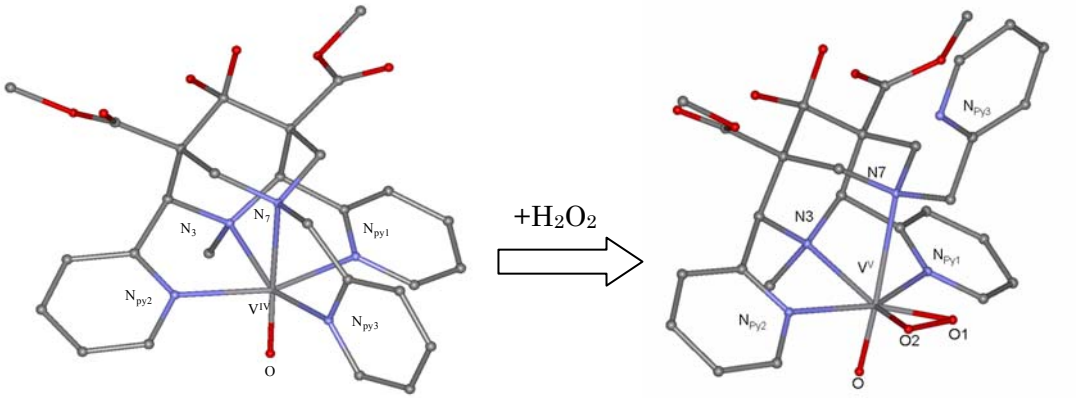

[V(IV) O(N2Py3o)](ClO$_4$)$_2$ [V(V)=O(O$_2$)(N2Py3o)]ClO$_4$

Abb. 5 Kristallstruktur von Vanadiumkomplexen mit 3,7-Diazabicyclo[3.3.1]nonan

Die Oxidation von Vanadium (IV) zu Vanadium (V) wurde erfolgreich mit Hydrogenperoxid durchgeführt und spektrophotometrisch untersucht.

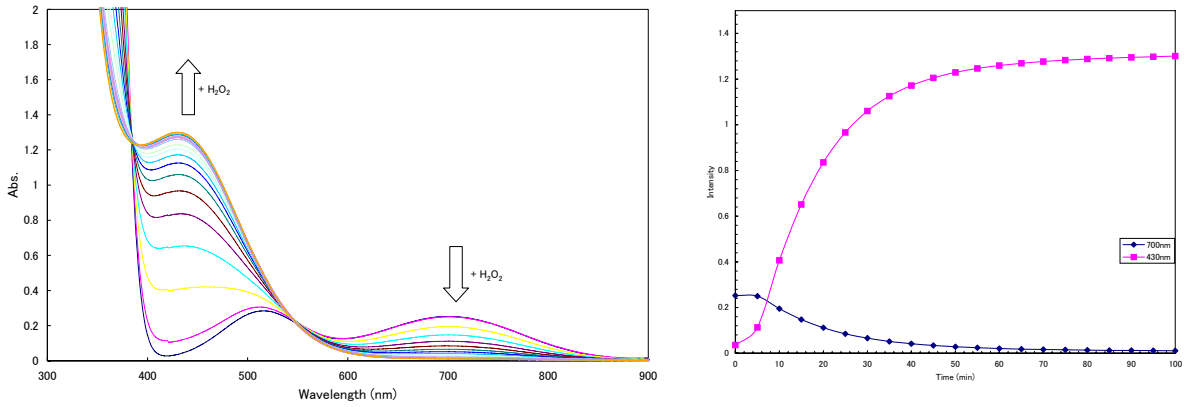

Abb. 6 Oxidationsreaktion von $[V(IV)=O\ (N2Py3o)]^{2+}$ in Methanol mit H_2O_2

1. Introduction

The geometry of a complex is the result of a variety of effects, which act together, some of them with less, others with more importance. It can generally be claimed that during coordination of a metal ion to a ligand, the geometry of the ligand around the metal are significantly changed. The ligand can show large conformational changes, with concomitant bond elongations or compressions. The changes in the coordination environment around the metal can have drastic effects on its properties, which are most obvious in the spectroscopic properties and explained by the **ligand field theory**[1,2].

The stabilization or destabilization of a metal complex depends on whether the metal fits to a given ligand. A high degree of stabilization of a complex results from the selectivity of a specific metal ion to a ligand, a high degree of destabilization (energization) leads to enhanced reactivities. To consider these features, **preorganization**[3], **complementarity**[4] and rigid ligands are important. The **elasticity** of coordination sphere is an important factor for the selectivity of specific metal ions. For example, very rigid such as 1,10-phenanthroline and bispidine (=3,7-diazabicyclo[3.3.1]nonane) might allow the coordination with a variety of metal ions. To tune the selectivity of a ligand, a good combination of the rigidity of backbone and elasticity of the coordination sphere are key tools. The metal ion selectivity of a ligand is not necessary only a ligand field effect, but also depends on the electronic preferences of the metal and the donor groups (**HSAB principle** [5]). The electronic configuration (**Irving-Williams series**[6,7]), the covalency of bonds, and the chelate effect[8] should also be taken into account. These various effects can result in a change in selectivity, allowing the coordination of a wider range of metal ions to the ligand.

Bispidines are known to be ligands with an extremely rigid backbone and additional functional groups can be introduced by a selection of the appropriate amines and aldehyde precursors.

For example, N2Py4 possesses two flexible picolyl groups and two pyridyl groups in the backbone which can be considered as a favourable combination of rigidity and elasticity of the coordination sphere. In Chapter 3, we report the coordination chemistry of the bispidine N2Py4 with cobalt (II), nickel (II), copper (II), zinc (II), lead (II), mercury (II) and lithium (I) including stability constants. Stability of the complexes depend not only on the ligand structure (hole size), but also on the metal ion and the donor groups. Electronic effects (number of d-electrons) play an important role: with the help of the Irving-Williams series, a prediction can be made for the stabilities of complexes of first-row transition metal ions,

taking primary electronic effects into account. It will be shown in Chapter 3 that the steric demand of the ligand is more important for bispidine complexes, since the stability constant values do not follow the expected Irving-Williams series behaviour.

Moreover computed hole size curves of the coordination sphere with regard to5 types of bispidine ligands are discussed. In addition, protonation constants of five kinds of bispidine ligands were determined potentiometrically and investigated to clarify the effects of the substitution of pyridyl groups and the build-up of intra-ligand van der Waals repulsion.

As mentioned above, a variation of metal-donor bond lengths can influence the strain energy of a ligand. For example, according to hole size calculations, the average Co(II)-N bond length is optimal for the coordination sphere of N2Py2 Co(II)-N bond leads to a minimum strain energy.In contrast, Co(III)-N (c.a. 1.95Å) distort the ligand-based angles and distances, and this leads to a increase of the strain energy and a concomitant build-up of intra-ligand van der Waals repulsion.

A simple one electron oxidation of a Co(II) complex to a Co(III) complex leads to significant differences in their properties. For example, the Co(III)-N donor distance is significantly smaller than the Co(II) -N donor distance, Co(II) complexes (d^7) are labile and paramagnetic, while Co(III) complexes (d^6) in low-spin configuration are inert and diamagnetic.

Co(II) bispidine complexes are usually inert, which indicates that the Co(II) ion is stabilized by bispidines. There might be two reasons for this: the stabilization by pyridyl groups π-donor of bispidine and the match of size in with the coordination sphere of the bispidine ligand. We report about the oxidation of Co(II) bispidine complexes together with the structural and electrochemical characterization of Co(II) and Co(III) complexes in Chapter 4.

Vanadium has been recognized to play an important role in biological systems. Currently, there is considerable interest in investigating mononuclear vanadium complexes because some of haloperoxidase enzymes.[9,10] Vanadium (V) peroxo complexes have been found to act as catalysts in the oxidation of organic substrates (e.g., epoxidation of alkenes, hydroxylation of alkanes and of aromatic compounds). [11,12]

The ion size of Vanadium (IV) (72.0pm) lays between Co(III) ions (68.5pm) and Co(II) ions (79.0pm), which therefore is a suitable metal ion size for the bispidine coordination sphere. Vanadium (IV) as a hard ion has a moderate affinity to the amine nitrogens of the bispidine ligands. Similar to Co(II) and Co(III), an oxidation from V(IV) to V(V) gives drastic changes in properties. For example, an oxidation from the paramagnetic V(IV) (d^1) yields the diamagnetic V(V) (d^0) complex. Therefore, there is no d-d transition observable in UV–Vis spectra of V(V) oxo complexes, the most remarkable features are charge transfer bands from

the interaction between coordinated anion and central V(V).

Similarly to cobalt, changing the valency of vanadium can alter metal-donor atom distances as well as the strain energy of the ligands. In Chapter 5, The influences of oxidation of a V(IV) bispidine complex on structural, spectroscopic and electrochemical properties is reported and discussed.

References

[1] L.H.Gade, *Koordinationschemie*, Wiley-VCH, Weinheim, **1998.**

[2] B. Figgis, M.Hitchman, *Ligand field theory and its application,* Wiley-VCH,Weinheim,2000.

[3] S. P. Artz, D. J. Cram, *J. Am. Chem. Soc.,* **1984**, *106*, 2160.

[4] D. J. Cram, *J. Inclusion Phenom.,***1988**, *6*, 397.

[5] R. G. Pearson, *J. Am. Chem.,* **1963**, *85*, 3533.

[6] H. M. Irving, R. J.P. Williams, *Nature*, **1948**, *162*, 746.

[7] H. M. Irving, R. J.P. Williams, *J.Chem. Soc.,* **1953**, 3192.

[8] D. H. Busch, N. A. Stephenson, *Coord. Chem. Rev.*, **1990**, *100*, 119.

[9] H. Sigel, A. Sigel, Eds. *Metal Ions in Biological Systems Vol.31: Vanadium and its Role in Life*, 31, Marcel Dekker, Inc., New York,**1995**.

[10]A. Butler, J. V. Walker, *Chem. ReV.,* **1993**, *93*, 1937.

[11] A. Butler, M. J. Clague, G. E. Meister, *Chem. ReV.,* **1994**, *94*, 625.

[12] H. Mimoun, L. Saussine, E. Daire, M. Postel, J. Fischer, R. Weiss, *J. Am. Chem. Soc.,* **1983**, *105*, 3101.

2. Ligand synthesis

2.1 Introduction

Sparteine derivatives with a ligand backbone similar to that of bispidines are found in nature as quinolizidine alkaloids. In the 1930's Mannich and Mohs obtained through the condensation of two piperidines with formaldehyde and primary amines, 3,7-diazabicyclo[3.3.1]nonane, subsequently named bispidine by Mannich. Generally, 3.7-diazabicyclo[3.3.1]nonane derivatives can be prepared in 3 different synthetic routes; i) ring-cleavage reaction of diazaadamantane under acidic condition ii) intramolecular cyclization of piperidine derivatives[1]. iii) Mannich reactions.[2]

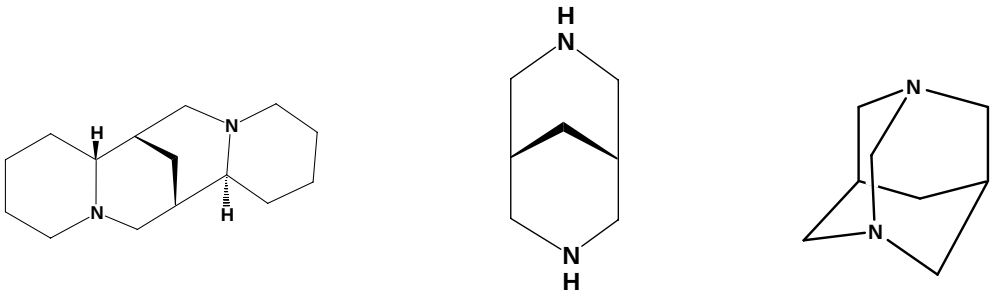

(a) (b) (c)

Fig. 2.1 Sparteine (a), bispidine (b), diazaadamantane (c)

There are three possible conformations of 3,7-diazabicyclo[3.3.1]nonane:
chair-chair, chair-boat and boat-boat. From the point of view of metal complexation, the chair-chair conformation is considered as the most favorable one due to the build-up of a cavity by two adjacent amines, yielding a specific coordination environment for metal ions. The bicyclic structure almost freezes conformational changes within the cavity.
The introduction of additional donors, e.g., pyridyl groups at the 3,7-positions of the rigid bispidine backbone leads to a large variety of ligands. Moreover, substitution of additional donors at 2 and 4 positions provide further pentadentate and hexadentate ligands.

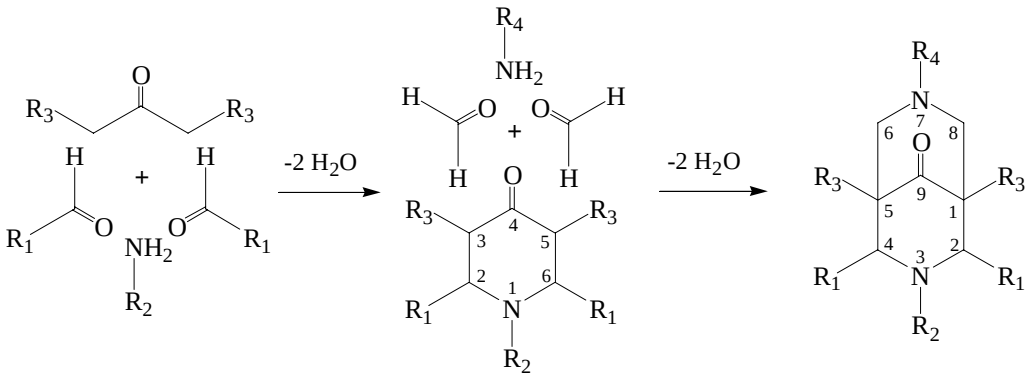

Piperidone Bispidine

Fig. 2.2 Syntheses of substituted 3,7-diazabicyclo[3.3.1]nonanes

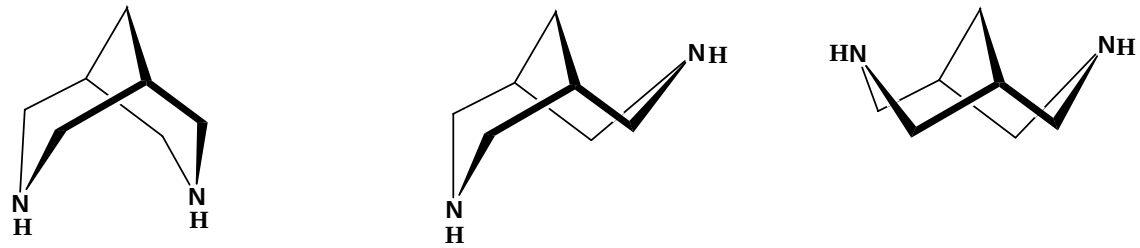

chair-chair chair-boat boat-boat

Fig. 2.3 Possible conformation of 3,7-diazabicyclo[3.3.1]nonanes

Strong antinociceptive activities[3] of 3,7-diazabicyclo[3.3.1]nonane derivatives have been revealed. In the pharmaceutical industry, bispidine derivatives are shown to be promising candidates, they are currently the targets of different pharmaceutical investigations[4,5,6].

A variety of derivatives can be prepared by using different combinations of aldehyde and primary amines as building blocks. In order to carry out the Mannich reaction successfully, it is necessary to use two equivalents of the aldehyde, equimolar amounts of the amine and one equivalent of the component which contains acidic protons; in our case this is the dimethyl or methyl ester of acetone dicarbonic acid. The introduction of methyl or ethylesters as R3 at the 1,5 positions leads to an increase of the yield of bispidine derivatives.

The distance between adjacent aliphatic nitrogen atoms in the chair-chair conformation is

remarkably short (~2.9Å). There are weak repulsions dipole-dipole interactions and orbital exchange effects between both nitrogen atoms, referred to as the 'hockey-stick-effect'[7]. Moreover, 3,7-diazabicyclo[3.3.1]nonane derivatives posses proton sponge properties, the first protonation occurs with log K_a values of between 11.2 to 12.2 (see in Chapter 3).

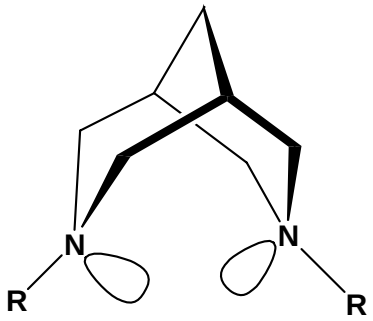

Fig. 2.4 Orbital exchange effect in 3,7-diazabicyclo[3.3.1]nonane

It is noteworthy that there are not only conformational isomers but also configurational isomers, which are endo/endo, exo/endo, exo/exo (R1 ligands attached in 2,4 position can occupy axial or equatorial position, and due to the rigidity of the bicyclic system, interconversion. At room temperature this isomerization does not occur.

The endo/endo configuration can build a highly preorganised coordination environment, having all donors in a favorable position for the complexation with metal ions. This endo/endo configuration is thermodynamically the most favorable one (both R1 groups are in the equatorial position).

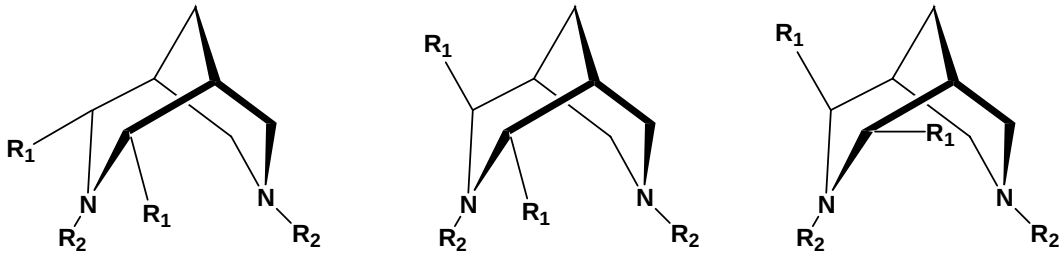

endo/endo exo/endo exo/exo

Fig. 2.5 Configurational isomers of substituted 3,7-diazabicyclo[3.3.1] nonane

A mixture of endo/endo and exo/endo isomers can often be generated during the syntheses of bispidine derivatives. Refluxing in methanol is an effective method to yield exclusively the endo/endo configuration, due to its high degree of thermodynamical stability. The inclusion of different configurations can efficiently be confirmed by ^{1}H-NMR technique.

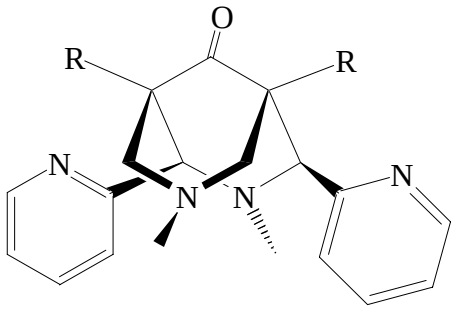

Fig. 2.6 N2Py2 in the thermodynamically most stable conformation and configuration.

2.2 Synthesis of the Piperidones

Throughout this work, piperidone derivatives have been prepared through the Mannich condensation as a first step in the syntheses of bispidine derivatives[8]. Generally the synthesis of piperidone derivatives was carried out with 1 eq. of the dimethyl ester of acetone dicarboxylic acid[9] and subsequent addition of, in slight excess, 2 eq. of the corresponding aldehyde and the corresponding primary amine, in methanol or ethanol, with stirring and ice cooling[10].

The desired piperidone derivatives were obtained from the resulting solution through recrystalization in a yields of 70-90%.

It is assumed that the piperidone derivatives exist in an equilibrium of the ketonic and enolic form, with the respective isomers, in alcoholic solution[11].

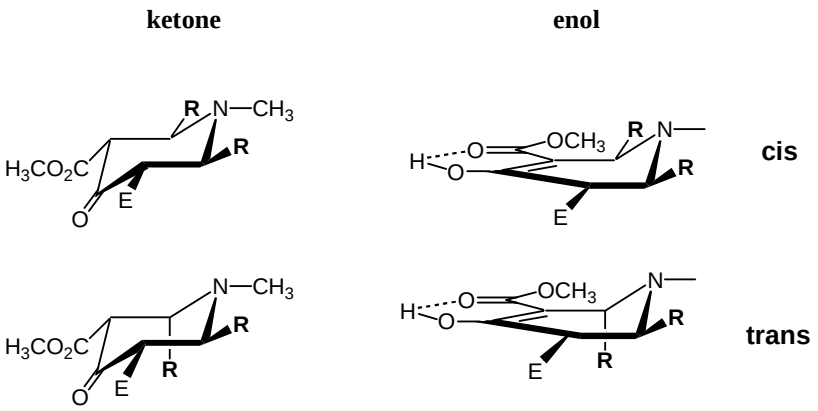

Fig. 2.7 Possible isomers and tautomers of piperidones

In polar solvents, bispidine forms both *cis*- and *trans*-ketone structures, the interconversions between cis-ketone and trans-ketone take place through the corresponding cis-enol and trans enol.

The ketone derivatives initially tautomerize into the enol form which can isomerize to the other enol structure through ring opening due to the ‘‘Retro Mannich reaction’’. The two enol isomers can again go through tautomerization to give the initial ketone isomer. The proposed mechanism of the isomerization is shown in Fig. 2.8

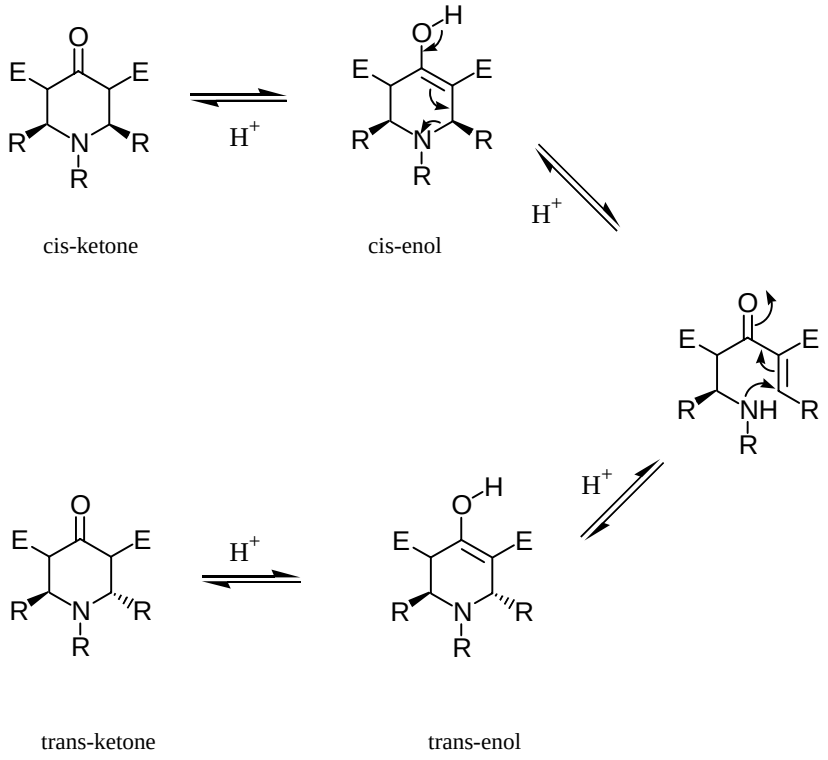

Fig. 2.8 Proposed mechanism of the piperidone isomerization

2.3 Synthesis of Bispidines

Derivatives of 3,7-diazabicyclo[3.3.1]nonane (bispidine) have been prepared through a variety of combinations of aldehydes and primary amines.

As shown in Fig. 2.9 2-pyridyl or 6-methyl-pyridyl groups were introduced as R1, methyl or 2-pyridyl-methyl (α-picolyl) groups as R2, methyl or 2-pyridyl-methyl groups as R3, respectively.All bispidine derivatives were synthesized by using ca. 20% excess amounts of the corresponding aldehydes and amines. The reactions were carried out under refluxing methanol or ethanol in 1-2 hours. Most of the products were isolated through recrystalization in methanol at ca. 5 ^{o}C for 48 hours. When no precipitate formed, the solvent was removed in *vacuo*, and a different solvent chosen e.g. ethanol (which more efficient in obtaining pure products in higher yields).

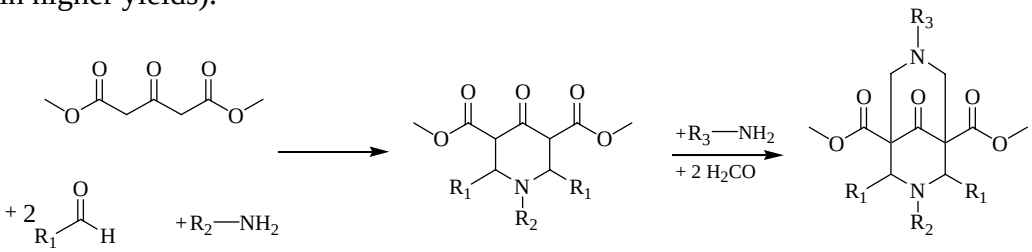

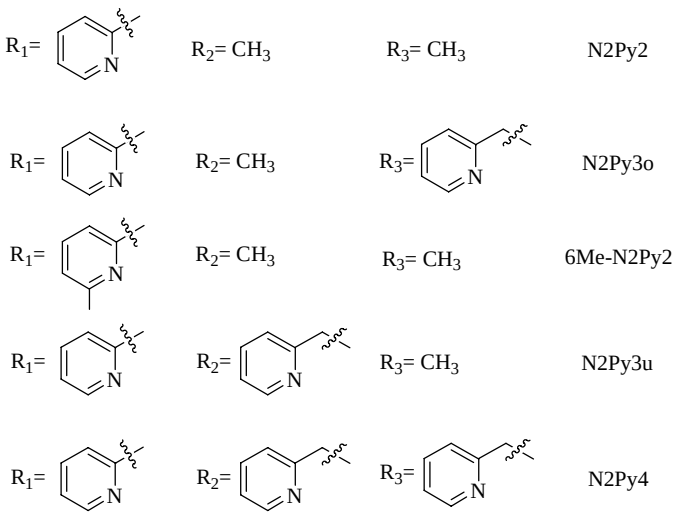

Fig. 2.9 Syntheses of substituted 3,7-diazabicyclo[3.3.1]nonane derivatives

References

[1] G. Dietz, W. Fiedler, G. Faust, *Chem. Ber.*, **1969**, *102*, 4147.

[2] H. Stetter, J. Schafer, K. Dieminger, *Chem. Ber.*, (II)**1958**, *91*, 598.

[3] B. Koegel, S. Dorsihn, M. Haurand, U. Holzgrabe, C. Nachtsteim. *Arch. Pharm. Pharm., Med. Chem.* **1996**, *329*, 311.

[4] T. Siener, A. Cambareri, U. Kuhl, W. Engelberger, M. Haurand, B. Koegel, U. Holzgabe, *J. Med. Chem.*, **2000**, 3746

[5] U. Holzgabe,E. Ericyas, *Arch. Pharm.*,**1992** ,*325*, 657.

[6] U. Holzgabe, A. Samhammer, R. Haller, *Arch. Pharm.*, **1989**, *322*, 551.

[7] N. S. Zefirov, *Russ. J. Org. Chem.*, **1970**, *6*, 1768.

[8] K. W. Merz, R. Haller, *Pharm. Acta Helv.* **1963**, *38*, 442.

[9] R. Haller; *Arzneim. Forsch.* **1965**, *15*, 1327.

[10] H. Quast, B. Müller, H. G. Schnering, *Chem. Ber.*, **1982**, *115*, 3631.

[11] M. J. Fernández, J. M. Casares, E. Gálvez, *J. Heterocycl. Chem.*, **1992**, *29*, 1797.

3. Complex Stabilities of 3,7-Diazabicyclo[3.3.1]nonane

3.1 Introduction

There is a considerable interest in developing ligands which coordinate to a specific metal ion, and which can build stable complexes with high selectivity. The metal selectivity of a ligand is essential in the development of new drugs, good structural and functional models for different enzymes, metal refinement, solvent extraction, metal ion sensors and so on[1,2,3,4,5]. To achieve metal ion selectivity, the design of a ligand with preorganization and complementarity is needed which satisfies the requirements of the metal ion, allowing the formation of the ideal coordination geometry. Fixation a given conformation of a ligand can lead to a higher level of preorganization which may enhance selectivity. The metal ion selectivity of a ligand is not necessarily only a ligand field effect[6], but also depends on the electronic preferences of the metal and the donor groups (HSAB principle[7]). The electronic configuration (Irving-Williams series[8,9]), the covalency of bonds, and the chelate effect[10] should also be taken into account. These various effects can result in a change in selectivity, allowing the coordination of a wider range of metal ions to the ligand.

Preorganization[11] and complementarity[12] are often considered as important factors in the macrocyclic ligands.[13,14] Rigid acyclic ligands have been shown to be able to enforce a specific shape on the chromophore.[15,16] It has been shown that increasing the rigidity of the ligand backbone leads to an enhancement of the selectivity for metal ions.[17,18,19,20]

Bispidine type ligands (bispidine = 3,7-diazabicyclo[3.3.1]nonane) are known to have a remarkable rigidity.[21] Ligand L^1 prefers metal ions which adopt distorted square planar geometries. These ligands were studied and compared with the bispidine-type ligands. Our bispidine-type ligands (N2Py2, N2Py3o, N2Py3u and N2Py4) enforce square pyramidal (N2Py2, with one co-ligand, strong in-plane bonding, N7 usually is the axial donor) or octahedral coordination geometry (N2Py2 with 2 co-ligands in cis-orientation; N2Py3u, N2Py3o with 1 co-ligand); seven-coordinate complexes with N2Py2, N2Py3u and N2Py3o have also been observed.[22] Other coordinating substituents than pyridine in 2-, 4-, 3-, 7-position have been reported,[23,24] and oligo-nucleating ligands, bridged through N7, have been prepared.[25,26,27]

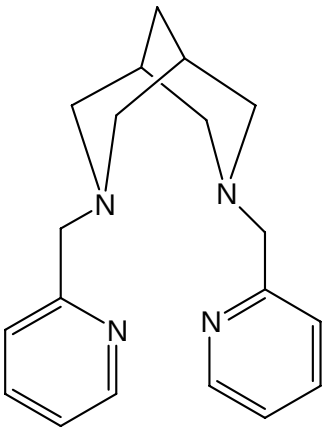

Fig. 3.1 Structure of L^1

3.2 Hole Size Calculations

The strain energies of tetra-, penta-, and hexadentate bispidine-type complexes have been investigated. Graphs showing the strain energy as a function of the average metal-bispidine-donor distance are shown in Fig. 3.2. These ‘‘hole size curves’’ have been obtained from empirical force field calculations with the established program MOMEC[28] and the force field developed in our group[29]. The model applied does not include metal-donor terms. The energies were calculated keeping the average metal-donor distance fixed, but allowing variation of each individual bond length. The calculated strain energy for each bispidine ligand showed a minimum and the corresponding distance was the optimum metal ion size for that particular ligand. The minimum energy of all curves was set to 0 $kJmol^{-1}$.

The hole size calculations of L^1 showed a flat curve. The differences of ΔE_{strain} between a bond length of 1.95 Å (which is the optimal Co(III)-N bond length) and 2.19Å (which is an ideal Zn(II) -N bond length) are only 4.4$kJmol^{-1}$. It emerges that L^1 tolerates a large difference in metal-donor distances, that is, L^1 it is not very size-selective. This is due to the elasticity of the coordination sphere. There is also no significant difference in steric energy for large metal ions (c.a. 2.0-2.2Å) with N2Py2, N2Py3o, N2Py3u and N2Py4, similarly for L^1.

This indicates that there is little constraint to fix the metal ion in a particular position in the ligand cavity, which is open on one side. However smaller metal ions (such as Co(III) bond length of ca. 1.95Å) distort the ligand-based angles and distances, and this leads to a dramatic increase of the steric energy, and a concomitant build-up of intra-ligand van der Waals repulsion. This is consistent with the relatively high redox potentials of Co(II)/(III) bispidine complexes. (e.g. $[Co(II)/(III)(N2Py2)(H_2O)_2]^{2+/3+}$ has 653mV of redox potential, see in Chapter 4).

Table 3.1 Steric energy at 1.95 Å which is an optimal Co(III)-N bond length

Ligand	**L1**	**N2Py2**	**N2Py3o**	**N2Py3u**	**N2Py4**
steric energy at 1.95Å	4.5kJ/mol	17.2kJ/mol	17.9kJ/mol	25.8kJ/mol	61.1kJ/mol

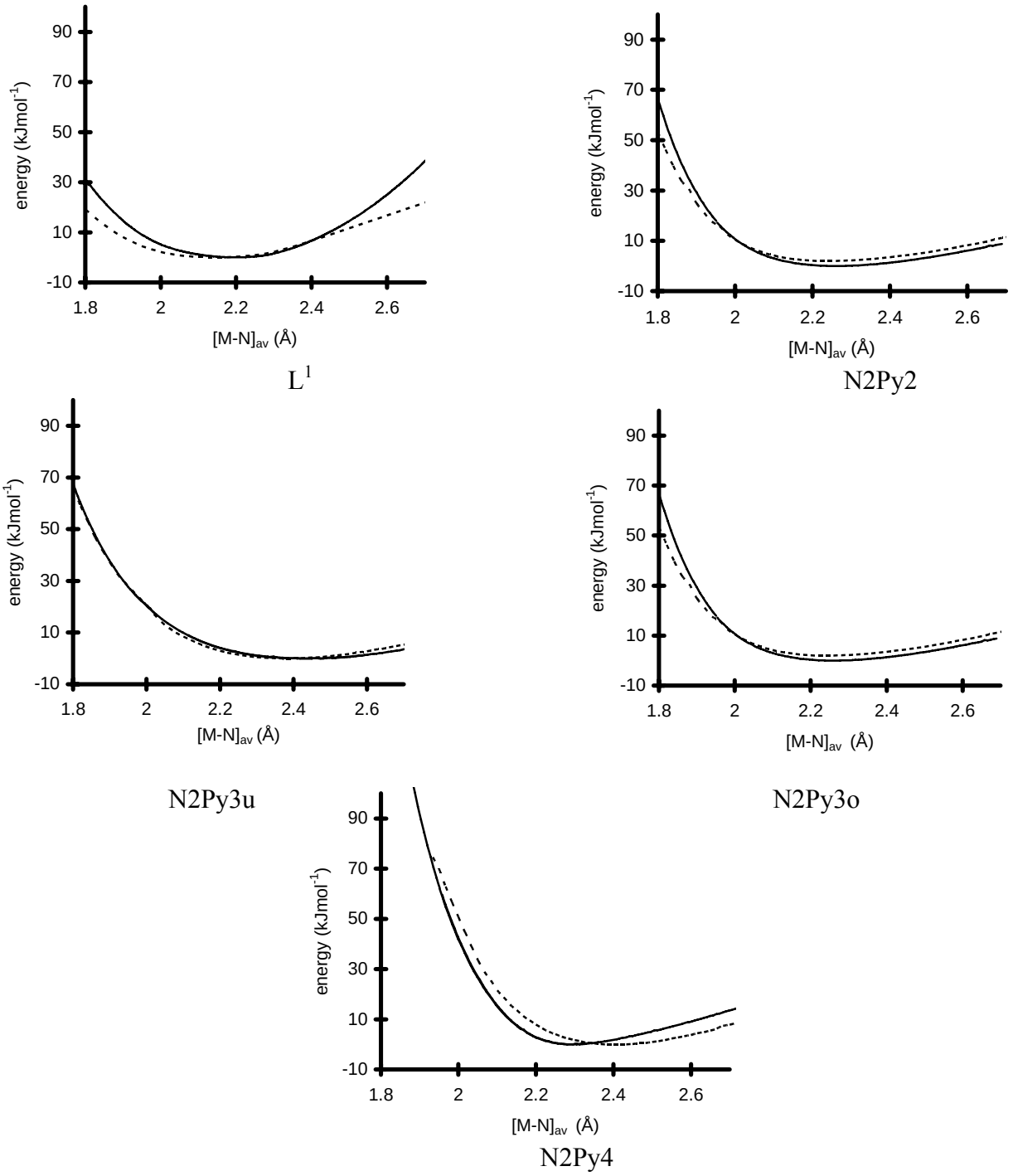

Fig. 3.2 Hole size curves for L^1, N2Py2, N2Py3o, N2Py3u and N2Py4

Table 3.2 Average of the experimentally determined and calculated M-N distance of complexes with N2Py4 and calculated relative strain energies by single point calculation of the optimized structure with all energies involving the metal ion set to zero.

	Co^{3+}(N2Py4)	Cr^{3+}(N2Py4)	Ni^{2+}(N2Py4)	Cu^{2+}(N2Py4)	Co^{2+}(N2Py4)	Zn^{2+}(N2Py4)
observed average (M-N) (Å)	-	-	2.10	2.13	2.17	2.19
computed average (M-N) (Å)	1.95	2.06	2.10	2.13	2.14	2.19
Ionic radii (pm)[30]	68.5	75.5	83.0	87.0	79.0	88.0
ΔE_{strain}(kJmol^{-1})	61.1	22.9	15.0	24.8	9.9	0.0

a) Jahn-Teller axis modeled along N7-Cu-py3

As a conclusion remarks from the hole size calculation from the comparison of ligands, it is proposed that in general the position of the minimum of ΔE_{strain} for the bispidine ligands is slightly shifted to smaller metal ions with respect to L^1 (L^1 : 2.15Å, N2Py2 : 2.25Å, N2Py3u : 2.38Å, N2Py3o : 2.24Å and N2Py4 : 2.29Å.). The hole size computations (though with another technique was applied for L^1 that we used) led to the conclusion that the bispidine cap in L^1 enforces small metal-N bispidine distances. Especially with regard to N2Py4, coordination to very small metal ions (Co(III), Cr(III)) leads to large distortions according to our calculations (loss of up to 60 kJ/mol with respect to the relatively unstrained geometry induced by Zn(II)), Redox potentials of the cobalt complexes support this (see in Chapter 4) Our calculation indicate that Zn(II) is the "optimal" ion with regard to the size to this ligand, coordination to Co(II) and Ni(II) still leads to a loss of more than 10 kJmol^{-1} relative to Zn(II). This is due to the rigidity of the backbone of N2Py4 (general effect of bispidine-type ligands) and also due to the elasticity of coordination sphere. The ligand N2Py4 is predicted not to be strongly size-selective for metal ions with average M-N bonds larger than approx. 2.1 Å Therefore, it was of particular interest to study this specific aspect experimentally. We are going to focus on the determination and comparison of their stability constants with transition-metal ions.

3.3 Acidity Constants

3.3.1 General

The stepwise acid protonation equilibrium of a ligand L can be described by the following equations:

$$L^{-m} + H^{+} \rightleftarrows HL^{1-m} \qquad \text{Eq. 3.1}$$

$$HL^{1-m} + H^{+} \rightleftarrows H_2L^{2-m} \qquad \text{Eq. 3.2}$$

$$H_2L^{m} + H^{+} \rightleftarrows H_3L^{3-m} \qquad \text{Eq. 3.3}$$

$$H_3L^{m} + H^{+} \rightleftarrows H_4L^{4-m} \qquad \text{Eq. 3.4}$$

where L is the ligand and m equals to 4, 5 or 6 for N2Py2, N2Py3u, N2Py4, respectively. The corresponding acid protonation constants are defined as:

$$Ka_1 = \frac{[HL]}{[H][L]} \qquad \text{Eq. 3.5}$$

$$Ka_2 = \frac{[H_2L]}{[H][HL]} \qquad \text{Eq. 3.6}$$

$$Ka_3 = \frac{[H_3L]}{[H][H_2L]} \qquad \text{Eq. 3.7}$$

$$Ka_4 = \frac{[H_4L]}{[H][H_3L]} \qquad \text{Eq. 3.8}$$

$$\vdots$$

where Ka is the concentration acid protonation constant; the concentrations of the species are given in molarity; the species charges in the above equations have been omitted. For example, N2Py2 has 4 basic sites so the stepwise acid protonation equilibria can be described by Eq. 3.5-3.8 with m = 4 . These constants were calculated from the potentiometric titration curve of the ligand by using the fitting program Hyperquad2000[31].

3.3.2 Measurements

Potentiometric titrations of the ligands in the absence (to determine ligand acidity constants) and in the presence of metal ions (to determine complex stability constants) were performed on 25 cm^3 samples, applying metal ion concentrations of $0.5 \times 10^{-3} – 1.0 \times 10^{-3}$ mol dm^{-3}. For the measurements 4:5 and 2:1 metal / ligand ratios were used, as solvent H_2O or dioxane/H_2O = 2:3 systems were applied.

For all ligands in the except for N2Py4, 40 vol% aqueous dioxane was used for the titration due to low solubility at higher pH region in pH meter. The experiments with ligand N2Py4 were carried out in both H_2O and 40 vol% aqueous dioxane.

3.3.3 Protonation Constants of Bispidine Ligands

The first log K_a value for all ligands was found to be in the range of 11.2 to 12.2.

These can be divided into two groups: to the first one belong N2Py2, N2Py3u , 6Me-N2Py2 which contain a methyl substituent at N7 position; to the second category fall N2Py3o and N2Py4 which have a picolyl group attached to the bispidine backbone at N7. The first log K_a value of ligands from the first group (N2Py2, N2Py3u, 6Me-N2Py2) are 11.2, 11.3 and 11.3, respectively. The first log K_a value of N2Py3o and N2Py4 were calculated to be 12.0 and 12.2, respectively. These values are somewhat higher, in comparison to results which were observed for ligands having only a methyl group attached to N7.

Alkyl groups are clearly electron donating, stabilizing the fully deprotonated neutral form and resulting in relatively small protonation constants while picolyl is less donating which make it more difficult to deprotonate the single positively charged species. However, this factor is proably not significant. This first protonation constant is relatively large due to two lone pairs involved (see Fig. 2.4).

The second log K_a value for N2Py2, N2Py3u and 6Me-N2Py2 8.8, 8.2 and 8.4, respectively, i.e., also similar each other. It seems likely that the structural difference in the ligands, the groups attached to N3, or the substituted/unsubstituted pyridine ring do not play a significant role in the values of the second protonation constant. Analogously the log K_{a2} values for N2Py3o and N2Py4 are 7.1 and 6.7, respectively. These values are smaller than those of the first group ligands, which might be due to the larger log Ka range (difference between the highest and lowest protonation constants).

Protonation constants log Ka1 and log K_{a2} are associated with the two aliphatic tertiary amines within the bispidine backbone.

As a result of the determination of protonation constants, it was found that these bispidine type ligands are not exceptionally strong 'proton sponges', but the configuration, where a proton bridges the two adjacent amine sites within the cavity, leads to a clear step between the first protonation, where the pair of secondary amines in the cavity can share a proton, and the second protonation, where each tertiary nitrogen accepts a proton and the original bridge is broken. By way of comparison, pK_a values for N,N,N',N'-tetramethylethylenediamine, which have no cavity effect, are several log units lower at 9.1 and 5.0[32].

The next steps are assigned to successive protonation of the pendant pyridine groups.

The final protonations take place in a very low pH region, their accurate determination by potentiometric titration is not possible, since the pH value at the beginning of the titration is already some units higher than these low log K_a values themselves, so the degree of protonation is minimal.

For tetraazamacrocycles, where two pairs of adjacent amines direct lone pairs into a cavity, two high log Ka values of ~11 are observed prior to a sharp drop to the third and successive protonations,[33] a comparable behavior to that observed here for this acyclic but structurally rigid molecule. The N,N,N',N'-tetrakis(2'-pyridylmethyl)ethane-1,2-diamine ligand (tpen) displays four log K_a values of 7.38, 4.84, 3.24 and 2.82;[34] the pKa of pyridine itself is 5.3. The second protonation constant (assigned to the second tertiary amine) is unexpectedly high, so is the third, associated with the first pyridine protonation. Apart from this, the observed trends are similar to those with other hexadentate pyridine/amine ligand systems.

It is also interesting to observe that out of the 6 protonable groups, only four of them could be determined, the largest two of them are aliphatic amine, which are much smaller than for macrocycles and proton sponge systems, it causes no further stabilization of the protonated species.

Among the pyridine pK_a, two of them are already smaller than for simple pyridine, and the other two are remarkably small. Due to possessing of amine and pyridine groups

simultaneously in a ligand, the pyridine pK_a will decrease significantly. In the case of bispidines, the effect of this decrease is combined with the proton sponge effect: the aliphatic amines have unusually large values, while pyridines have smaller ones. Another effect is the counter-compensation: due to the proton sponge effect, the pyridine nitrogens tend to have much smaller values due to the remarkably large range of pK_a values.

Comparing the distribution curves of the species for all five bispidine-type ligands, it can be seen that at pH ca.10, LH_1 exist to almost 100%. Further rise in pH results in gradual formation of the fully deprotonated species. There is no remarkable difference between the bispidine-type ligands.

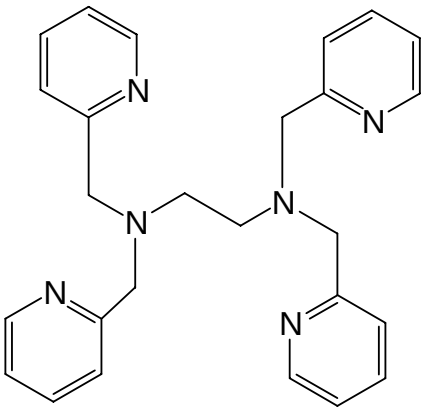

Fig. 3.3.2 Structure of N,N,N',N'-tetrakis(2'-pyridylmethyl)ethane-1,2-diamine (TPEN)

Table.3.3 Potentiometrically determined protonation constants

	N2Py2 (H_2O/Dioxane=3:2)	N2Py3u (H_2O/Dioxane=3:2)	N2Py3o (H_2O/Dioxane=3:2)	6Me-N2Py2 (H_2O/Dioxane=3:2)	N2Py4 (H_2O/Dioxane=3:2)	N2Py4 (H_2O)	TPEN (H_2O)
$L+H^+ = [LH]^+$	11.2	11.3	12.2	11.3	12	11.8	7.4
$L + 2H^+ = [LH_2]^{2+}$	8.8	8.2	7.1	8.4	6.7	6.9	4.8
$L + 3H^+ = [LH_3]^{3+}$	2.3	4	2.8	2	4.1	5.1	3.2
$L + 4H^+ = [LH_4]^{4+}$	≥2	≥2	2.4	≥2	2.2	2.2	2.8
$L + 5H^+ = [LH_5]^{5+}$	-	≥2	≥2	-	≥2	≥2	≥2
$L + 6H^+ = [LH_6]^{6+}$	-	-	-	-	≥2	≥2	≥2

3.4 Stability Constants

3.4.1 Chemical Species Distribution

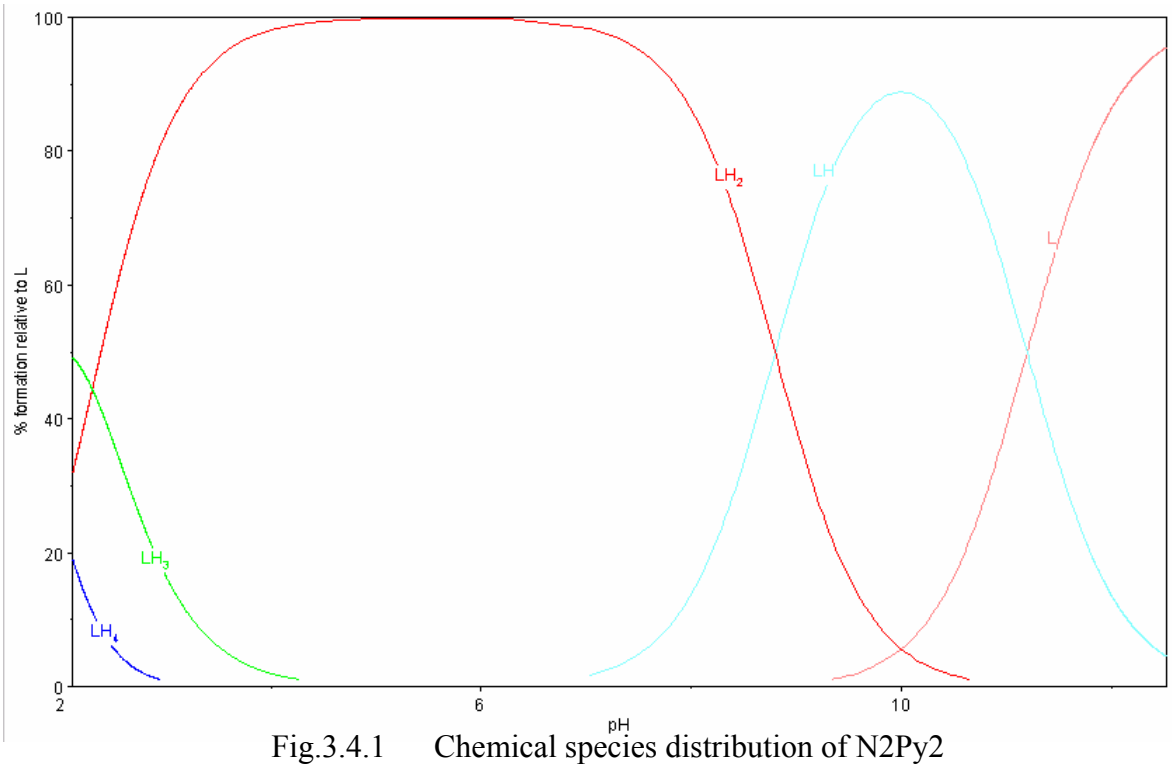

Fig.3.4.1 Chemical species distribution of N2Py2

(H_2O, T=25°C, μ =0.1M(KCl)

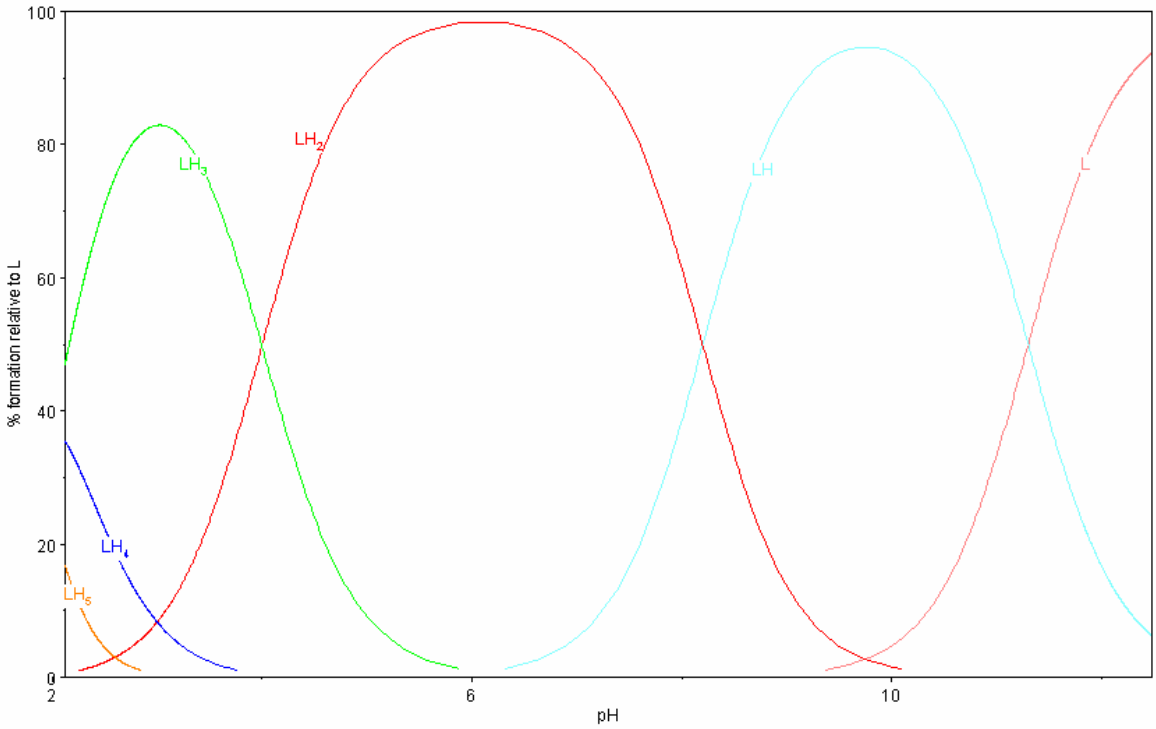

Fig.3.4.2 Chemical species distribution of N2Py3u

(H_2O, T=25°C, μ =0.1M(KCl)

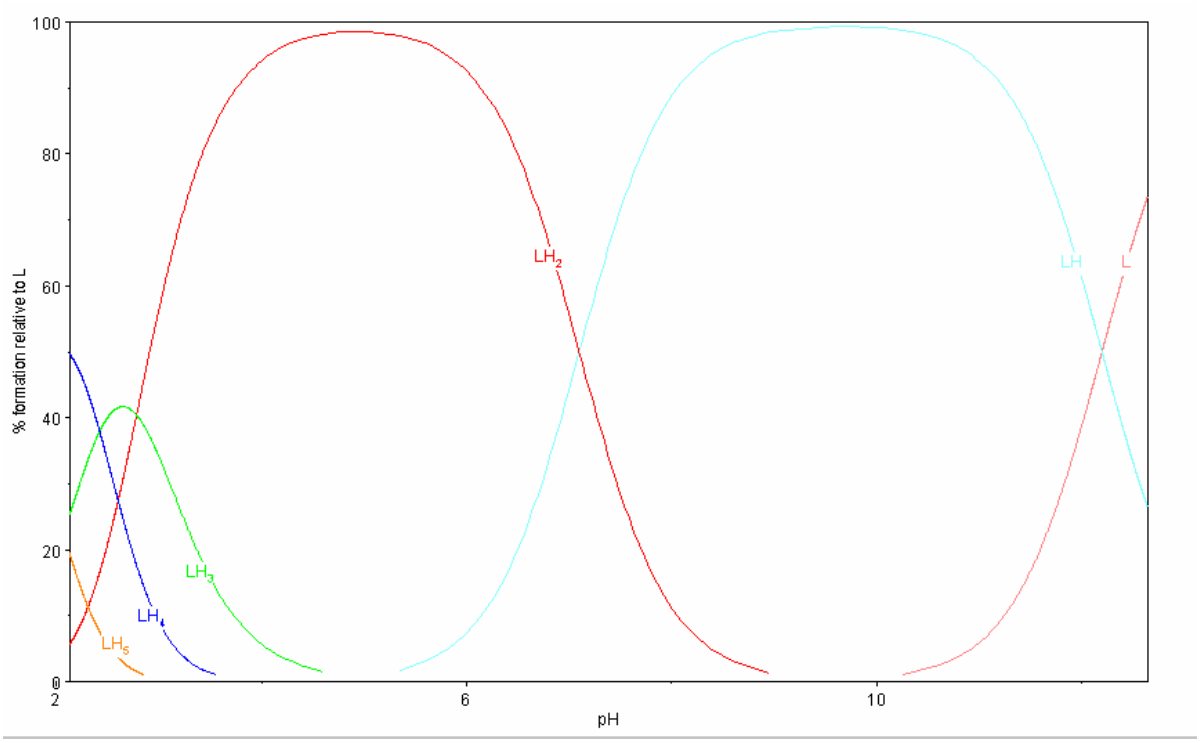

Fig.3.4.3 Chemical species distribution of N2Py3o

(H_2O, T=25°C, μ =0.1M(KCl)

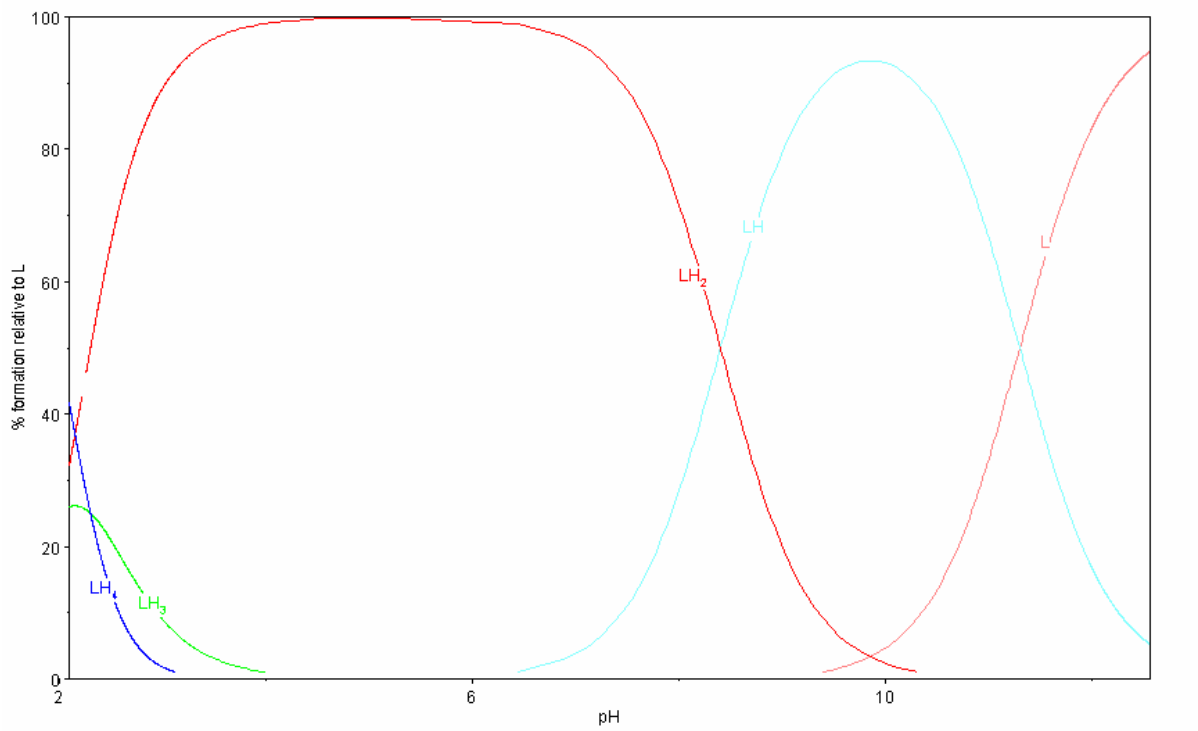

Fig.3.4.4 Chemical species distribution of 6Me-N2Py2

(H_2O, T=25°C, μ =0.1M(KCl)

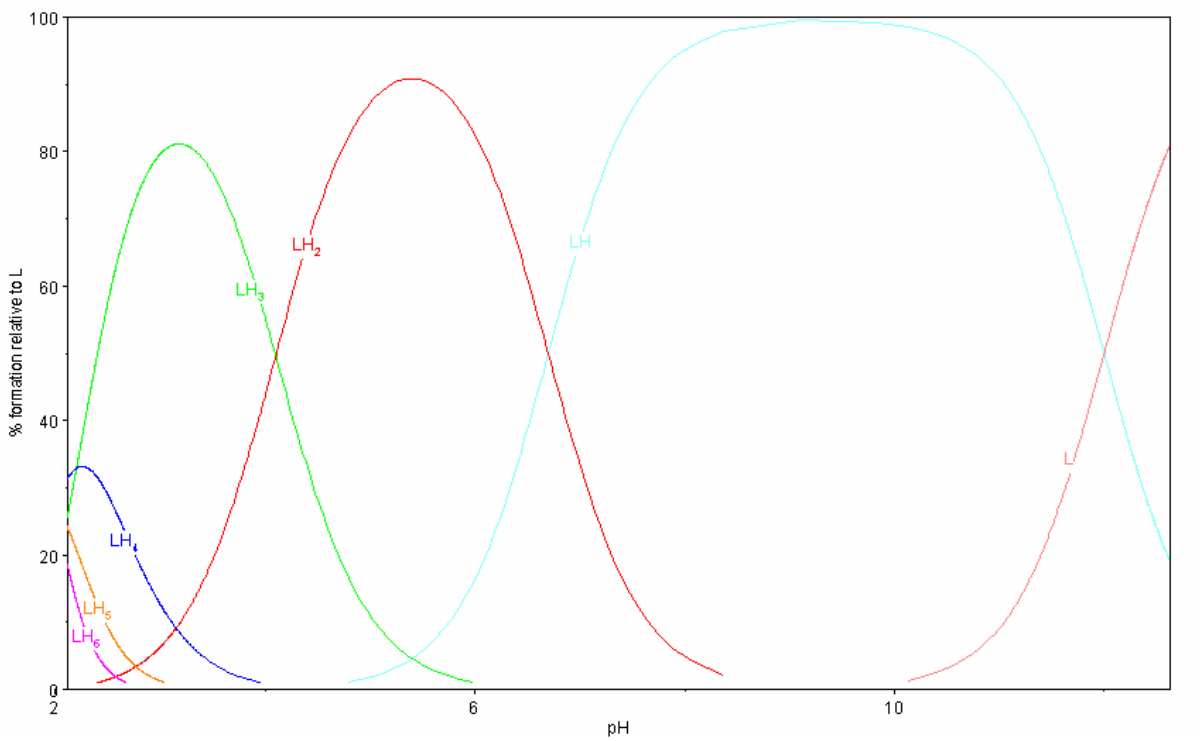

Fig.3.4.5 Chemical species distribution of N2Py4

(H_2O, T=25°C, μ =0.1M(KCl)

3.4 .2 Stability Constants

Table 3.4 Potentiometrically determined protonation and complex stability constants (logK values) of N2Py4 (H_2O, T=25°C, μ =0.1M KCl)

Stability constants	Co^{2+}	Ni^{2+}	Cu^{2+}	Zn^{2+}	Hg^{2+}	Pb^{2+}	Li^{+}
$M^n + L + 2H^+ \rightleftarrows [MLH2]^{n+2}$	23.8	24.4	-	-	-	-	24.8
$M^n + L + H^+ \rightleftarrows [MLH]^{n+1}$	20.8	20.4	22.9	24.7	20.3	18.9	20.4
$M^n + L \rightleftarrows [ML]^n$	**15.0**	**14.1**	**19.8**	**21.5**	**15.8**	**14.0**	**13.2**
$M^n + L + OH^- \rightleftarrows [ML(OH)]^{n-1}$	5.0	6.2	9.2	10.8	7.2	4.4	3.2
$M^n + L + 2OH^- \rightleftarrows [ML(OH)_2]^{n-2}$	-	-4.0	-	-	-	-	-

The stability constants of N2Py4 ligand with Co(II), Ni(II), Cu(II), Zn(II), Hg(II), Pb(II) and Li(I) were determined potentiometrically. The hexadentate bispidine-based ligand, N2Py4, with four pyridine and two tertiary amine donors, based on a very rigid backbone, is coordinated to a range of metal ions. Based on experimental and computed structural data, spectroscopy and electrochemistry the ligand was predicted to build very stable complexes. This is confirmed by potentiometrically determined stability constants which indicate that, in general, stabilities comparable to those with macrocyclic ligands are observed.

The main feature of the log $_{KM}$ values of the series Co(II)(d^7), Ni(II)(d^8), Cu(II)(d^9), Zn(II)(d^{10}) Co(II)(15.0)>Ni(II)(14.0)<<Cu(II)(19.8)<Zn(II)(21.5) which are in sharp contrast to usual Irving-Williams behavior Co(II) < Ni(II) < Cu(II) > Zn(II).

This feature can be explained by the force field calculations (see above) that indicate that short metal-donor distances lead to a build-up of strain in the ligand and that there is no size-match selectivity for large metal ions as shown in Fig.3.2.

The ionic radii (Co(II) 0.75, Ni(II) 0.69, Cu(II) 0.75, Zn(II) 0.74) and the observed average bond distances of M-N ; Co(II) 2.17, Ni(II) 2.10, Cu(II)2.13, Zn(II) 2.17 suggest that Ni(II) is

smaller (~ 2.1 Å) than optimal in terms of the ligand preference. This might be one of the reason for the relatively low stability of the Ni(II)complex. The larger Zn(II) center with relatively weak M-N force constants and virtually no angular directionality also ideally fits the ligand requirements.

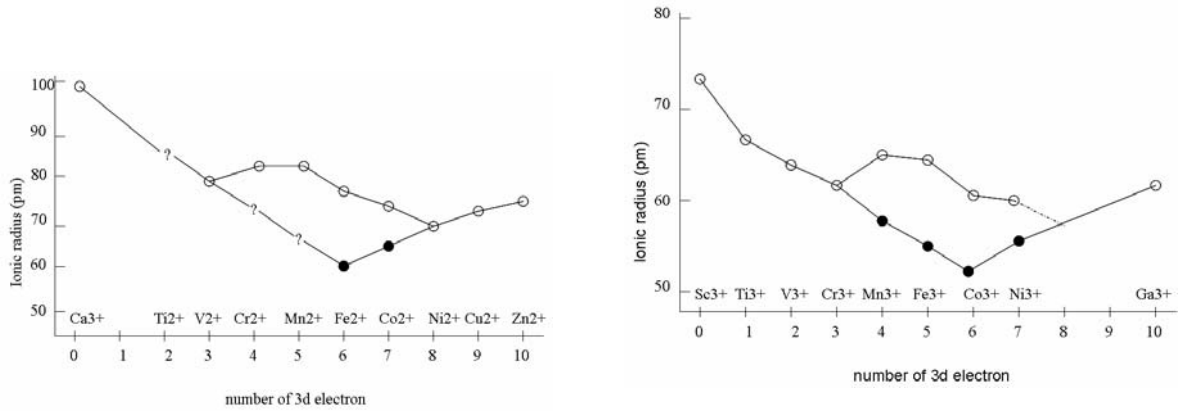

Fig. 3.4.6 Relationship between the number of d-electrons and ionic radius for first row transition metal ions (white dots (○) represent low-spin, black dots (●) show high-spin metal ions, respectively.[35])

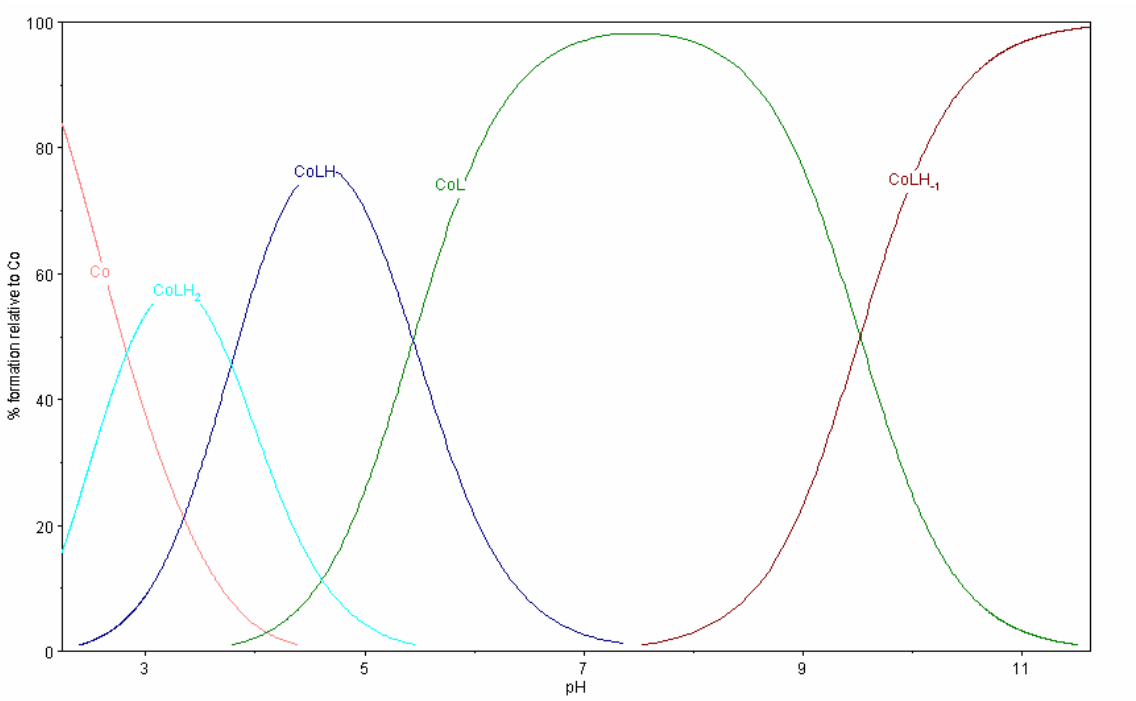

Fig. 3.5.1 Chemical species distribution of N2Py4 with Co^{2+}

(H_2O, T=25°C, μ =0.1M(KCl)

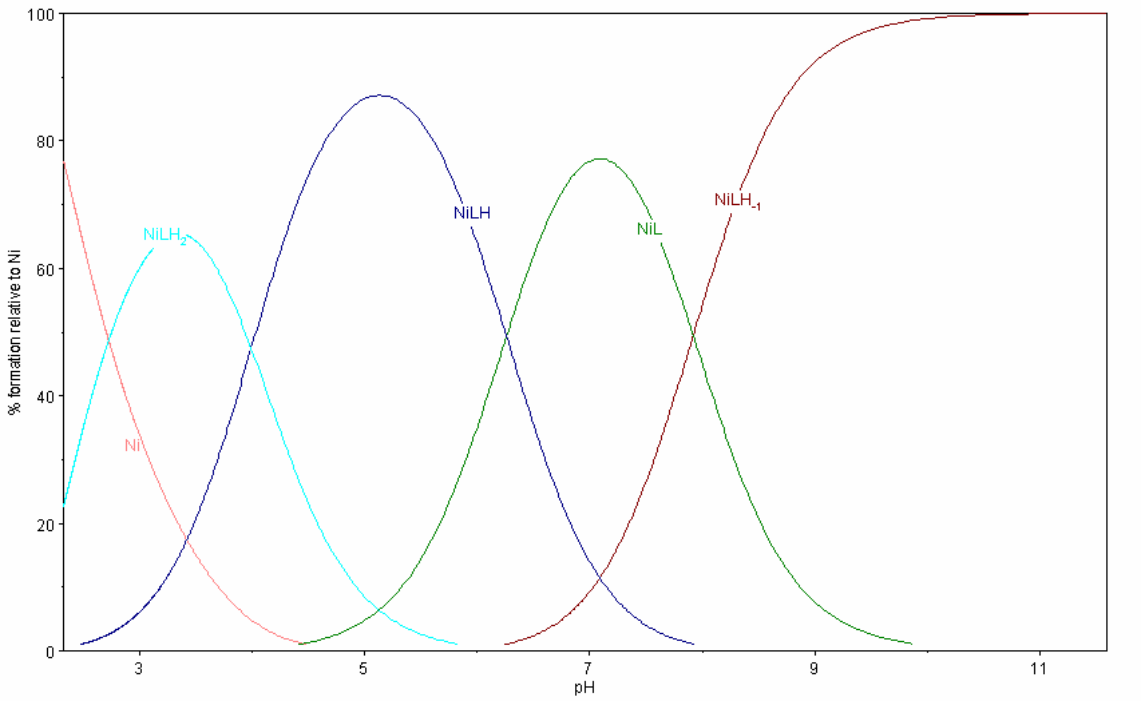

Fig.3.5.2 Chemical species distribution of N2Py4 with Ni^{2+}

(H_2O, T=25°C, μ =0.1M(KCl)

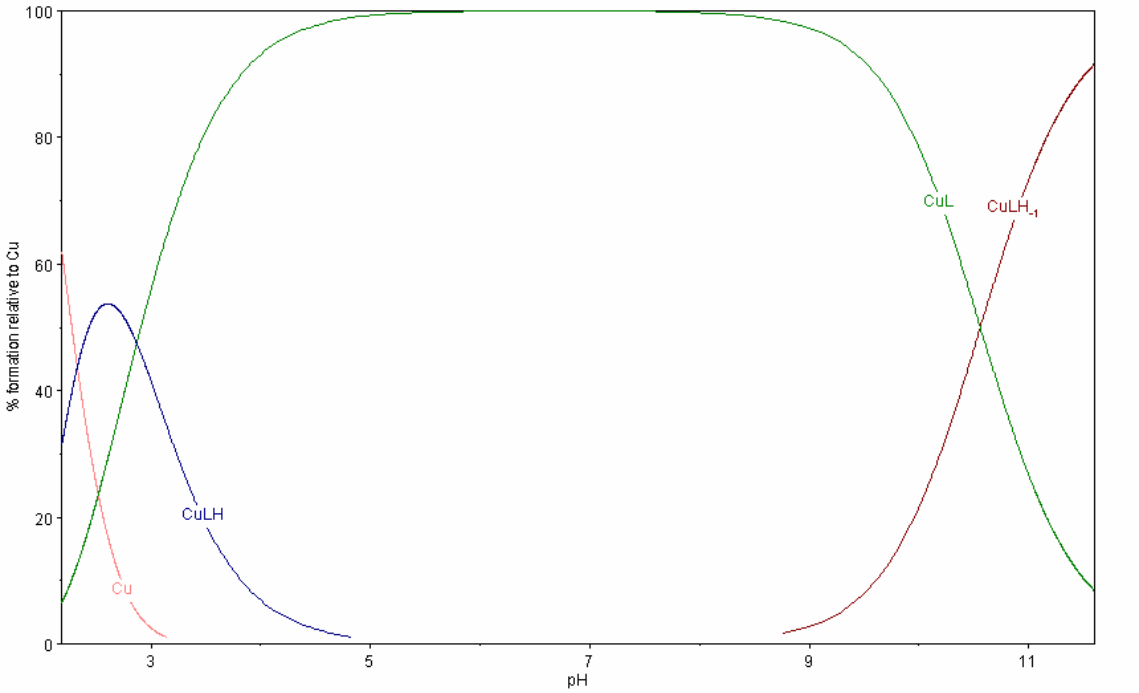

Fig.3.5.3 Chemical species distribution of N2Py4 with Cu^{2+}

(H_2O, T=25°C, μ =0.1M(KCl)

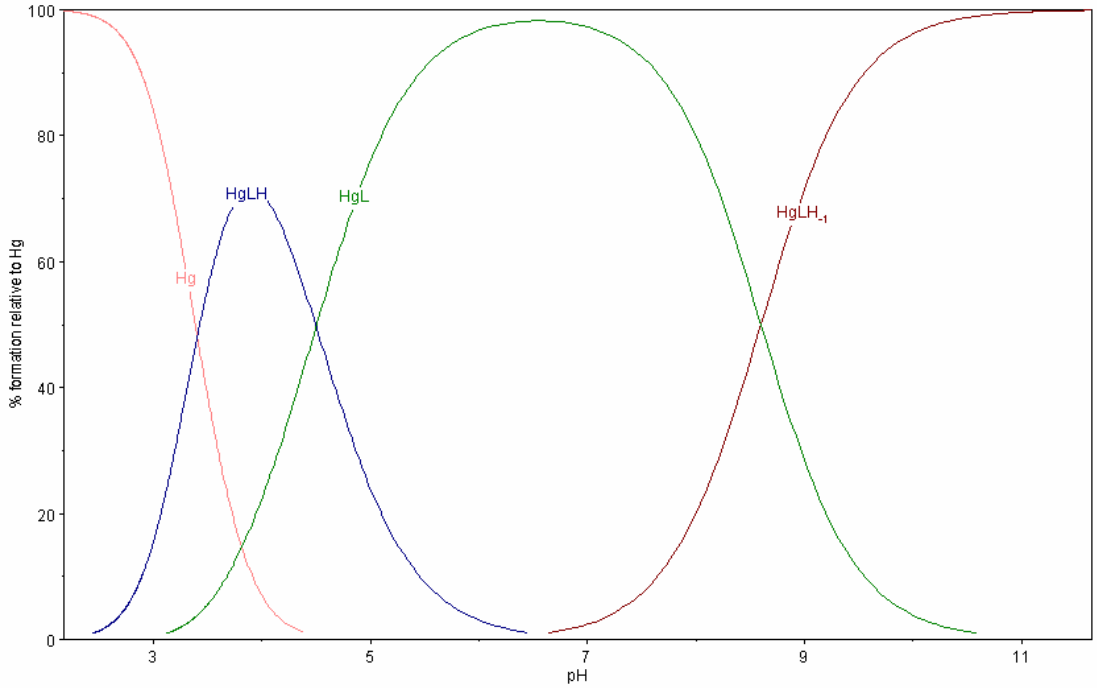

Fig.3.5.4 Chemical species distribution of N2Py4 with Hg^{2+}

(H_2O, T=25°C, μ =0.1M(KCl)

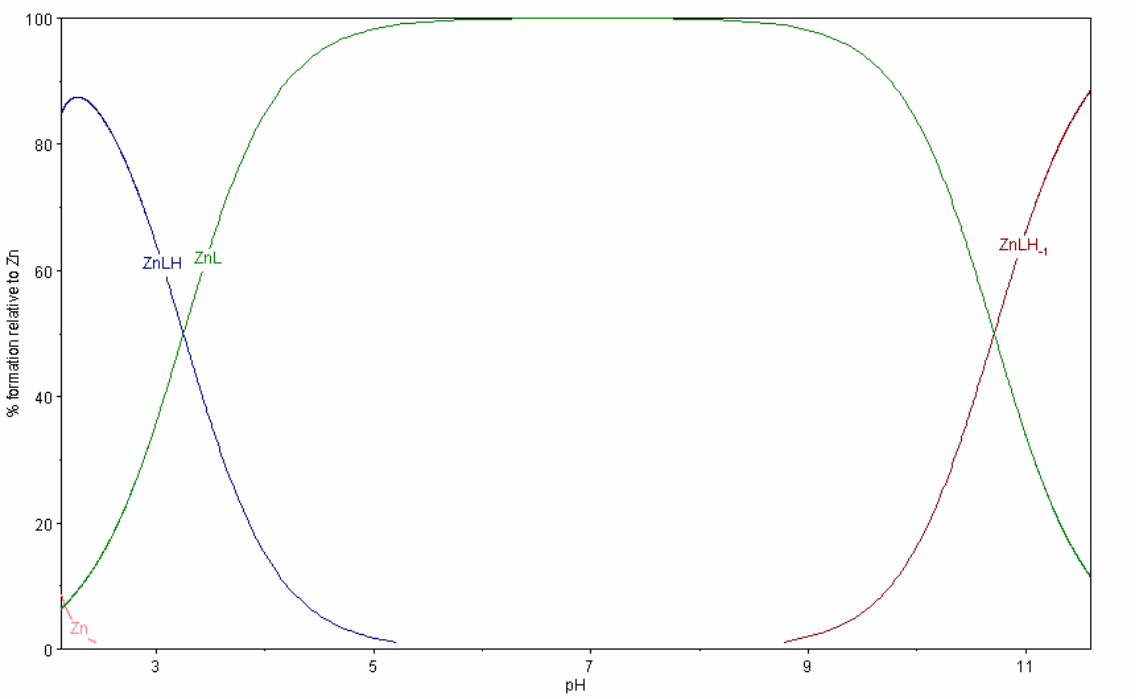

Fig.3.5.5 Chemical species distribution of N2Py4 with Zn^{2+}

(H_2O, T=25°C, μ =0.1M(KCl)

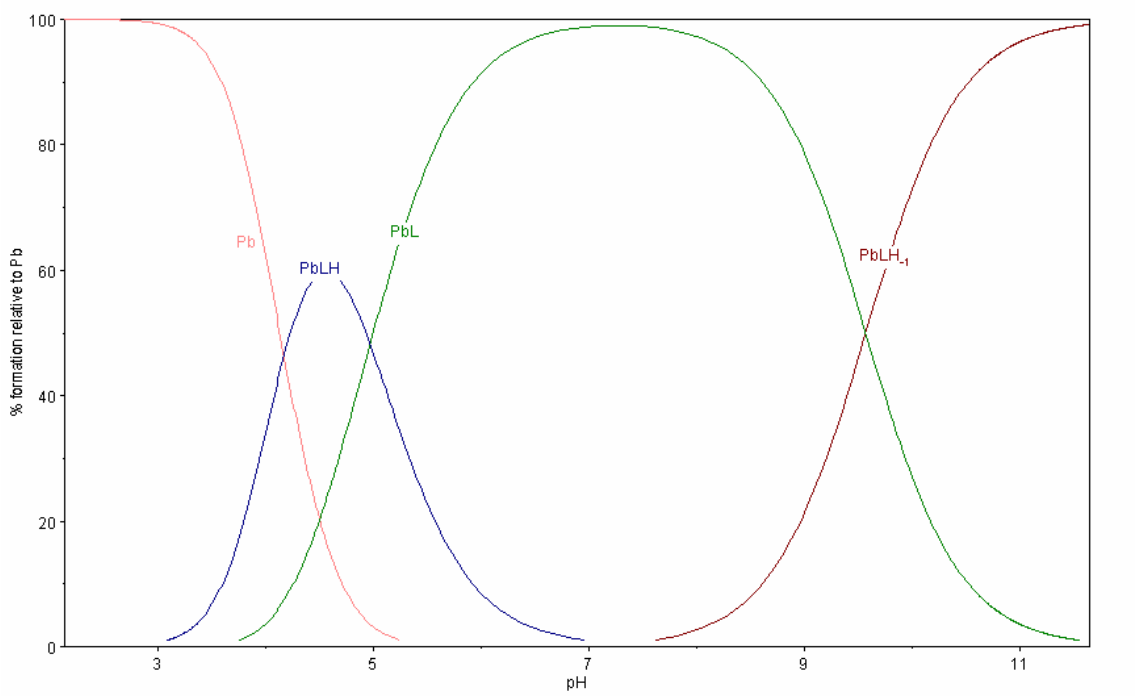

Fig.3.5.6 Chemical species distribution of N2Py4 with Pb^{2+}

(H_2O, T=25°C, μ =0.1M(KCl)

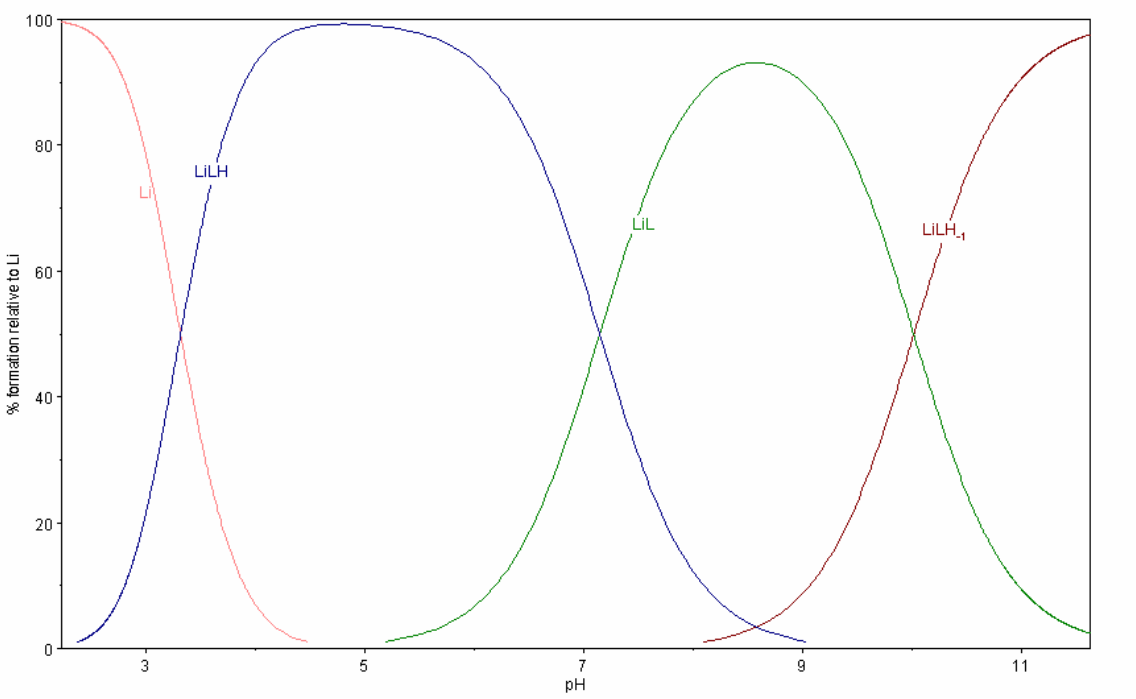

Fig.3.5.7 Chemical species distribution of N2Py4 with Li^+

(H_2O, T=25°C, μ =0.1M(KCl)

References

[1] P. Comba, W. Schiek, *Coord. Chem. Rev* **2003**, *21*, 238.

[2] R. Hancock, D. Martell, *Chem. Rev.* ,**1989**, 1975, 89.

[3] P.Comba, *Coord. Chem. Rev.* ,**1999** , *185*, 81.

[4] P. Comba, *Coord. Chem. Rev.* ,**2000**, *217*,200.

[5] J. J. R Frausto da Silva, R. J. P. Williams, *The Biological Chemistry of the Elements*; Clarendon Press: Oxford, **1999**.

[6] L. H. Gade, *Koordinationchemie*,Wiley-VCH,Weinheim,1998

[7] R. G. Pearson, *J. Am. Chem.,* **1963**, *85*, 3533.

[8] H. M. Irving,R. J.P. Williams, *Nature*, 1948, 162, 746.

[9] H. M. Irving, R. J.P. Williams, *J.Chem. Soc.* **1953**, 3192.

[10] D. H. Busch, N. A. Stephenson, *Coord. Chem. Rev.*, **1990**,*100*,119.

[11] S. P. Artz, D. J. Cram, *J. Am. Chem. Soc.*,**1953**,3192

[12] D. J. Cram, *J. Inclusion Phenom.*,**1988**,*1*,1

[13] L. F. Lindoy, *The chemistry of macrocyclic ligand complexes*; Cambridge University Press: Cambridge New York, 1989.

[14] B. Dietrich, P. Viout, J. M. Lehn, *Macrocyclic chemistry. Aspects of organic, inorganic and supramolecular chemistry*; VCH: New York Weinheim, **1993**.

[15] G. D. Hosken, R. D. Hancock, *J. Chem. Soc., Chem. Commun.* **1994**, 1363.

[16] C. C. Allan, J. C. A. Boeyens, R. D. Hancock, *J. Chem. Soc., Dalton Trans.* **1995**, 3705.

[17] G. Schwarzenbach, R. Gut, G. Anderegg, *Helv. Chim. Acta* **1954**, *37*, 937.

[18] K. P. Wainright, A. Ramasubby, *J. Chem. Soc., Chem. Commun.,* **1982**, 277.

[19] K. P. Wainright, *Inorg. Chem.,* **1980**, *19*, 1396.

[20] R. D. Hancock, *Pure and Appl. Chem.,* **1993**, *65*, 941-946.

[21] P. Comba, M.Kerscher, *Cryst. Eng.,* **2004**, *6*, 197.

[22] P. Comba, M.Kerscher, M.Merz, V.Müller, H.Pritzkow, R.Remenyi, W.Schiek, Y. Xiong,

Chem. Eur. J., **2002**, *8*, 5750.

[23] H. Börzel, P. Comba, K. S. Hagen, M. Merz, Y. D. Lampeka, A. Lienke, G. Linti, H. Pritzkow, L. V. Tsymbal, *Inorg. Chim. Acta.,* **2002**, 337, 407.

[24] P. Comba, M. Merz, H. Pritzkow, *Eur. J. Inorg. Chem. ,* **2003**, 1711.

[25] H. Börzel, P. Comba, K. S. Hagen, M.Kerscher, H. Pritzkow, M. Schatz, S. Schindler, O. Walter, *Inorg. Chem.,* **2002**, *41*, 5440.

[26] H. Börzel, P. Comba, C. Katsichtis, W. Kiefer, A.Lienke,V.Nagel, H.Pritzkow, *Chem. Eur. J.,* **1999**, *5*, 1716.

[27] P. Comba, A. Hauser, M. Kerscher, H. Pritzkow, *Angew. Chem.,* **2003**, *115*, 4675.

[28] P. Comba, T. W. Hambley, G. Lauer, M. Melter, N. Okon, *MOMEC97, a molecular modeling package for inorganic compounds*: University of Heidelberg, www.combagroup.uni-hd.de, 1997.

[29] J. E. Bol, C. Buning, P. Comba, J. Reedijk, M. Stroehle, *J.Comput.Chem.*,**1998**, *19*, 512

[30] R. D. Shanon, *Acta Crystallogr.*, **1976**, *32*, 751

[31] P. Gans, A. Sabatini, A. Vacca, *Talanta.*, **1996**, *43*, 1739.

[32] L. G. Sillén, A. E. Martell, *Stability Constants of Metal-Ion Complexes, Supplement No1*; The Chemical Society: London, **1971**.

[33] Y. Baran, G. A. Lawrance, E. N. Wilkes, *Polyhedron,* **1997**, *16*, 599.

[34] I. Cukrowski, E. Cukrowska, R. D. Hancock, G. Anderegg, *Anal. Chim. Acta.,* **1995**, *312*, 307.

[35] R. D. Shannon, C. T. Prewitt, *Acta Crystallogr.*, **1970,** *26*,1076

4. Cobalt Complexes of 3,7-Diazabicyclo[3.3.1]nonane Derivatives

4.1 Introduction

Cobalt is a component of enzymes such as vitamin B_{12}, which has various functions in biological systems[1]. In the series of first row transition metals, cobalt represents the transition between hard and soft metal ions.

The two most investigated oxidation states of cobalt are the divalent and the trivalent forms. Co(II) is d^7 and paramagnetic (EPR active), its complexes are kinetically labile and they can usually be oxidized by, for example, using H_2O_2 or air. In contrast, Co(III) is d^6 and diamagnetic (EPR inactive) in its low spin configuration. Their complexes are mostly kinetically inert and are resistant usually even to concentrated acid.

Co(III) complexes can be regarded as one of the archetypes of an inert metal complex and have been at the forefront of coordination chemistry for more than 130 years.

The simple ammine-aqua derivatives were extensively investigated by Jørgensen[2] and Werner[3]. Since the discovery that vitamin B12 is a macrocyclic complex of Co(III), there has been interest due to the inert property of low spin Co(III) complexes, in their application as models for enzymatic reactions[4,5].

It is known that aliphatic nitrogen donors have a high affinity for cobalt (III). The complexity of the different effects steric and electronic which play a role in the metal-ligand interactions, allows us to tune the coordination properties of the complexes. In the case of the bispidine chemistry the harder nature of Co(III) can somewhat counterbalance the effect of the smaller ion size in comparison with Co(II). Co(II)/(III) complexes of tetra- or pentadentate bispidines have one or two open sites due to the hexa-coordinate central metal ion, which can be used for binding a co-ligand or a substrate molecule. Besides the difference in ion size (and therefore also in the metal-donor distances), the charge transfer effect can also influence the stability of the complexes. A negatively charged co-ligand can increase the electron density around the

central cobalt ion.

As reported in Chapter 3, force field calculations indicate that there is significant strain in Co(III) bispidine complexes. Moreover Co(II) bispidine complexes are unusually inert due to the stabilization by the pyridyl π-donor groups of bispidine.

Thus, a oxidation of Co(II) complex gives significant steric and electronic differences. There is, therefore, much interests in investigating the oxidation process from Co(II) to Co(III) in bispidine complexes.

4.2 Preparation

4.2.1 Preparation of Co(II) Bispidine Complexes

Cobalt (II) complexes with variousbispidine-type ligands (N2Py2, N2Py3o, N2Py3u and N2Py4) have been obtained in MeOH or EtOH solution using reported procedures[6,7,8,9,10,11]. $Co(II)(ClO_4)_2 \cdot 6H_2O$ and $Co(II)(BF_4)_2 \cdot 6H_2O$ were applied as cobalt sources. For same applications it is useful to use counter anions which hardly coordinate to the cobalt center (e.g., perchlorate or tetrafluoroborate), because it can be advantageous to leave open coordination sites for the exchange with co-ligands. However complexes are more difficult to crystallize in comparison with e.g. chloro complexes. Cobalt (II) complexes of all ligands were prepared by the following method: 0.9 eq. of cobalt salt and 1 eq. of ligand were dissolved separately in methanol. These solutions were then mixed and refluxed for 5-10 minutes. After further stirring for 2-3 hours at room temperature, methanol was completely evaporated by means of a rotary evaporator and an appropriate amount of ethylacetate added to the crude complex to wash off unreacted ligand. The resulting pure complex was filtered and dried in vacuum. Single crystals of Co(II) complexes, suitable for structure determination were grown by ether diffusion into their methanolic solution. Two of the experimentally determined structures are shown in Fig. 4.3.1.

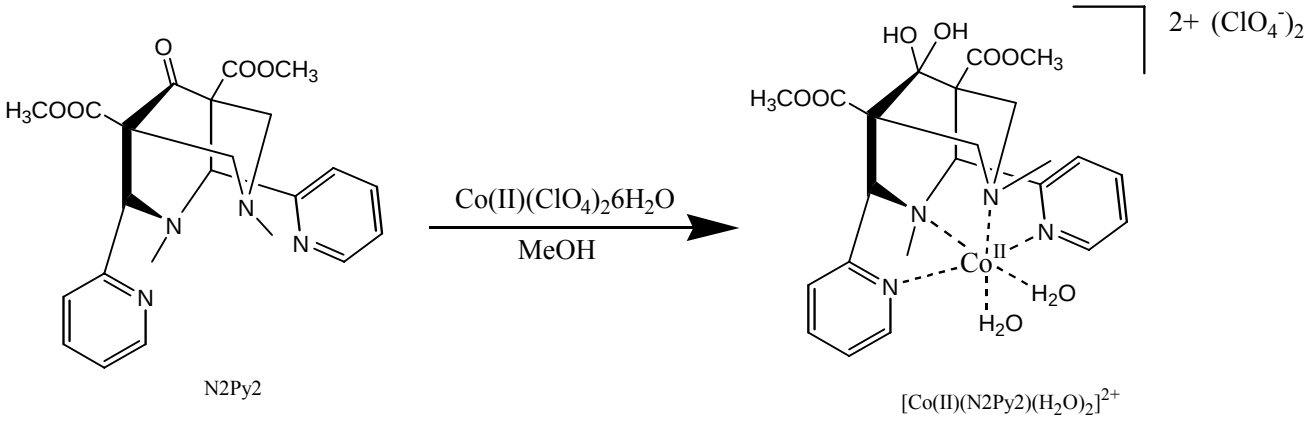

Fig. 4.2.1 Complexation of Co(II) with N2Py2

4.2.2 Preparation of Co(III) Bispidine Complexes

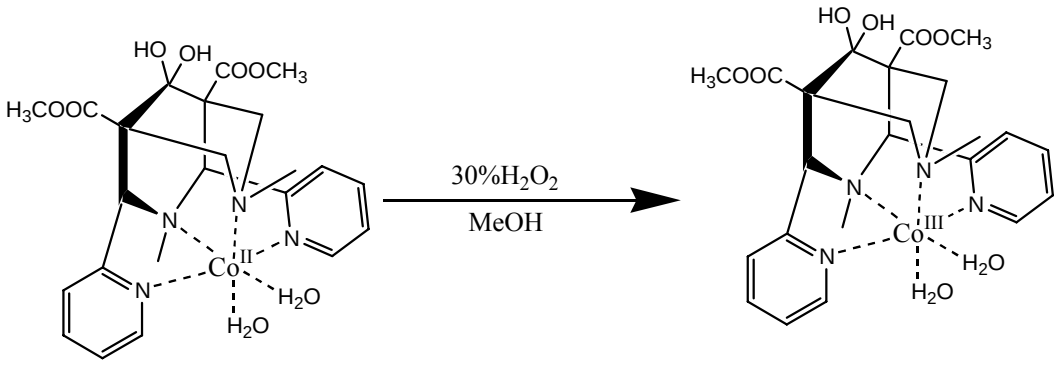

Fig. 4.2.2 Oxidation from $[Co(II)(N2Py2)(H2O)_2]^{2+}$ to $[Co(III)(N2Py2)(H2O)_2]^{3+}$

Oxdation of Co(II) complexes to the corresponding Co(II) usually is done with pure O_2, air or hydrogen peroxide as oxidant. Another known method to prepare Co(III) complexes is the exchange reaction between ligands and $K_3[Co(III)(OCO_2)_3]$ or $Na_3[Co(III)(OCO_2)_3]$ [12] $[Co(III)(acac)_3]$ [13],and $[Co(III)(NO_3)_6]^{3-}$ [,14] are also operative.

Initially air and pure O_2 were used as oxidants to obtain Co(III) complexes with bispidine-type ligands. However, these attempts proved to be unsuccessful due to the high redox potentials of the Co(II)/(IIII) bispidine complexes (e.g. E_0=0.65V vs. $Ag/AgNO_3$ for Co(II)/(IIII)(N2Py2).) The failure of oxidation by oxygen and air can be also explained by the unusual inertness of Co(II) bispidine complexes due to the stabilization by the π-donors (pyridyl groups) and the hole size effect of the bispidine backbone: the size of Co(III) leads to a significant increase of the steric energy (See in Chapter 3)

Attempts to obtain Co(III) complexes by oxidation of the corresponding Co(II)complexes with hydrogen peroxide, a more powerful oxidant, were successful with all bispidine-type ligands. These oxidation reactions were carried out in methanol at room temperature. Furthermore, $[Co(III)(N2Py2b)CO_3]PF_6$ has also been obtained by an exchange reaction using $K_3[Co(OCO_2)_3]$ [15] as the cobalt source, in refluxing methanol.

4.3 Crystal structures of Cobalt (II) and (III) Bispidine Complexes

4.3.1 Crystal Structures of Cobalt (II) and (III) Complex with N2Py2

Selected bond lengths, bond angles and torsion angles of $[Co(III)(N2Py2a)Cl_2]ClO_4$, $[Co(III)(N2Py2a)(EtO)(H_2O)](ClO_4)_2$, $[Co(III)(N2Py2b)CO_3]PF_6$, $[Co(II)(N2Py2)(H_2O)_2]Cl_2$ and [Co(II)(N2Py2)OAc]OAc are listed in Table 4.1, structural plots are presented in Fig. 4.3.1.

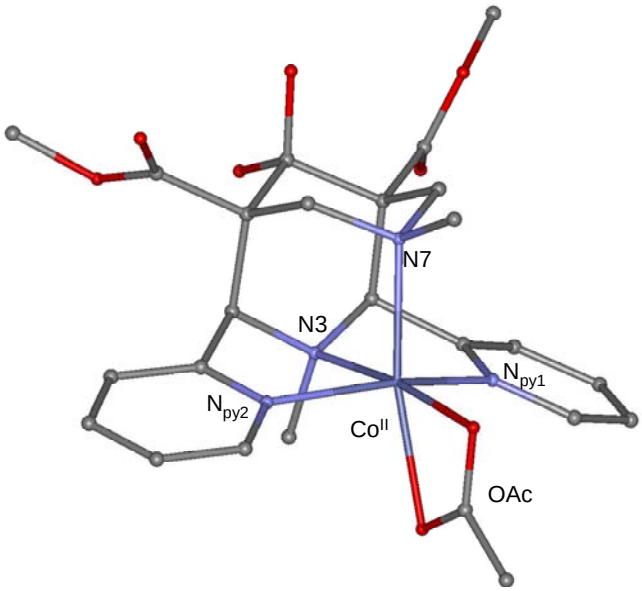

$[Co(II)(N2Py2)(OAc)]^+$

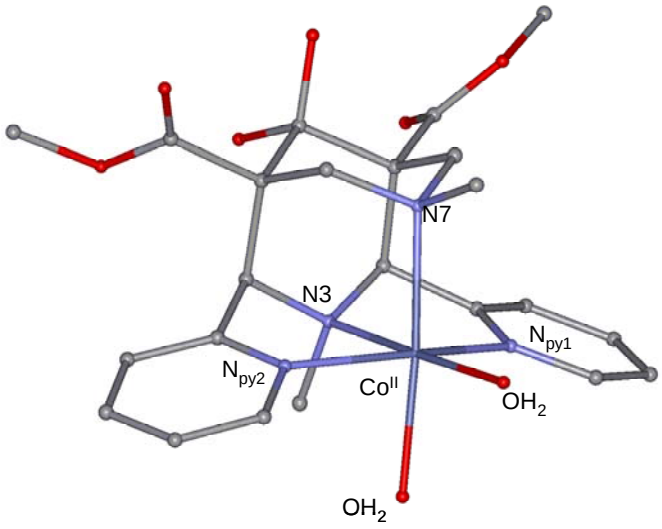

$[Co(II)(N2Py2)(H_2O)_2]^{2+}$

Fig. 4.3.1 Crystal structures of $[Co(II)(N2Py2)(OAc)]^+$ and $[Co(II)(N2Py2)(H_2O)_2]^{2+}$

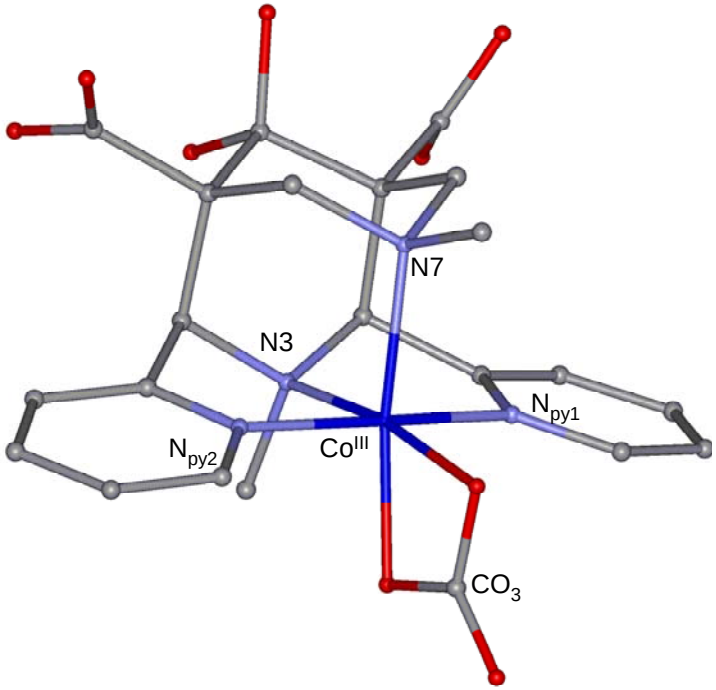

$[Co(III)(N2Py2_b)(CO_3)]^{2+}$

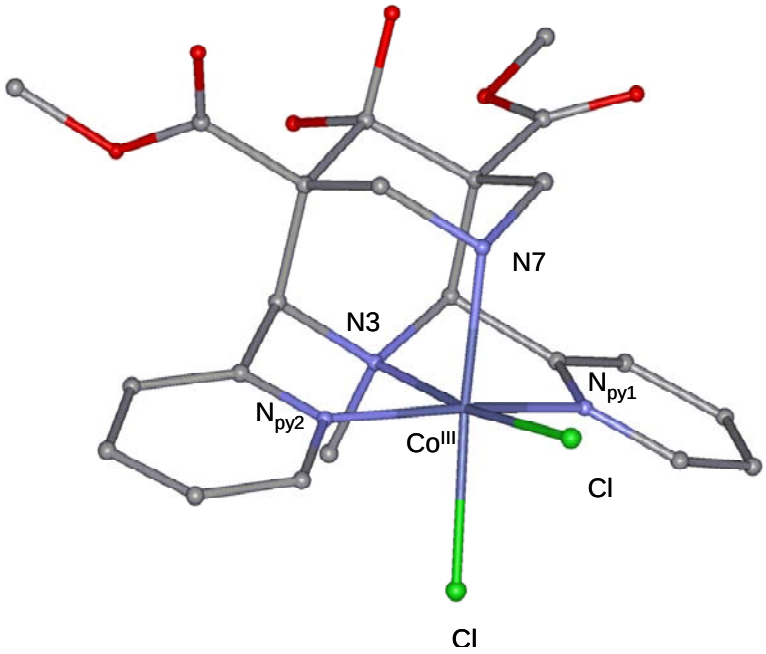

$[Co(III)(N2Py2_a)(Cl)_2]^{+}$

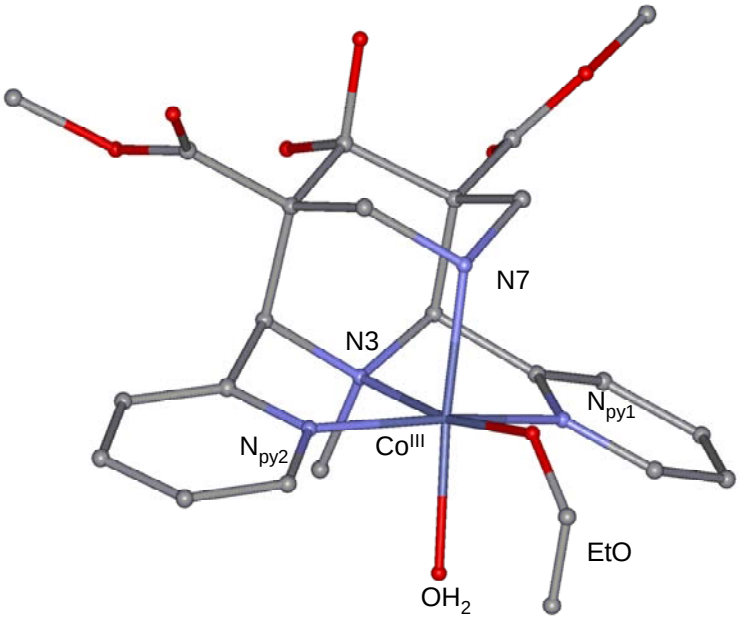

$[Co(III)(N2Py2_a)(EtO)(H_2O)]^{2+}$

Fig. 4.3.2 Crystal structure of $[Co(III)(N2Py2_a)(Cl)_2]^{+}$, $[Co(III)(N2Py2_a)(EtO)(H_2O)]^{2+}$ and $[Co(III)(N2Py2_b)(CO_3)]^{2+}$

Table 4.1 Structural data of $[Co(III)(N2Py2a)(Cl)_2]ClO_4$, $[Co(III)(N2Py2a)(EtO)(H_2O)](ClO_4)_2$, $[Co(III)\ (N2Py2b)(CO_3)]PF_6$, $[Co(II)\ (N2Py2)(H_2O)_2]Cl_2$, [Co(II)(N2Py2)(OAc)]OAc and $[Co(III)(N2Py2)(NH_3)_2MM]$, $[Co(II)(N2Py2)(NH_3)_2MM]$

	$[Co^{III}(N2Py2^a)Cl_2]ClO_4$	$[Co^{III}(N2Py2^a)(EtOH)\ (H_2O)](ClO_4)_2$	$[Co^{III}(N2Py2^b)CO_3]PF_6$	$[Co^{II}(N2Py2)2H_2O]Cl_2$	$[Co^{II}(N2Py2)OAc]OAc$	$Co^{III}(N2Py2)momec$	$Co^{II}(N2Py2)momec$
X(plane)	Cl	EtOH?	CO_3	H_2O	OAc	NH_3	NH_3
Y(axial)	Cl	H_2O		H_2O		NH_3	NH_3
distances[Å]							
Co-N3	1.96	1.95	1.94	2.15	2.15	1.97	2.14
Co-N7	2.02	1.98	2.03	2.21	2.17	2.04	2.25
Co-N_{py1}	1.96	1.93	1.91	2.12	2.10	1.93	2.12
Co-N_{py2}	1.92	1.94	1.93	2.14	2.11	1.93	2.12
Co-X	2.25	1.91	1.90	2.07	2.06	1.97	2.18
Co-Y	2.25	1.96	1.92	2.14	2.23	1.98	2.16
averaged (Co-N)	1.97	1.95	1.95	2.16	2.13	1.97	2.16
N3-N7	2.75	2.73	2.78	2.90	2.90	2.79	2.87
N_{py1}-N_{py2}	3.84	3.84	3.83	4.18	4.09	3.81	4.12
angles[°]							
N3-Co-N7	87.5	88.1	89.0	83.4	84.6	88.4	81.6
N3-Co-N_{py1}	83.8	84.3	85.9	78.8	78.7	83.9	78.1
N3-Co-Npy2	83.5	84.2	84.8	79.0	77.8	83.3	78.1
N3-Co-X	172.8	170.2	169.9	177.7	172.8	177.3	178.0
N3-Co-Y	98.1	97.5	101.1	94.0	111.7	95.5	97.9
Npy1-Co-N_{py2}	165.1	166.3	169.8	156.6	153.2	162.9	153.6
torsion[Å]							
C1-C2-CA-N_{py1}	84.2	84.2	84.6	86.8	85.4	91.8	96.9
C5-C4-CA2-N_{py2}	-85.1	-82.4	-83.3	-80.6	-87.5	-92.7	-96.9

N2Py2a): CH_3 group N7 substituted by H

N2Py2b):Methyl ester groups hydrolyzed.

For the comparison of the crystallographic data of the cobalt complexes with N2Py2, it emerges ;

① The observed metal-donor distances in the complex with the trivalent cobalt ion in $[Co(III)(N2Py2a)(H_2O)(EtO)]^{2+}$ are related to the different size of the coordinated metal ion. The rigidity of the bispidine backbone plays an important role in how deeply the metal ion can be in the cage. For the Co(III) complex, the N-Co-N angles are close to 90 and 180 degrees, indicating a small distortion from the ideal octahedral geometry around the metal ion. Interestingly, coordination of cobalt(III) leads to significant changes in the structure of the rigid ligand : while the distance between the two aliphatic amino nitrogens in the free N2Py2 ligand is 2.90Å, this value in $[Co(III)(N2Py2a)(H_2O)(EtO)]^{2+}$ decreases to 2.73Å. This may indicate that the forming of this complex is favored due to its high stability and the formation of the close to ideal octahedral geometry(strong bonding) ; and that these effects over compensate the loss of energy loss to the compression of the ligand cavity. In contrast, the separation of the two tertiary nitrogens in $[Co(II)(N2Py2)(H_2O)_2]^{2+}$ is 2.90Å, a value which coincides exactly with the unstrained value, measured for the free ligand. This can be interpreted by the fact that the coordination of the divalent cobalt does not require changes in geometry in the bispidine backbone, rather the geometry around the central cobalt (II) will be more distorted. Indeed, the N-Co-N angles are smaller than the corresponding values measured in $[Co(III)(N2Py2a)(H_2O)(EtO)]^{2+}$ The longer Co-N bonds are partially consequences of the position of cobalt (II) ion, which is out of the cavity.

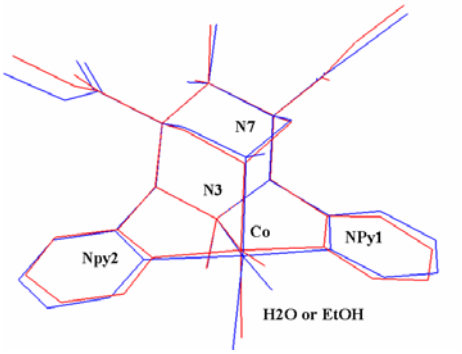

Fig. 4.3.3 Overlay crystal structures of $[Co(II)(N2Py2)(H_2O)_2]^{2+}$ (blue) and $[Co(III)(N2Py2a)(H_2O)(EtO)]^{2+}$ (red).

② The Co-N7 distance in $[Co(III)(N2Py2a)(Cl)_2]^+$ is 2.02Å, which is somewhat larger than the value of 1.98Å found in $[Co(III)(N2Py2a)(H_2O)(EtO)]^{2+}$ This longer bonds may be due to the different co-ligands. Coordination of chloride ions can lead to ligand-to-metal charge transfer, which then increases the electron density around the cobalt (III) center.

③ The effect of the charge at the co-ligand can also be illustrated with the example of $[Co(III)(N2Py2a)(H_2O)(EtO)]^{2+}$ and $[Co(III)(N2Py2b)(CO_3)]^+$ in Fig. 4.3.2 and Table 4.1.

The axially bound water in the mixed aqua/ethanol complex binds to cobalt with a bond distance of 1.96Å. The corresponding distance for the carbonato complex (considering the axially bound oxygen of the bidentate carbonate ion) is 1.92Å. This structural difference may be the result of the different charge, π-bonding and the rigid and strained for chelate ring of carbonate.

④ Comparing the Co-N bond lengths and N-Co-N value angle data of the dichloro and carbonato complexes $[Co(III)(N2Py2a)(Cl)_2]^+$ and $[Co(III)(N2Py2b)(CO_3)]^+$ we find that all corresponding value pairs are quite close to each other. This indicates that the denticity of the co-ligand probably has no significant effect the geometry of the ligand backbone.

⑤ Exchange of a monodentate neutral co-ligand for a charged bidentate donor (with the same donor atoms) leads to more pronounced distortions for Co(II)-complexes than for Co(III)-complexes, with respect to both the bispidine backbone and the geometry around the metal center. In $[Co(III)(N2Py2a)(H_2O)(EtO)]^{2+}$ the N3-Co-O(axial) angle is 97.5, and the analogous angle in $[Co(III)(N2Py2b)(CO_3)]^+$ (considering the axially bound carbonate oxygen) is 101.1; the change in angle is less than 3 degrees. However, when we compare these angles in the divalent Co-complexes, in $[Co(II)(N2Py2)(H_2O)_2]^{2+}$ and $[Co(II)(N2Py2)(OAc)]^+$ these values are 94.0 and 111.7 degrees, respectively. This means that the substitution of a neutral monodentate O-donor co-ligand to a bidentate one leads here to almost 18 degrees difference in the N3-Co-O angle. This difference is much larger than what is observed for the trivalent complexes (3 degrees): the geometry around Co(II) is more

dependent on the type of co-ligand, on their charge and density. This is due to the fact in general, the geometry around Co(III) is more rigid than around Co(II).

Also the separation of the two pyridine nitrogens is again, for the divalent complexes, more "sensitive" to the co-ligands. While N_{py}-N_{py} distances for $[Co(III)(N2Py2a)(H_2O)(EtO)]^{2+}$ and $[Co(III)(N2Py2b)(CO_3)]^{+}$ are 3.84 and 3.83Å, respectively; these values for $[Co(II)(N2Py2)(H_2O)_2]^{2+}$ and $[Co(II)(N2Py2)(OAc)]^{+}$ are 4.18 and 4.09Å. Not surprisingly the N_{py}-N_{py} distances are larger for the divalent than for the trivalent complexes, which is mainly due to the difference in the size of the metal ions.

As reported in chapter 3, empirical force field calculations were carried out with MOMEC, and s force field tuned to bispidine complexes[16]. Comparing the energies belonging to the average Co-N bond distances, the hole function calculation[17,18,19] shows approximately 10 $kJmol^{-1}$ difference in strain energy between cobalt (II) and cobalt (III). This difference is considered to be rather small. It indicates that although N2Py2 itself is quite a rigid as ligand, its coordination sphere is remarkably flexible.

Although the range of optimal metal-N-donor distances for N2Py2 is quite wide, it falls around 2.15-2.3Å, which means that complexes with such average M-N separations are the most favorable for N2Py2. Coordination with such metals leads to complexes in which the geometry of the ligand backbone is almost the same as in the unstrained free form. Co(II) complexes, showing $[M\text{-}N]_{av}$ of 2.13 and 2.16Å for $[Co(II)(N2Py2)(H_2O)_2]^{2+}$ and $[Co(II)(N2Py2)(OAc)]^{+}$, respectively, fall in this optimum range obtained from the hole size calculation. In parallel, the N3-N7 distance (which is characteristic for the bispidine backbone geometry) remains 2.90 Å, which value is exactly the same as was observed for the free ligand.[20]

The average metal-nitrogen distances for Co(III) complexes are 1.95-1.97Å, which fall somewhat out of the optimal range, as seen from N2Py2 hole size. As the calculation shows, yielding such a complex costs the ligand around 10 - 15 kJ/mol in energy. If there are

compensating effects arising from complexation, this energy loss is still bearable. Indeed, cobalt (III) complexes were successfully obtained, and as expected, there is a significant distortion of the bispidine cavity: N3-N7 distance (2.90Å) for the unstrained free ligand decreases to 2.73-2.78Å in the Co(III) complexes.

These examples show that the level of distortion in the bispidine backbone, as seen from the crystal data, confirm the hole size calculations. However, considering the compensating effect of complexation, the N2Py2 ligand can accommodate both Co(II) and Co(III) ions, although there is a significant difference in the ionic radii of the two ions.

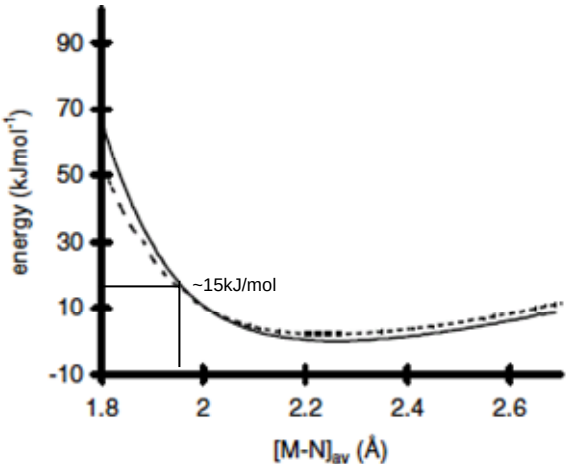

Fig. 4.3.4 Hole size calculation of N2Py2 with the metal ion by Momec97[21].

4.3.2 Crystal Structures of $[Co(III)(N2Py3u)(OH)](ClO_4)_2$ and $[Co(III)(N2Py3o)(H_2O)](ClO_4)_3$

Crystals suitable for structure determination were obtained by vapor diffusion of ether into the methanolic solution of the complexes. It was found that the structure of $[Co(III)(N2Py3u)(OH)](ClO_4)_2$ and $[Co(III)(N2Py3o)H_2O](ClO_4)_3$ are in good agreement with the computed structures. The measured distances are only slightly different (±0.01-0.03 Å) from the calculated values.

Comparing the structures of $[Co(III)(N2Py3u)(OH)]^{2+}$ and $[Co(III)(N2Py2a)(H_2O)(EtO)]^{2+}$ it can be seen that $[Co(III)(N2Py3u)OH]^{2+}$ has slightly longer Co-N7 distance (2.05Å) than $[Co(III)(N2Py2a)(H_2O)(EtO)]^{2+}$ (1.98Å), in parallel, $[Co(III)(N2Py3u)(OH)]^{2+}$ has a 0.02 Å shorter Co-N3 distance. This indicates that the cobalt metal center is pulled by the N3-bound picolyl unit away from the center of the cavity.

Furthermore, the bond distance between co-ligand oxygen and central Co(III) (Co-Y) is 1.88 Å for $[Co(III)(N2Py3u)(OH)]^{2+}$ and 1.96 Å for $[Co(III)(N2Py2a)(H_2O)(EtO)]$. The electrostatic attraction between the hydroxide oxygen and Co(III) causes extra stabilization and thus shorter bonds in comparison with the other complex with an equatorial ethanol at co-ligand, where this effect does not play role. In addition, the N3-N7 distance for $[Co(III)(N2Py3u)(OH)]^{2+}$ is 0.07 Å longer than for $[Co(III)(N2Py2a)(H_2O)(EtO)]$. This phenomenon is caused by increasing of the electron density of metal center due to the coordination of OH groups, which leads to increasing of metal ionic radius.

Comparing the structures of $[Co(III)(N2Py3u)(OH)]^{2+}$ and $[Co(III)(N2Py3o)H_2O]^{3+}$, it can be seen that and $[Co(III)(N2Py3o)H_2O]^{3+}$ has a longer Co-N3 distance (1.98Å) than $[Co(III)(N2Py3u)(OH)]^{2+}$ (1.93Å). It indicates that the cobalt metal center of $[Co(III)(N2Py3u)(OH)]^{2+}$ is affected by the N7-bound picolyl unit.

Moreover, distances of N3-N7 for all Co(II) and Co(III) bispidine complexes (N2Py2,

N2Py3o, N2Py3u) were found to have N3---N7 in the small range of 2.73Å to 2.90Å. This indicates the significant rigidity of bispidine backbone.

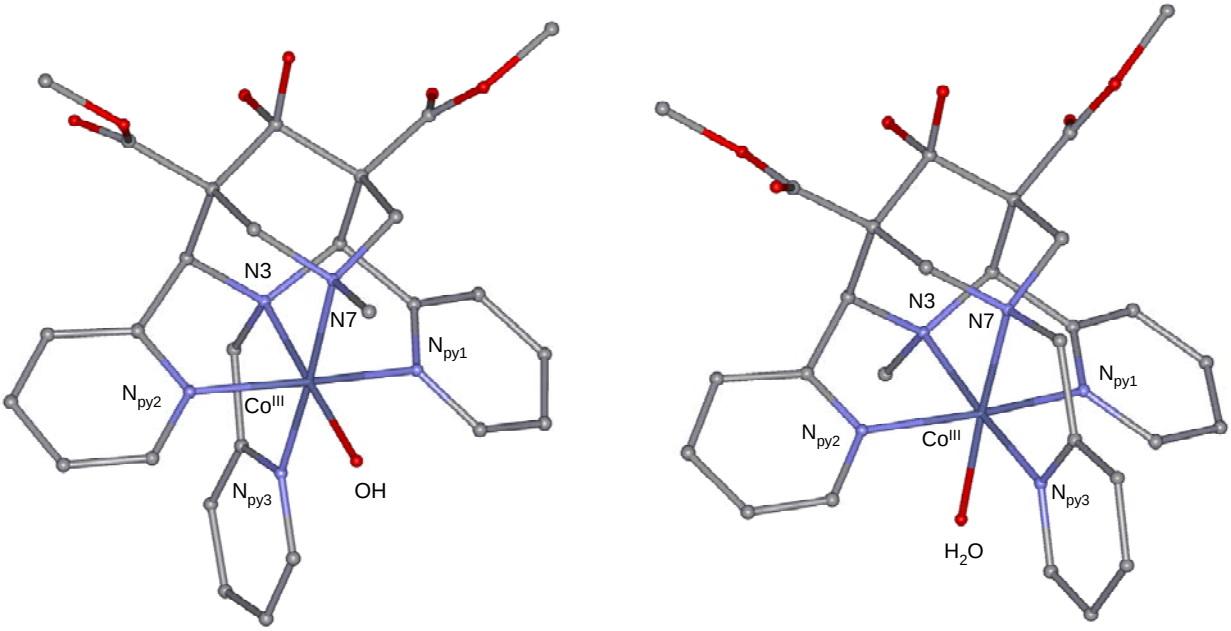

$[Co(III)(N2Py3u)(OH)]^{2+}$ $[Co(III)(N2Py3o)H_2O]^{3+}$

Fig. 4.3.5 Crystal structure of $[Co(III)(N2Py3u)(OH)](ClO_4)_2$ and $[Co(III)(N2Py3o)H_2O](ClO_4)$

Table 4.2 Structural data of Cobalt bisbidone complexes

	$[Co^{III}(N2Py3u)OH]$	$Co^{III}(N2Py3u)momec$	$[Co^{III}(N2Py3o)H_2O]$	$Co^{III}(N2Py3o)momec$	$[Co^{III}(N2Py2a)(H2O)(EtOH)]$	$Co^{II}(N2Py3u)momec$	$Co^{II}(N2Py3o)momec$
X=(plane)	–	–	H2O	NH3	EtOH	–	NH3
Y=(axial)	OH	NH3	–	–	H_2O	NH3	–
distances[Å]							
Co-N3	1.93	1.96	1.98	1.97	1.95	2.19	2.14
Co-N7	2.05	2.04	2.02	2.02	1.98	2.17	2.20
Co-N_{py1}	1.95	1.92	1.93	1.92	1.93	2.16	2.12
Co-N_{py2}	1.93	1.94	1.97	1.91	1.94	2.14	2.12
Co-N_{py3}	1.93	1.95	1.94	1.93	–	2.15	2.10
Co-X	–	–	1.96	1.97	1.91		2.10
Co-Y	1.88	1.95	–	–	1.96	2.16	–
averaged (Co-N)	1.95	1.96	1.98	1.95	1.95	2.16	2.14
N3-N7	2.80	2.81	2.80	2.78	2.73	3.03	2.95
N_{py1}-N_{py2}	3.85	3.81	3.87	3.80	3.84	4.16	4.13
angles[°]							
N3-Co-N7	89.6	89.3	88.8	88.2	88.1	88.0	85.4
N3-Co-N_{py1}	83.8	84.6	83.8	83.8	84.3	77.8	78.7
N3-Co-N_{py2}	84.8	82.3	84.0	84.4	84.2	78.1	78.4
N3-Co-N_{py3}	87.2	86.5	174.8	174.0	–	79.4	165.5
N7-Co-Npy1	95.3	91.9	91.7	97.1	91.8	96.5	96.9
N7-Co-Npy2	93.1	100.8	94.6	92.2	92.7	95.6	78.4
Npy1-Co-Npy2	165.8	161.6	166.1	164.8	166.3	152.5	154.2
Npy1-Co-Npy3	85.8	80.3	96.3	94.2	–	82.4	98.3
torsion[Å]							
C1-C2-CA-N_{py1}	82.6	91.2	83.4	91.5	84.2	84.7	90.3
C5-C4-CA2-N_{py2}	−83.8	−93.2	−86.1	−91.1	−82.4	−84.6	−92.2

4.4 Proposed Reaction Mechanism for Intermolecular Reactions

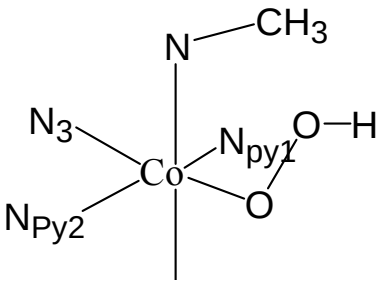

Fig. 4.4 Proposed reaction mechanism for removal of the methyl group

Interestingly, when the Co(III)N2Py2 complex was formed by oxidation with H_2O_2, the methyl group at N7 was removed (the demethylation was confirmed by ^{1}H-NMR, XRD, and Mass-spectra).

It has recently been reported that Co(II) and H_2O_2 can catalyze intermolecular reactions with 1,4-diazacyclononane Co(III) complexes. [22] There probably is first an interaction between Co(II) and H_2O_2. Binding of peroxide (subsequent to deprotonation) can be divided into two modes: **end-on** hydroperoxo (monodentate) or **side-on** peroxo (bidentate). In the peroxo form, the distance between the oxygen of the peroxo co-ligand and the methyl group of N7 is too large and the reaction seems unlikely to occur. For this reason, a monodentate binding of a hydroperoxide is thought rather to occur. The unbound oxygen of the co-ligand can then freely flip around and, in a given conformation, reach the methyl group at N7. After attack of the C-H bond, there may be cleavage of the bond between N7 and the methyl group.

Large groups attached to N7 can cause a serious steric hindrance for the hydroperoxide. This might be explain the failure to cleave N7 bound.

Interestingly, the removal of the methyl group at N7 was observed only in the case of the N2Py2 complex, but not for the corresponding complex of N2Py3u. This may be due to the differences in redox potentials: the significantly lower half-wave potential of Co(II)/(III)N2Py3u (300 mV) in comparison with Co(II)/(III)N2Py2 (653

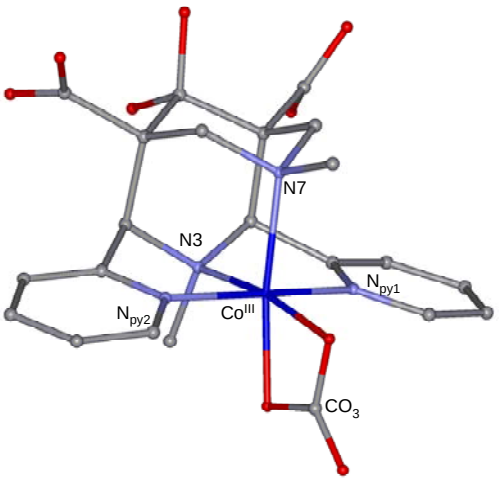

Fig. 4.4b $[Co(III)(N2Py2b)CO_3]^+$

mV) leads to the stabilization (less activation) of Co(III)N2Py3u complex.

During a ligand exchange reaction of $K_3[Co(OCO_2)_3]$ and N2Py2, hydrolysis of the methyl ester groups of the bispidine ligand occurred. This is probably due to the presence of CO_3^{2-}. Hydrolysis has not observed for the other bispidine reactions and may have occurred during the complexation.

4.5 UV Spectrum of Cobalt Bispidine Complexes

Coordination of Co(II) (d^6) to strong donor groups such as nitrogen donors leads to a high degree of splitting of the d-orbitals. Due to the large energy difference between the ground state and the excited state(s), Co(III) complexes usually are diamagnetic in the ground state.

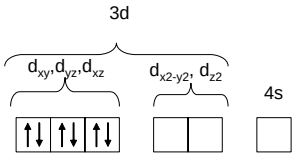

Fig. 4.5.1 Electron configuration of a low-spin complex with a d^6 metal ion.

The state of lowest energy for a low-spin Co(III) complex has t_{2g}^6 configuration (characterized by a $^1A_{1g}$ term). Electron transfer is possible to the following terms: $^1A_{1g} \rightarrow {}^1T_{2g}$, $^1A_{1g} \rightarrow {}^1T_{1g}$, $^1A_{1g} \rightarrow {}^3T_{2g}$ and $^1A_{1g} \rightarrow {}^3T_{1g}$.[23]

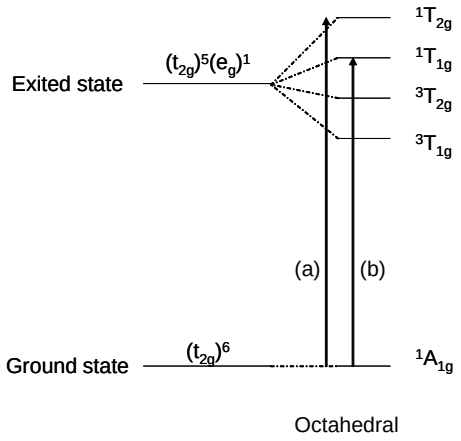

Fig. 4.5.2 Electron excitation of the ground state of a low-spin d^6 complex in octahedral field.

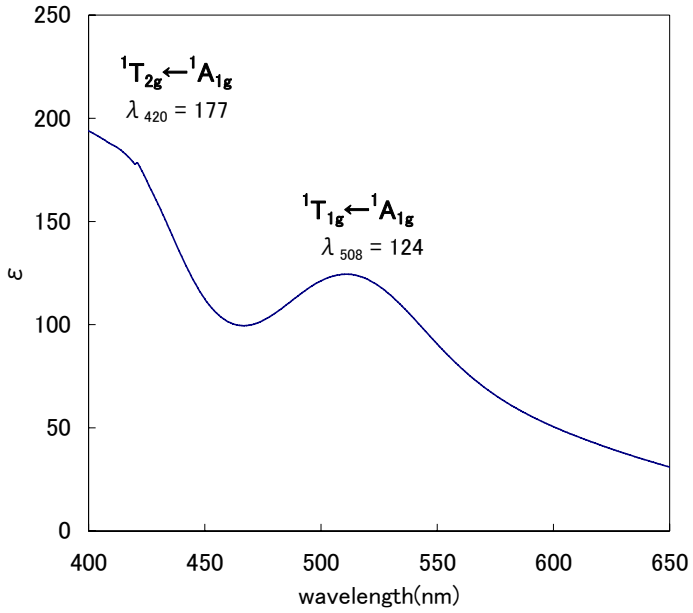

Fig. 4.5.3 UV-Vis spectrum of $[Co(III)(N2Py2)(H_2O)_2](ClO_4)_3$ in MeOH at 25°C.

The UV-Vis spectrum of $[Co(III)(N2Py2)(H_2O)_2](ClO_4)_3$ was measured in MeOH at 25°C. Two bands are observed, at 420 nm and 508 nm. The peak at 420 nm is assigned to a $^1A_{1g}\rightarrow{}^1T_{1g}$ d-d transition and the peak at 508nm to a $^1A_{1g}\rightarrow{}^1T_{2g}$ d-d transition. Other theoretically possible excitations ($^1A_{1g}\rightarrow{}^3T_{1g,}$ $^1A_{1g}\rightarrow{}^3T_{2g}$) are not observed.

Table 4.3 UV-Vis spectra of Co(II) and Co(III) bispidine aqua complexes in MeOH at 25°C, Co(III)N2Py3o was measured in acetonitrile.

	N2Py2	N2Py3o	N2Py3u	N2Py4
Co(II)	ε 425=13.8 ε 486=19.0 ε 533=16.6	ε 383=37.3 ε 446=23.5 ε 483=34.6 ε 542=17.9		ε 457=43.1 ε 492=56.2 ε 551=21.3
Co(III)	ε 508=124 ε 420=177	ε 498=115.9	ε 490=215.0	ε 447=273.0

4.6 Oxidation of Co(II) Bispidine Complexes

4.6.1. Oxidation from Co(II)N2Py2 to Co(III)N2Py2

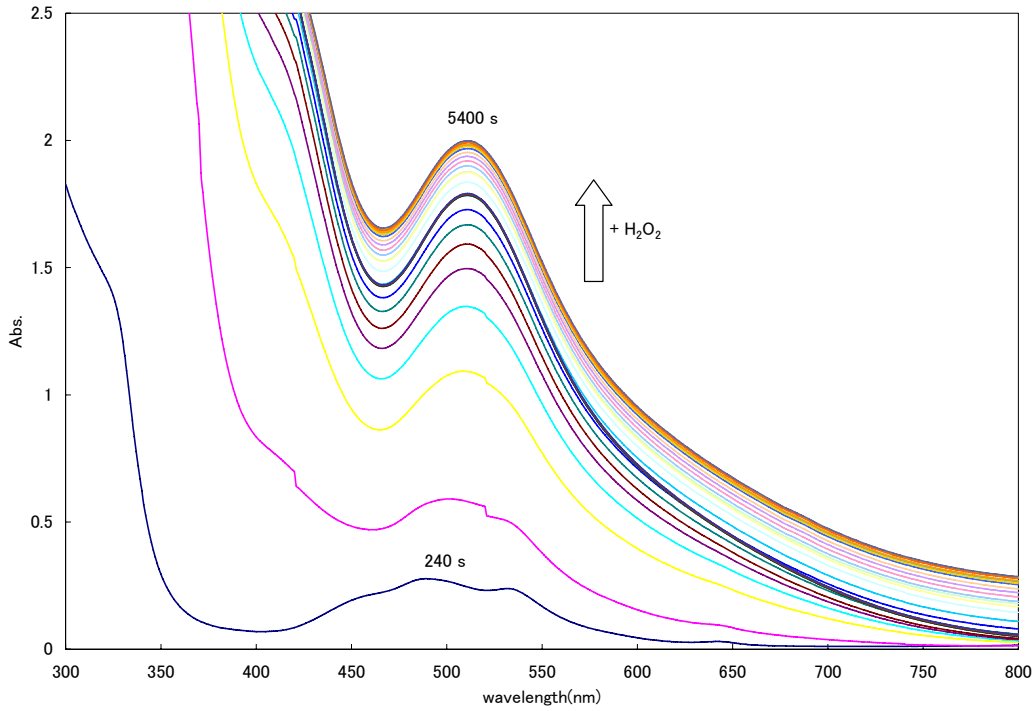

Fig.4.6.1 Time-dependent UV-Vis spectra following the oxidation of Co(II) to Co(III)N2Py2

The oxidation of the Co(II)N2Py2 complex to Co(III) was measured by UV-Vis spectrophotometer.

For the experiment 11 mM of $[Co(II)(N2Py2)(H_2O)_2](ClO_4)_2$ and 170 eq. of 30% hydrogen peroxide were used. The measurements were carried out in methanol at 25°C. A spectrum was recorded every 4 minutes. According to the UV-Vis spectra the expected conversion occurred successfully, three weak bands of Co(II)N2Py2 complex (ε_{452}=13.8, ε_{486}=19.0, ε_{533}=16.6) changed to two more intense bands (ε_{420} = 177, ε_{508}=124.2) which show undoubtedly the formation of the Co(III)N2Py2 product. The oxidation reaction was almost complete in 3000 seconds.

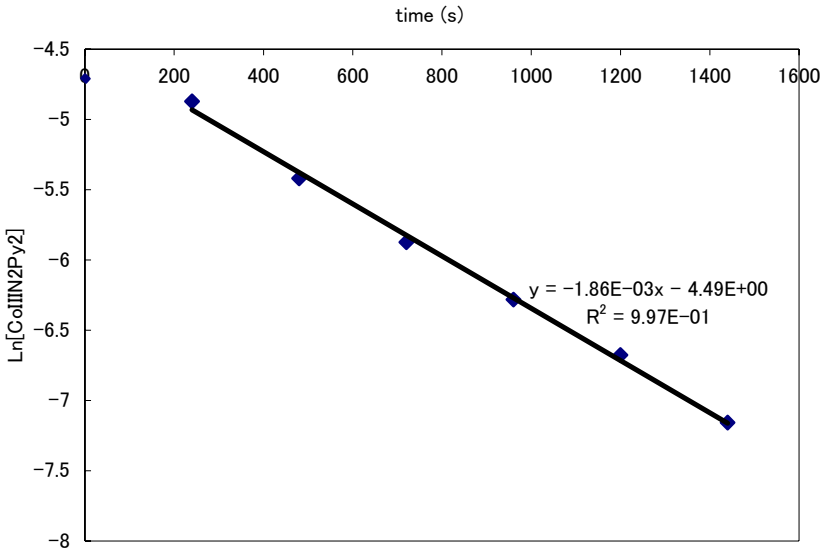

Fig.4.6.2 Half logarithmic plot (ln[Co(II)N2Py2] vs. time) for the determination of the rate constants for the oxidation of the Co(II)N2Py2 complex

The half logarithmic plot (the logarithm of the concentration of Co(II)N2Py2 complex against the reaction time) is shown in Fig.4.3.2. The decreasing concentrations of Co(II)N2Py2 was determined by the intensity of the peak at 510 nm. For a first order reaction, the relationship between the concentration of the reactant and the rate constant can be shown as **(4.1).**

$$-\frac{d[C]}{dt} = k[C] \qquad \textbf{(4.1)}$$

$$\int_{C_0}^{C_t} \frac{dC}{C} = -k\int_0^t dt \Leftrightarrow C_t = C_0 e^{-kt} \qquad \textbf{(4.2)}$$

$$\ln[C_t] = -kt + \ln[C_0] \qquad \textbf{(4.3)}$$

$$t_{1/2} = \frac{\ln 2}{k} \qquad \textbf{(4.4)}$$

It was observed that the reaction is first order, due to the linearity of the half logarithmic plot (Fig.4.6.2).The first point measured was that after 240s. The correlation coefficient of the fitted line (R^2) is 0.997, the determined first-order rate constant k_{obs} is $1.86*10^{-3}$ s^{-1} according to the slope of the line **(4.3)** and the half life $t_{1/2}$ is estimated as 372.66 s. The half-lives for all first order reactions are independent of the initial concentration as shown in **(4.4)**. Non-linearity was observed for the interval 0-240 seconds, which is a significant difference to the reaction which takes place after 240 s. This might indicate that the reaction follows a different mechanism for this time period.

4.6.3 Oxidation of Co(II)N2Py3o to Co(III)N2Py3o

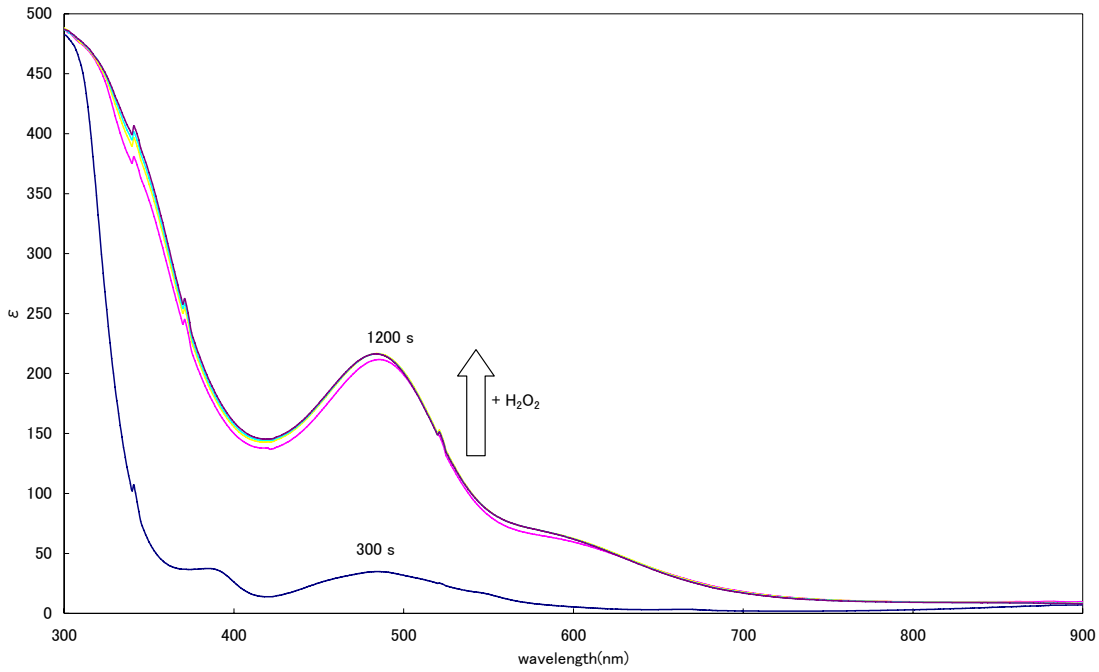

Fig. 4.6.3a UV-Vis spectra of the oxidation of [Co(II)N2Py3o] to the Co(III) complex

The oxidation of the Co(II) to the Co(III)N2Py3o complex was measured by UV-Vis spectroscopy. For the experiment, 10 mM of $[Co(II)(N2Py3o)(H_2O)_2]$ $(ClO_4)_2$ and 170 eq. of 30% hydrogen peroxide were used. Four weak bands of Co(II)N2Py3o complex (ε_{383}=37.3,ε_{446}=23.5, ε_{483}=34.6, ε_{542}=17.9) changed to a single, much more intense band, which is clear evidence for the formation of Co(III)N2Py3o complex (ε_{481}=215.9). There are remarkable differences in the oxidation of the Co(II) N2Py3o compared to the Co(II)N2Py2, both in the solubility of complex in methanol and the rate of reaction. Acetonitrile was used as solvent for the experiment with Co(II)N2Py3o, because of the low solubility of the complexes in methanol. The conversion from Co(II) to Co(III) was almost complete within 5 minutes, which indicates a much faster reaction than in the case of Co(II)N2Py2 where around 120 minutes were needed for the completion.

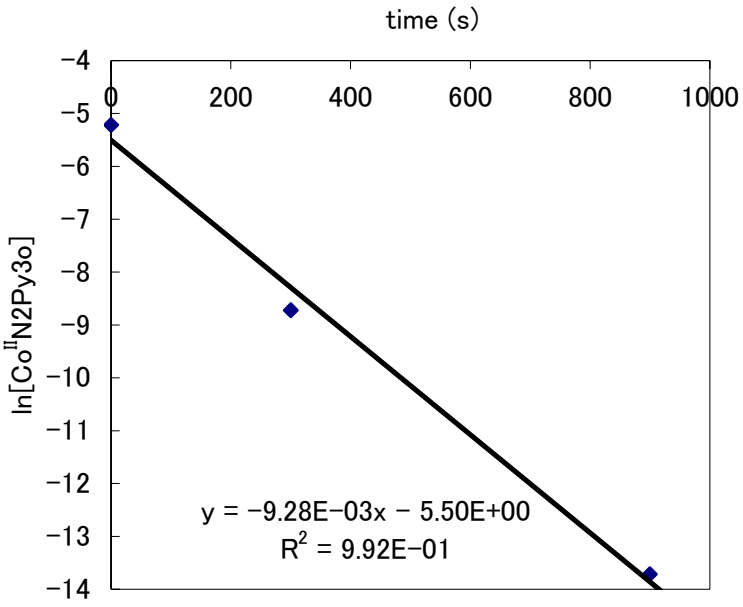

Fig. 4.6.3b Half logarithmic plot (ln[Co(II)N2Py3o] vs. time) for the determination of rate constants for the oxidation of Co(II)N2Py3o complex

A plot of logarithm of the decreasing concentration of the Co(II)N2Py3o complex vs. time (s) is shown in Fig. 4.6.4. This shows a linear relationship with a good correlation coefficient (R^2=0.992).The rate constant was estimated as $9.28*10^{-3}s^{-1}$ from the slope of the line fitted to the points of the half logarithmic plot **(4.3)**.

In comparison with rate constant of the Co(II)/(III)N2Py2 complex, the rate constant of Co(II)/(IIII)N2Py3o is ~10 times larger (k_{obs}= $1.02*10^{-3}$ s^{-1}). The half life of the reaction is estimated as 74.69 s by equation **(4.4)**. The same concentrations of complex and H_2O_2 were applied in both reactions. It is possible that the difference in solvents leads to such a huge increment in reaction rates.

4.6.4 Oxidation of Co(II)N2Py4 to Co(III)N2Py4

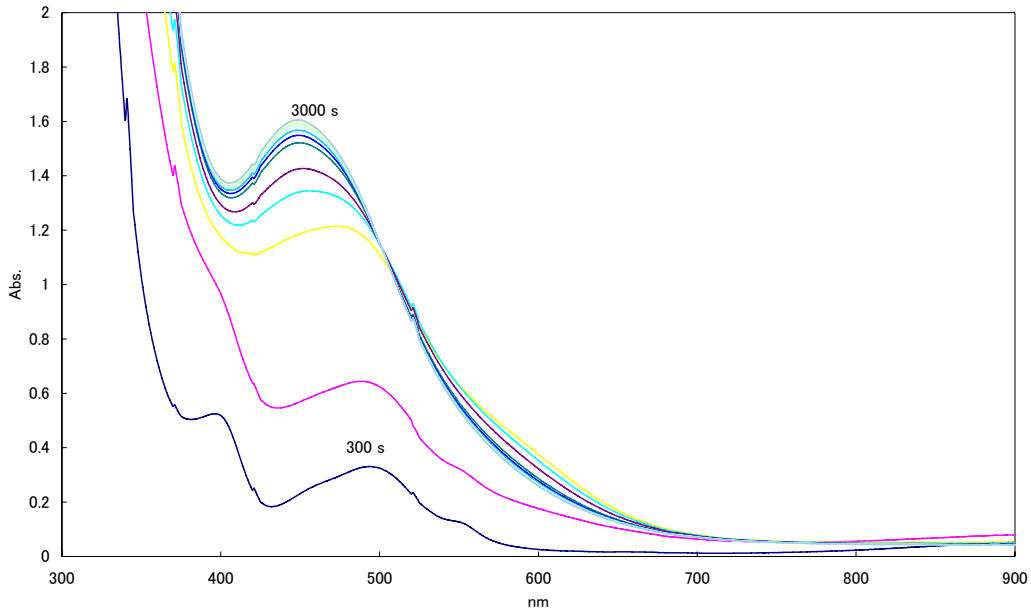

Fig. 4.6.4a UV-Vis spectra for the oxidation of the Co(II) to the Co(III) N2Py4 complex

The conversion of the Co(II)N2Py4 complex to Co(III)was also measured by UV-Vis spectroscopy. For the experiment, 10 mM of $[Co(II)(N2Py3o)(H_2O)](ClO_4)_2$ and 170 eq. of 30% hydrogen peroxide were used. Four less intense bands of $Co^{II}N2Py2$ complex (ε_{395}=89.0, ε_{457}=43.1, ε_{492}=56.2, ε_{551}=21.3) changed to a stronger absorbing single band which is clear evidence for the formation of the Co(III)N2Py3o complex (ε_{447}=273.0). The measurement was carried out in methanol at 25°C.

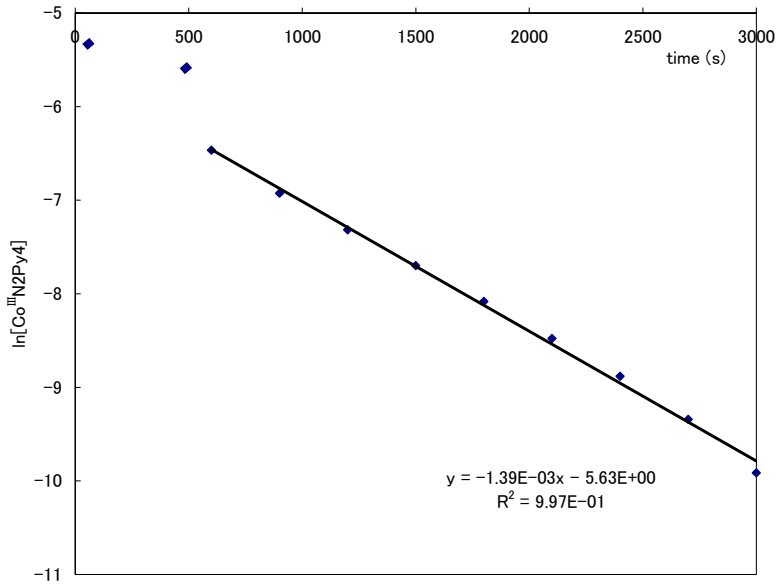

Fig. 4.6.4b Half logarithmic plot (ln[Co(II)N2Py4] vs. time) for the determination of the rate constant for the oxidation of the Co(II)N2Py4 complex

A plot of the logarithm of the concentration of Co(II)N2Py4 complex as a function of reaction time is shown in Fig. 4.3.6. It shows a linear relationship with a good correlation coefficient (R^2=0.997). The first-order rate constant was estimated to be $1.39*10^{-3}$ s^{-1} from the slope of the line fitted to the points of the half-logarithmic plot (4.3).

The rate constant of Co(II)/(IIII)N2Py4 is comparable to the rate constant of Co(II)/(IIII)N2Py2, which is k_{obs}= $1.86*10^{-3}$ s^{-1}. The half life of the reaction is estimated as 372.66 s .

4.7 ^{1}H-NMR spectrum of the Co(III)(N2Py2a) complexes

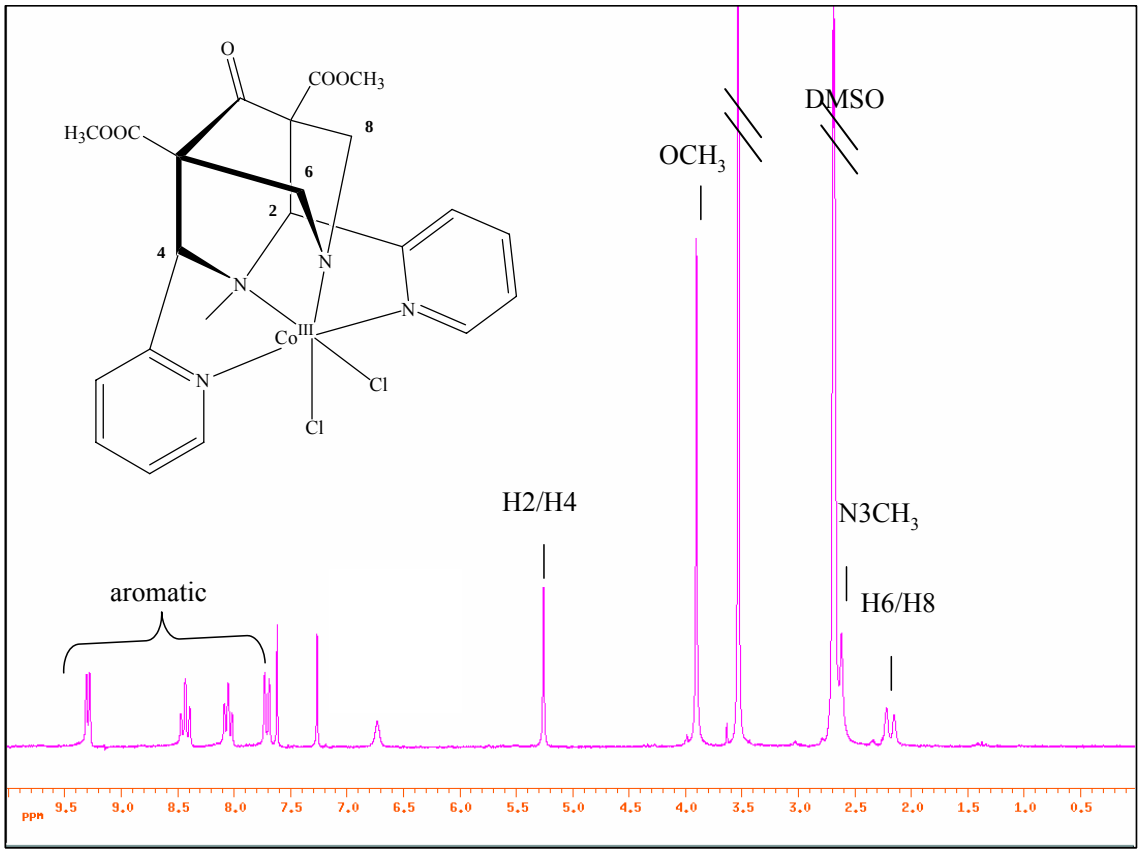

Fig. 4.7 ^{1}H-NMR spectrum of $[Co(III)(N2Py2a)Cl_2]ClO_4$ (200MHz, in d_6-DMSO)

The ^{1}H-NMR-spectrum of $[Co(III)(N2Py2a)Cl_2]ClO_4$ was measured in d_6-DMSO at 300 K. Sharp single peaks were observed at 3.9 ppm and 5.3 ppm, which were assigned to methoxy protons and H2/H4 CH protons respectively. These peaks indicate a high level of symmetry in the entire Co(III)complex: the protons on either side of the metal centre are chemically undistinguishable from each other. As the demethylation of -N7CH_3 has been identified by crystal structure, ESI-mass spectrum and elemental analysis; it is not surprising that the peak of the methyl group of N7CH_3 was not observable.

4.8 Electrochemistry of Cobalt Bispidine Complexes

Table 4.8.1 Redoxpotentials of cobalt bispidine complexes vs $Ag/AgNO_3$

	N2Py2	N2Py3o	N2Py3u	N2Py4
Cl	−18	92	136	−
ClO_4	653	519	300	170 (*)
$\Delta(Cl-ClO_4)$	671	427	164	−

(*) only Ox. Potential

The redox potentials of the cobalt complexes of N2Py2, N2Py3o, N2Py3u, N2Py4 were measured by cyclic voltammetry using BAS-100B electrochemical analyzer with a scan rate of 100mV/s. The measurements were carried out in acetonitrile containing 0.1 M tetra-n-butyl ammonium hexafluorophosphate as supporting electrolyte at 25℃, $Ag/AgNO_3$ electrode was used as reference electrode.

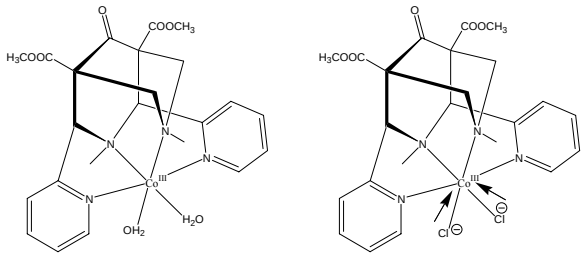

Fig. 4.8.2 Charge transfer to cobalt metal center.

The differences in redox potentials between aqua complexes (perchlorate anion) and chloro complexes are compared in Table 4.8.1. The chloro complexes show lower redox potential than the aqua complexes in the case of all ligands. A lower redox potential in the same complex indicates higher stability of the oxidized form.

The charge transfer from chloride to cobalt causes an increasing of charge density at the metal center, which results in ionic attraction and thus in higher complex stabilities. The effect of charge transfer is more significant for higher charged central metal ions, which

are then more stabilized in comparison with the reduced form.

It was shown that for N2Py2 the difference in the redox potential between the chloro and aqua complex is significantly larger (671mV) than for N2Py3o (427mV) and N2Py3u (164mV). As the crystal structure of Fig. 4.1.2 reveals, two chlorides coordinate to the Co(III) center with N2Py2 while for N2Py3o, N2Py3u only one chloride ligates to the central cobalt ion. Coordination of two chlorides has more influence on the redox potential than one, an effect which is simply additive.

According to the crystal structure of Co(III) with N2Py2, the average bond lengths in the aqua and chloro complexes with N2Py2 are 1.97Å, and 1.95Å, respectively. The reason for this relatively small difference can also be explained by the charge transfer from chloride to cobalt center. Furthermore, it was also observed that there is a large difference between N2Py3o(427mV) and N2Py3u(164mV), both of which are pentadentate ligands.

This may be explained by the diffidence in bond distances from cobalt to the co-ligand. The computed structure shows Co(III)N2Py3o (NH_3-Co : 1.95) has slightly shorter distances between co-ligand and Co than Co(III)N2Py3u (NH_3-Co : 1.97). That is , the CoN2Py3o complex is more significantly affected by the coordination to a chloride anion.

Fig.4.8.3 shows CV's of $[Co(III)(N2Py2)(H_2O)_2](ClO_4)_3$ and $[Co(III)(N2Py2)Cl_2]Cl$. The aqua complex (perchlorate complex) shows an ideal, symmetric redox couple, which is quasi-reversible. On the other hand, for the chloro complex, the curve is asymmetric and shows smaller currents for the reduction process of Co(III) to Co(II) complex. It is considered as a partially quasi-reversible process.

Fig. 4.8.4 shows CV curves of $[Co(III)(N2Py3o)(H_2O)](ClO_4)_3$ and $[Co(III)(N2Py3o)Cl]Cl_2$. The curves of both the aqua complex (perchlorate) and the chloro complex show an ideal symmetric pattern, having both the oxidation and reduction peaks around the same absolute intensity. There is a considerable difference in the distance of the reduction-potential and the oxidation-potential of the two complexes. This difference for the aqua complex and the chloro complex was 498 mV and 137 mV respectively. It is considered that the aqua complex is quasi-reversible and the chloro complex is reversible

Fig. 4.8.5 shows CV of $[Co(III)(N2Py3u)(H_2O)](ClO_4)_3$ and $[Co^{III}(N2Py3u)Cl]Cl_2$. The curve of both complexes show ideal patterns during the oxidation of Co(II) to Co(III). On the other hand, the reduction of Co(III) to Co(II) half wave was not complete, being far from reversible. Aqua complexes with N2Py3u also reveals higher redox potentials compared with chloro complexes as it was observed for the case of the complexes of other ligands.

Fig. 4.8.6 shows CV of $[Co(III)(N2Py4)(ClO_4)_3$. For N2Py4 there is no peak for the reduction of Co(III) to Co(II). This process is considered as irreversible. it might be due to the build-up of strain energy. This is proposed by force field calculations, as mentioned in Chapter 3, which indicate that short metal-donor distances such as Co(III)-N lead to a build-up of strain (loss of up to 60 kJ/mol with respect to the relatively unstrained geometry induced by Zn(II)) in N2Py4. The strain causes the destabilization of the Co(III)N2Py4 complex.

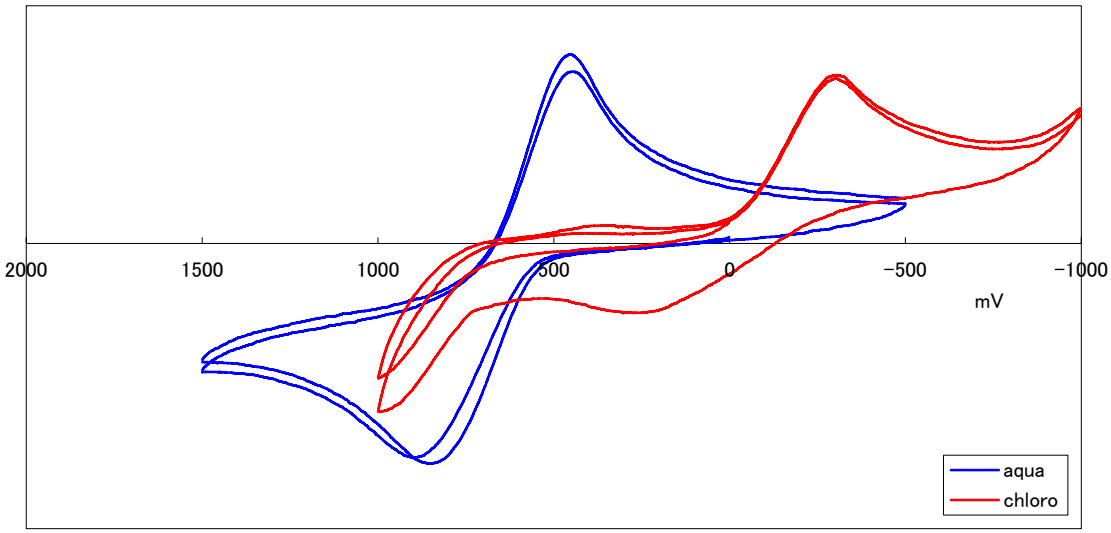

Fig. 4.8.3 Cyclovoltammetric curves of $[Co(III)(N2Py2)(H_2O)_2](ClO_4)_3$ and $[Co(III)(N2Py2)\ Cl_2]Cl$

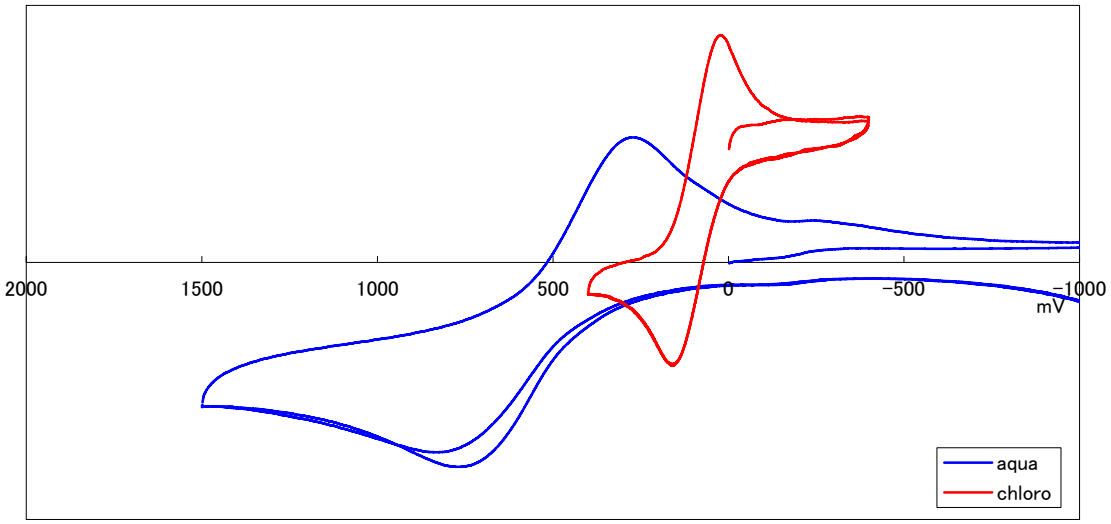

Fig. 4.8.4 Cyclic voltammetry of $[Co(III)(N2Py3o)(H_2O)](ClO_4)_3$ and $[Co(III)(N2Py3o)Cl_2]Cl$

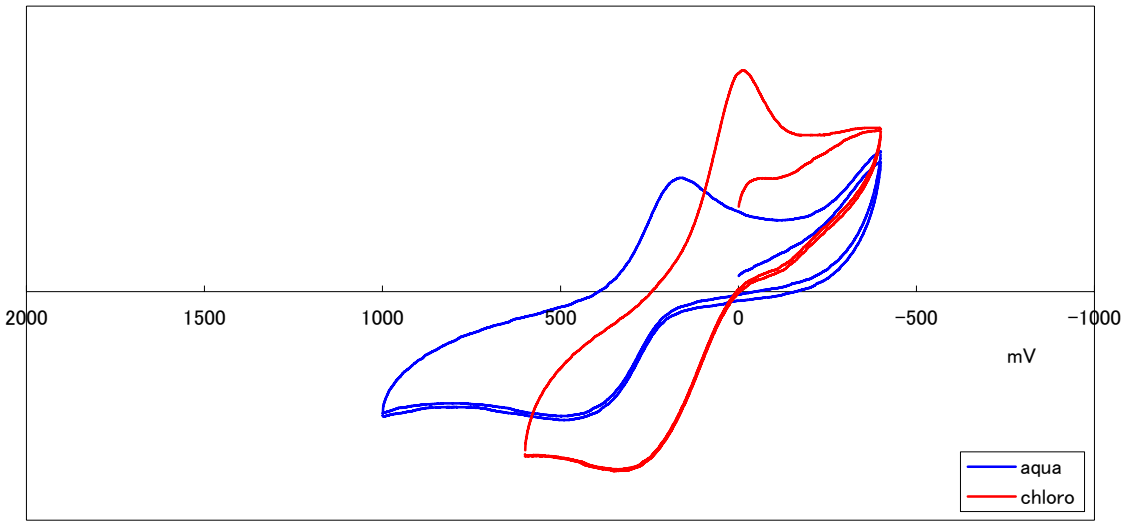

Fig. 4.8.5 Cyclic voltammetry of $[Co(III)(N2Py3u)(H_2O)](ClO_4)_3$ and $[Co(III)(N2Py3u)Cl_2]Cl$

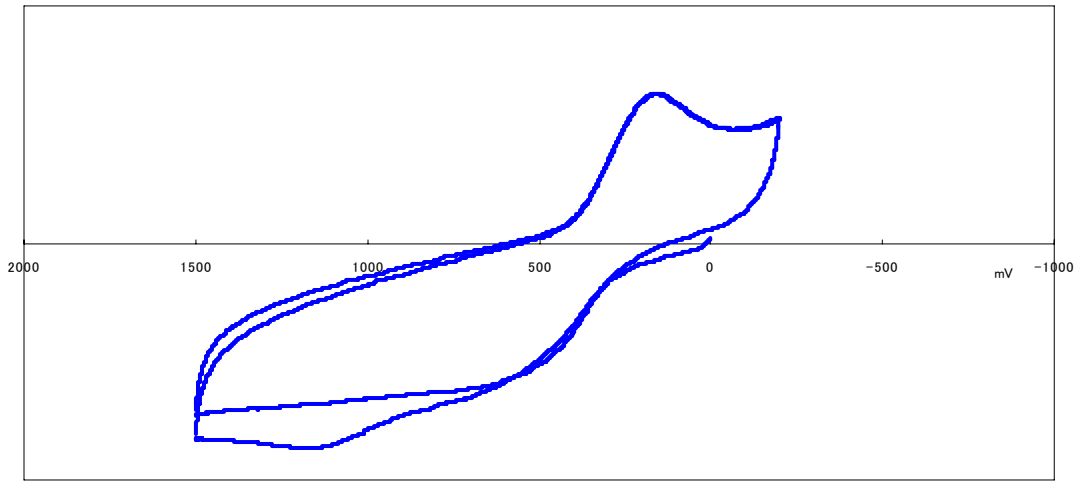

Fig. 4.8.6 Cyclic Voltammetry of $[Co(III)(N2Py4)](ClO_4)_3$

References

[1] W. Kaim, B.Schwederki. *Bioinorganic Chemistr*y, Inorganic Elements in the Chemistry of Life . Wiley Ed. N.Y.

[2] S. Jörgensen, *Z. Anorg. Chem.,***1898**, *17*, 455

[3] A.Werner, *Ber.* ,**1906**, *39*, 2673.

[4] I. Bertini, H. Gray, S. Lippard, J. Valentine, *Bioinorganic Chemistry* (University Science Books; Mill Valley, CA, 1994)

[5] C. E. Schäffer, P. Steenberg, *J. Chem. Educ.* **2002** *,9* ,958.

[6] M. Kerscher, *Ph.D. dissertation Uni-HD***, 2003**.

[7] M. Merz, *Ph.D. dissertation Uni-HD*, **2002**.

[8] H. Boerzel, P. Comba, K. S.Hagen, C. Katsichtis, H. Pritzcow, *Chem.Eur.J*., **2000**, 6, 914.

[9] R. Haller, *Arch. Pharm*. **1968**, 301,741.

[10] P. Comba, B. Kanellakopulos, C. Katsichts, A. Lienke, H. Pritzkow, F. Rominger, *J. Chem. Soc.Dalton*.**1998**, 3997.

[11] U. Holzgrabe,E. Ericyas, *Arch.Pharm*.(Weinheim,Germany)**1992**,325,657

[12] M. Shibata,. *In topics in Current Chemistry*; Springer-Verlag:Berlin, **1983**, *110*, 1.

[13] H. Nishikawa, K. Konya, M. Shibata, *Bull. Chem.Soc.Jpn.,* **1973**,*46*, 3453.

[14] K. Khalil, N. Logan, A. Harris,*J. C. S. Dalton.,***1980**,314.

[15] D. A. Buckingham, C. R, Clark, *In Middle Transition Elements*, Pergamon: New York, **1987**, *4*, 635

[16] P. Comba, W. Schiek, *Coord. Chem. Rev. ,***2003***, 238,* 21.

[17] C. Bleiholder, H. Börzel, P. Comba, M. Heydt, M. Kerscher, S. Kuwata, G. Laurenczy, G. A. Lawrance, A. Lienkea, B. Martina, M. Merz, B. Nuber H. Pritzkow, *accepted to Inorganic Chemistry*,**2005**.

[18] P. Comba, M. Kerscher, M. Merz,V. Müller, H. Pritzkow,R. Remenyi, W. Schiek, Y. W. Xiong, *Chem. Eur. J.,* **2002**, *8*, 5750.

[19] P. Comba, N. Okon, , R. Remenyi. *J. Comput. Chem.,* **1999**, *20*, 781.

[20] H.Börzel, *Ph.D. dissertation Uni-HD*, **2000**.

[21] P. Comba, T. Hambley, G. Lauer, M. Melter, N. Okon,. *MOMEC97, a molecular modeling package for inorganic compounds*: University of Heidelberg, **1997**.

[22] X. Zhou, A. I. Day, A. J. Edwards, A. C. Willis, W. G. Jackson, *Inorg. Chem.*, **2005,** *44***,** 452.

[23] O. Yamauchi, H. Ogino,Y. Hisashi, *Daigakuin Sakutaikagaku*, **2000**.

5. Vanadium Complexes of 3,7-Diazabicyclo[3.3.1]nonane Derivatives

5.1 Introduction

Vanadium has been recognized to play an important role in biological systems. Currently, there is considerable interest in investigating mononuclear vanadium complexes because of haloperoxidase enzymes, which catalyze the peroxide-dependent halogenation of organic substrates, have been shown to contain vanadium in their active sites.[1,2,3,4]

Furthermore, peroxo vanadium (V) complexes have been found to act as catalysts in the oxidation of organic substrates (e.g., epoxidation of alkenes, hydroxylation of alkanes and aromatic compounds).[5,6] It has been discovered that some of mononuclear oxo vanadium (IV) and peroxo vanadium (V) complexes have insulin-mimetic properties.[7,8,9,10]

Therefore, developing further vanadium complexes is a flourishing field in bioinorganic chemistry.

The structural features, thermodynamic stability and kinetic lability are all important factors playing a crucial role in the mechanisms of the catalytic cycles of the enzymatic reactions. Rigid bispidine ligands (N2Py2, N2Py3o, N2Py3u and N2Py4) which contain only nitrogen donor atoms were tested for complexation with vanadium ions. Metal sources of different oxidation states and different anions were applied. According to the HSAB concept, vanadium ions (V^{3+},VO^{2+},VO_2^{+}) are all relatively hard, i.e., weakly polarizable, and interaction with nitrogen donors are expected to be not especially favored. But a manifold of effects influencing complexation (preorganization, hole size) can tune the reaction in the direction of completion.

Vanadium (IV) as a hard ion has a high affinity to amine nitrogens of the bispidine backbone. An oxidation from paramagnetic V(IV) (d^1) yields diamagnetic V(V) (d^0) complex. There is no d-d transition band observable in UV–Vis spectra of V(V) oxo complexes, the most

remarkable features can be some charge transfer band from possible interaction between coordinated anions and the central V(V) ion. A change of the valency of vanadium can alter metal-donor atom distances as well as the strain energy of the ligands.

The influences of oxidation of a V(IV) bispidine complex on structural, spectroscopic and electrochemical properties is reported and discussed.

5.2 Synthesis of Vanadium Bispidine Complexes

5.2.1 Synthesis of $[V(IV)O(N2Py3o)]^{2+}$

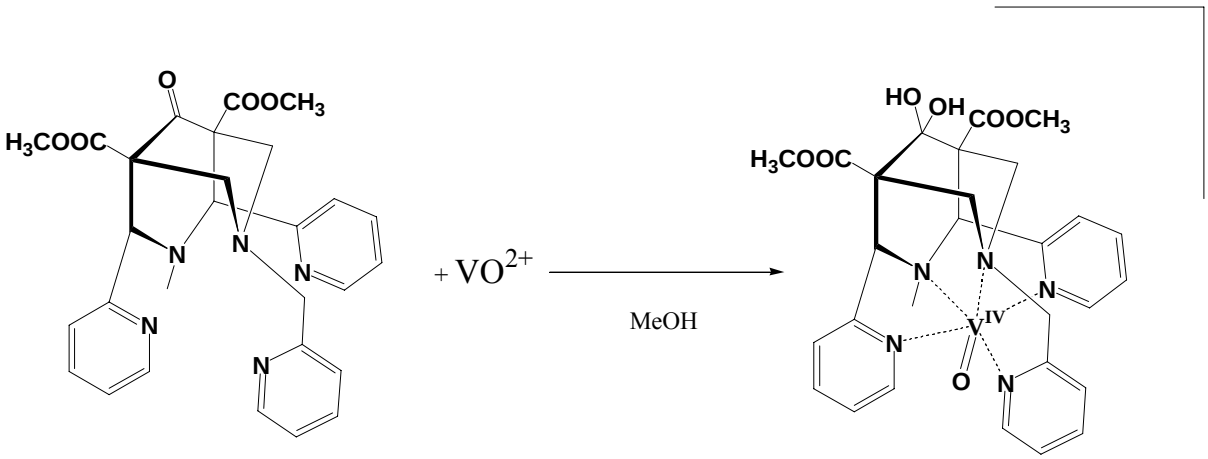

Fig. 5.2.1 Synthetic route of $[V(IV)=O(N2Py3o)]^{2+}$

The synthesis of a vanadyl complex with the pentadentate ligand N2Py3o was carried out by the following method: 1 eq. of vanadyl sulfate hydrate was stirred in the presence of 1 eq. N2py3o ligand in refluxing methanol for 2 hours. The resulting solution was diluted with water and the complex separated on a Sephadex CM-C25 column using 0.1M aqueous $NaClO_4$ as eluent.

Attempts were made to synthesize vanadyl complexes of the ligands N2Py2, N2Py3u and N2Py4. However no complexation took place, even after trying several different reaction conditions. This indicates that the pentadentate ligand N2Py3o has a high affinity towards vanadyl ions in comparison to the other ligands.

The vanadyl(IV) ion possesses only a single electron on the outer d-shell, which gives it a relatively low electron density in this shell. In comparison to Cu(II) or Zn(II), which have d^9 or d^{10} configuration, the ionic radius is comparable. The effect of valence shell electrons is less pronounced. The single d electron of vanadium can interact weakly with the lone pairs of the ligand in a "covalent" way. The nitrogens of the bispidine backbone, due to their lower electronegativity, represent a soft to border line donor, which prefer covalent interactions with the empty d-orbitals of the central metal ion. In our case vanadium is a rather hard acceptor

(due to the d^1 configuration), prefers bind to ligands with donors of ionic nature. Thus, coordination of the π -donor of the pyridine of the bispidines to vanadium is expected not to be of importance, on the other hand on pyridine donors not very difficult in π-bonding.

The distance between the metal and the ω-ligand is strongly dependent on the ligand configuration. For example copper (II) complexes of N2Py3o and N2py3u show remarkably different M-Cl distances, revealing the importance of the ligand field effect on this bond.

Such an effect may play an important role in the success or failure of the synthesis of the corresponding vanadyl complexes. A fit or misfit between the rigid bispidine backbone and the ‘‘quasi rigid’’ vanadyl ion is a different problem. Also, under the influence of the ligand field the double bond between oxygen and vanadium can elongate or compress. However, this double bond seems to be insusceptible to the ligand effect, as an analysis of the large number of crystal structures obtained so far shows.

5.2.2 Synthesis of $[V(V)=O(O_2)(N2Py3o)]ClO_4$

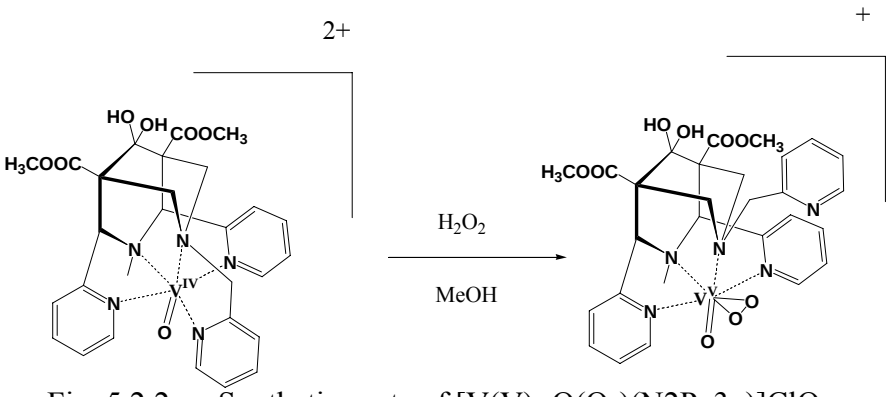

Fig. 5.2.2 Synthetic route of $[V(V)=O(O_2)(N2Py3o)]ClO_4$

$[V(V)=O(O_2)(N2Py3o)]ClO_4$ was obtained by the oxidation of the $[V(IV)O(N2Py3o)](ClO_4)_2$ complex using the following method: $[V(IV)O(N2Py3o)](ClO_4)_2$ was stirred in the presence of 10eq. H_2O_2 in methanol. The resulting solution was diluted with water and separated on a Sephadex CM-C25 column using aqueous 0.1M $NaClO_4$ as eluent. The solvent was removed in vacuo, 0.11g (0.14mmol, 47% yield) of product was obtained by precipitation.

5.3 Crystal Structures of Vanadium Bispidine Complexes

5.3.1 Crystal structures of $[V(IV)O(N2Py3o)]Cl_2$, $[V(V)O(N2Py3o)](ClO_4)_2$ and $[V(V)=O(O_2)(N2Py3o)]ClO_4$

Single crystals suitable for X-ray analysis of and $[V(IV)O(N2Py3o)](ClO_4)_2$ were obtained from crystallization in aqueous solution after about 1 week. The resulting purple crystals were stable in air for several days.

The crystal structure and selected bond lengths and bond angles of $[V(IV)O(N2Py3o)]Cl_2$, $[V(IV)O(N2Py3o)](ClO_4)_2$ are shown in Fig. 5.3.1a , Fig. 5.3.1b and Table 5.1,respectively.

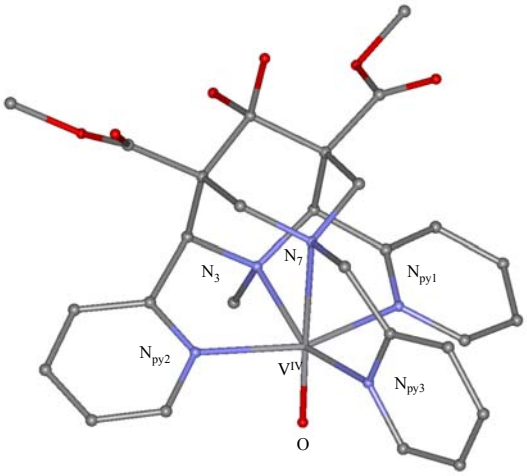

Fig. 5.3.1a Crystal structure of $[V(IV)O(N2Py3o)](ClO_4)_2$

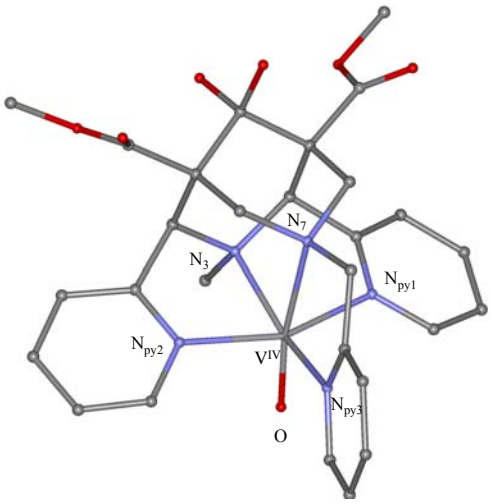

Fig. 5.3.1b Crystal structure of $[V(IV)O(N2Py3o)]Cl_2$

The vanadyl ion coordinates octahedraly to N2Py3o. In the ClO_4^- salt complex, the axis of the V-N_{py1}, V-N_{py2} and V-N_3 bonds are located almost on the same plane (the central vanadium almost falls on the plane determined by N_{py1}, N_{py2} and N_3) but the two pyridyl rings are not in the plane. The length of the V=O bond is consistent with values measured for other vanadyl group [1.59Å].[11] On the other hand, the length of the V-N_7 bond, which is perpendicular to this plane, is 2.36Å. This bond is rather long for V-N_{amine}.[12] The average for a V(IV)-N bond lengths is 2.15Å. The hydrolysis of the ketone groups are observed which is often observable for bispidine complexes.

Table 5.1 Crystal structure data of $[V(IV)O(N2Py3o)]Cl_2$, $V(IV)O(N2Py3o)](ClO_4)_2$ and $[V(V)O(O_2)(N2Py3o)]ClO_4$

	$[V^{IV}(N2Py3o)=O](ClO_4)_2$	$[V^{IV}(N2Py3o)=O]Cl_2$	$[V^{V}=OO_2(N2Py3o)]ClO_4$
distances[Å]			
V–N3	2.10	2.12	2.19
V–N7	2.36	2.34	2.56
V–N_{py1}	2.11	2.11	2.11
V–N_{py2}	2.10	2.10	2.11
V–N_{py3}	2.08	2.09	[5.54]
V=O	1.59	1.60	1.60
$\sum_{i=1}^{4(5)} (M-N)_i$	2.15	2.15	2.24
V–O1			1.81
V–O2			1.84
O1–O2			1.28
N3–N7	2.84	2.87	2.90
N_{py1}–N_{py2}	4.13	4.13	4.09
angles[°]			
N3–V–N7	78.7	80.1	75.1
N3–V–N_{py1}	79.6	79.0	76.0
N3–V–N_{py2}	78.9	78.5	74.6
N3–V–N_{py3}	154.5	156.0	–
N3–V=O	106.3	109.4	98.3
Npy1 –V–N_{py2}	158.3	157.4	150.5
torsion[Å]			
C1–C2–CA–N_{py1}	84.3	81.6	89.8
C5–C4–CA2–N_{py2}	–87.0	–83.2	–94.7

5.3.2 Crystal Structure of $[V(V)=O(O_2)(N2Py3o)]ClO_4$

Single crystals of $[V(V)=O(O_2)(N2Py3o)]ClO_4$, suitable for XRD, were obtained by slow evaporation at the solvent (water / acetonitrile, ca. 1:10). The resulting orange crystals were stable in air for several days.

The crystal structure of $[V(V)=O(O_2)(N2Py3o)]ClO_4$ clearly shows that oxidation from V(IV)complex to V(V) complex had occurred. Furthermore, there is a side–on bound peroxide anion at the metal center. The O-O is 1.28 Å, which is quite a short distance for a bidentate peroxo ligand (this will be discussed in greater detail in 5.8). The crystal structure also confirmed that N_{py3} does not coordinate to the metal center.

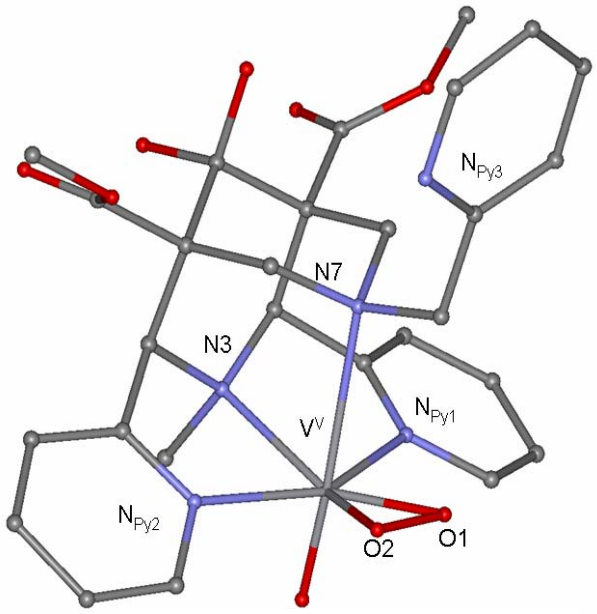

Fig. 5.3.2 Crystal structure of $[V(V)=O(O_2)(N2Py3o)]ClO_4$

The distances of N_{py1}-V, N_{py2}-V, N_3-V and V=O are 2.11 Å, 2.11 Å 2.19 Å

and 1.60Å, respectively, which are expected for V(IV) complexes.[11]

However, the V-N_7 bond is remarkably elongated to 2.56Å. This is an extremely long bond length

for V-N_{amine}.[6]

5.3.3 Comparison of the Crystal Ctructure of $[V(IV)O(N2Py3o)]Cl_2$ and $[V(V)=O(O_2)(N2Py3o)]ClO_4$

An overlay of the crystal structures of $[V(IV)O(N2Py3o)]Cl_2$ and $[V(V)=O(O_2)(N2Py3o)]ClO_4$ is shown in Fig. 5.3.3.

As it can be seen from the figure, there are no remarkable differences for the V-NPy1, V-Npy2 and V-N3 bond distances. However, the distance of V-N7 is much longer in the V(V) complex(2.56Å) than in of the V(IV) complex (2.34Å).

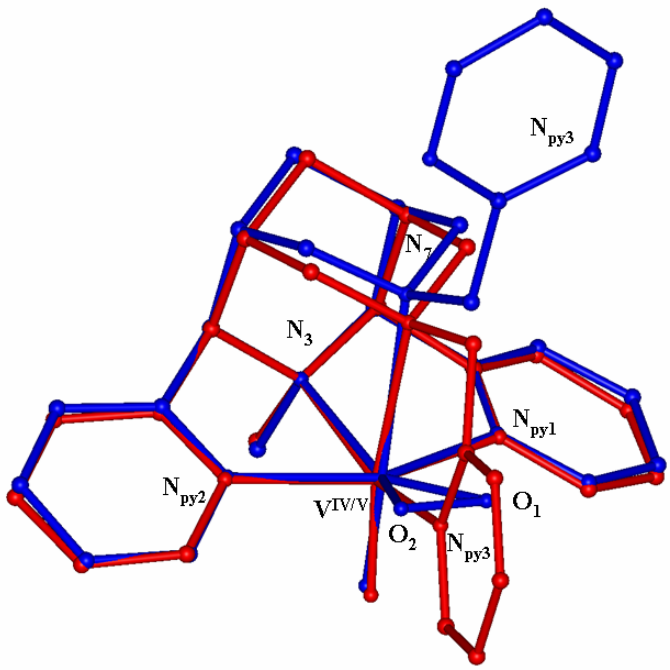

Fig. 5.3.3 Overlay of the crystal structure of $[V(IV)O(N2Py3o)]^{2+}$ and $[V(V)=O(O_2)(N2Py3o)]^{+}$ without substituents to the bispidine backbone

5.4 EPR spectra of the Vanadium(IV) Bispidine complexes

5.4.1 EPR spectrum of [V(IV) O(N2Py3o)]$(ClO_4)_2$

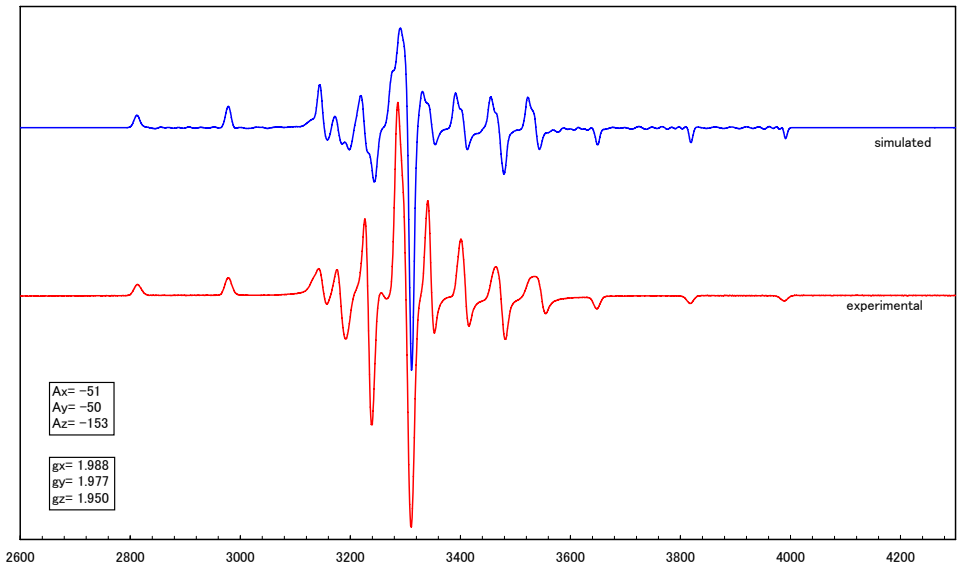

Fig. 5.4.1 EPR spectrum of [V(IV) O(N2Py3o)] $(ClO_4)_2$ in DMF/H_2O (2:1) with ν=9.2920 [Hz], frozen solution, (^{51}V; I=7/2; natural abundance 99.76%)

(red) experimental, (blue) simulated

The EPR spectra were measured at 110.3K using approx. 1 mM solutions of $[V(IV)O(N2Py3o)]^+$ complex in DMF/H_2O(2:1). Anisotropic spectra were recorded at the frozen sample. The g value and A^V values were determined by simulation using the program XSophe.

A_{xx}=-51cm^{-1}, A_{yy}=-50 cm^{-1}, A_{zz}=-153 cm^{-1} ($A_{xx}<A_{yy}>>A_{zz}$) A_{iso}=-84 cm^{-1}

g_{xx}=1.988, g_{yy}=1.977, g_{zz}=1.950 (gxx > gyy>gzz) g_{iso}=1.9717

All spin-Hamiltonian parameters were in the range expected for axially symmetric vanadyl complexes.[13] There is no difference in the EPR spectra of the two salts of the vanadyl complexes [V(IV)O(N2Py3o)]$(ClO_4)_2$ and [V(IV)O(N2Py3o)]Cl_2.

5.5 Electrochemistry of the Vanadium Bispidine

5.5.1 Electrochemical Properties of $[V(IV)O(N2Py3o)]Cl_2$ and $[V(IV)O(N2Py3o)](ClO_4)_2$

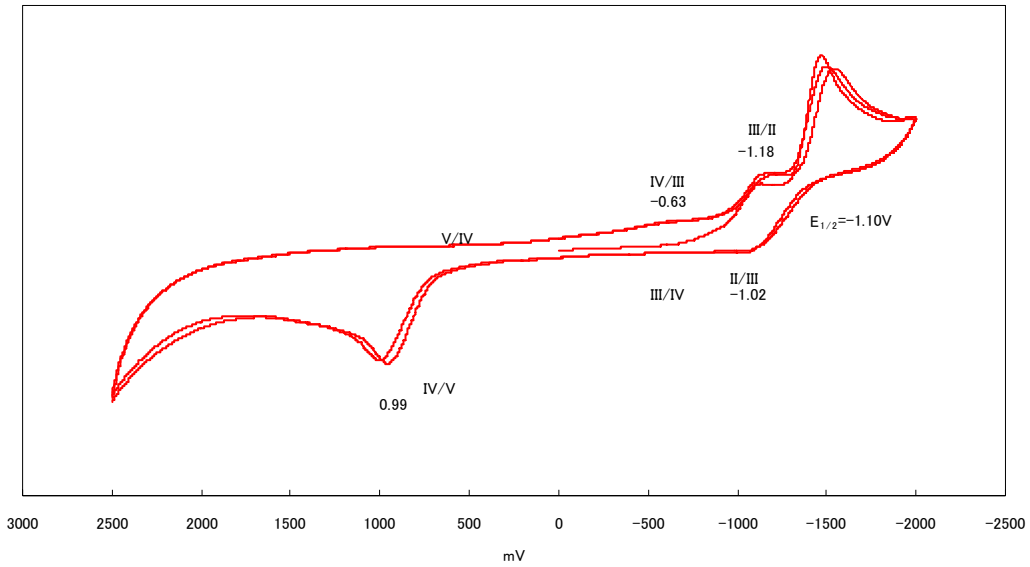

Fig. 5.5.1 Cyclic voltammogram of $[V(IV)O(N2Py3o)]Cl_2$ in CH_3CN

(scan rate: 100 mV/s, reference electrode 0.01 M $AgNO_3$/Ag)

The redox potential of the vanadium complexes of $[V(IV)O(N2Py3o)]Cl_2$ and $[V(IV)O(N2Py3o)](ClO_4)_2$ were measured by cyclic voltammetry using the BAS-100B electrochemical analyzer with a scan rate of 100mV/s. The measurements were carried out in dry acetonitrile containing 0.1 M tetra-n-butyl ammonium hexafluorophosphate as supporting electrolyte at 25°C, $Ag/AgNO_3$ was used as reference electrode. The cyclic voltammgramms are presented in Fig. 5.5.1. As can be seen, the redox step of the V(II)/(IIII) couple at a potential of -1.1V is quasi-reversible. Further at -0.63V, a reduction peak was observed but a peak for oxidation from III to IV was not found. There is an oxidation peak at 0.99V from IV to V but no reduction peak i.e., the oxidation to V(V) is irreversible.

5.5.2 Electrochemical Properties of $[V(V)=O(O_2)(N2Py3o)]ClO_4$

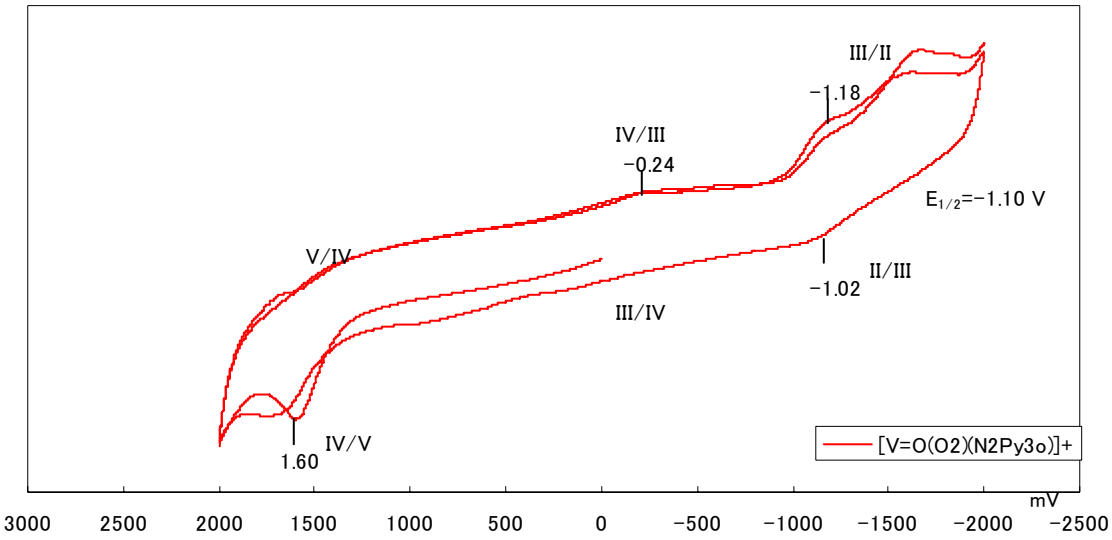

Fig. 5.5.2 Ccyclic voltammograms of $[V(V)=O(O_2)(N2Py3o)]ClO_4$ in CH_3CN (scan rate: 100 mV/s,against $AgNO_3$/Ag electrode)

The redox potential of V(II)/(III) redox couple is observed at -1.10V which is quasi-reversible similarly to $[V(IV)O(N2Py3o)]Cl_2$ complex. Furthermore, a reduction peak was observed at -0.24V, but a peak for oxidation from III to IV was not observed. There is an oxidation peak at 1.60V from IV to V but no reduction peak which is irreversible.

5.6 UV-Vis Spectra of the Vanadium Bispidine Complexes

5.6.1 UV-Vis spectrum of $[V(IV)O(N2Py3o)](ClO_4)_2$

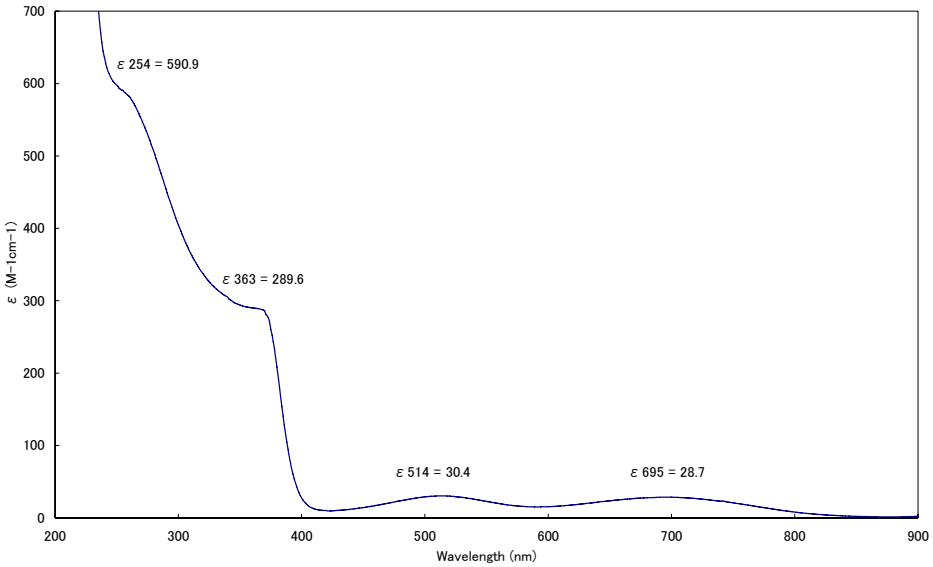

Fig. 5.6.1a UV-vis spectrum of $[V(IV)O(N2Py3o)](ClO_4)_2$ in methanol

Table 5.2 Assignment of electronic transition of $[V(IV)O(N2Py3o)](ClO_4)_2$

assignment	wavelength(nm)	wave number (cm^{-1})	ε
$\pi \rightarrow \pi^*$	254	39370	590.9
$xy \rightarrow z^2$ a)	363	27548	289.6
$xy \rightarrow x^2-y^2$ b)	514	19455	30.4
$xy \rightarrow xz, yz$ c)	695	14388	28.7

The electronic spectra of $[V(IV)O(N2Py3o)](ClO_4)_2$ was measured in methanol at 25°C. $[V(IV)O(N2Py3o)](ClO_4)_2$ has two sharp absorptions at 254nm, 363nm with shoulders and two broad peaks centered at 514nm and 695nm.

The band at 695 nm is tentatively assigned the promotion of an electron from the half-filled d_{xy} orbital to the empty or d_{yz} (xy→xz, yz). The band at 514nm is assigned as the promotion from the half-filled d_{xy} orbital to the d_{x2-y2} orbital ($xy \rightarrow x^2-y^2$). The peak at 363 nm is assigned as the promotion from the half-filled d_{xy} orbital to the d_{z2} orbital ($xy \rightarrow z^2$).The peak at 254nm is assigned as a $\pi \rightarrow \pi^*$ transition from within the pyridine groups.

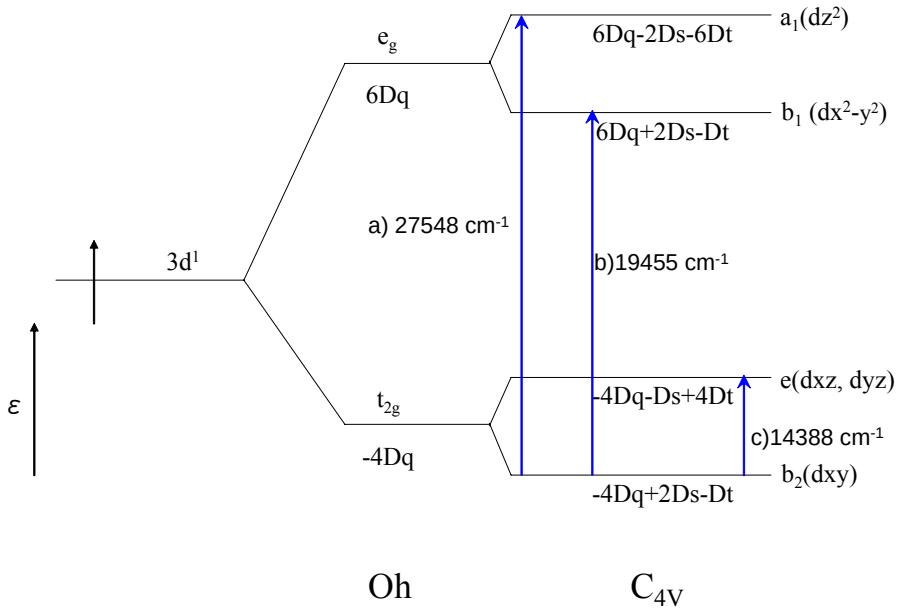

Fig. 5.6.1b Energy levels of an Oh ligand field (C_{4v} symmetry, (-3Ds+5Dt)>0)

The crystal field energy level diagram for $[V(IV)O(N2Py3o)]^{2+}$ is given in Fig. 5.6.1c. The parameters Ds and Dt specify the degree of tetragonality present in the ligand field.[14,15] The energies of the d states are given by the 3 parameter[16,17] as follows:

$$E(dz^2) = 6Dq - 2Ds - 6Dt \qquad (5.1)$$

$$E(dx^2 - y^2) = 6Dq + 2Ds - Dt \qquad (5.2)$$

$$E(dxy) = -4Dq + 2Ds - Dt \qquad (5.3)$$

$$E(dxz/dyz) = -4Dq - Ds + 4Dt \qquad (5.4)$$

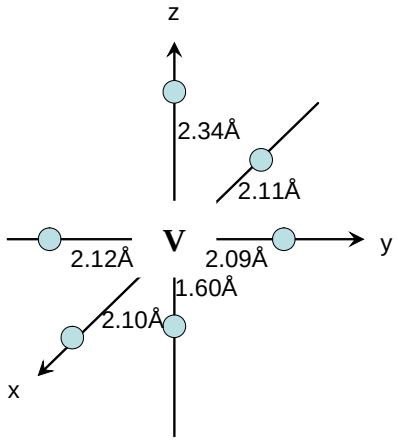

Fig. 5.6.1c X-ray data of $[V(IV)O(N2Py3o)]^{2+}$

From (5.1)-(5.4)

b2→e -3Ds+5Dt = 14388cm^{-1}

b2→b1 10Dq = 19455cm^{-1}

b2→a1 10Dq-4Ds-5Dt = 27548cm^{-1}

The value of 10Dq is obtained directly from the Δb2→b1transition,which gives Dq=1946cm^{-1}. ($VOSO_4 \cdot 5H_2O$: Dq= 1600 cm^{-1} [18,19])

From (5.1)-(5.4) it emerges that Ds = -3212, Dt = 951. The parameters of Ds and Dt specify the degree of tetragonality present in the field.[14]

5.6.2 UV-Vis Spectrum of $[V(V)=O(O_2)(N2Py3o)]ClO_4$

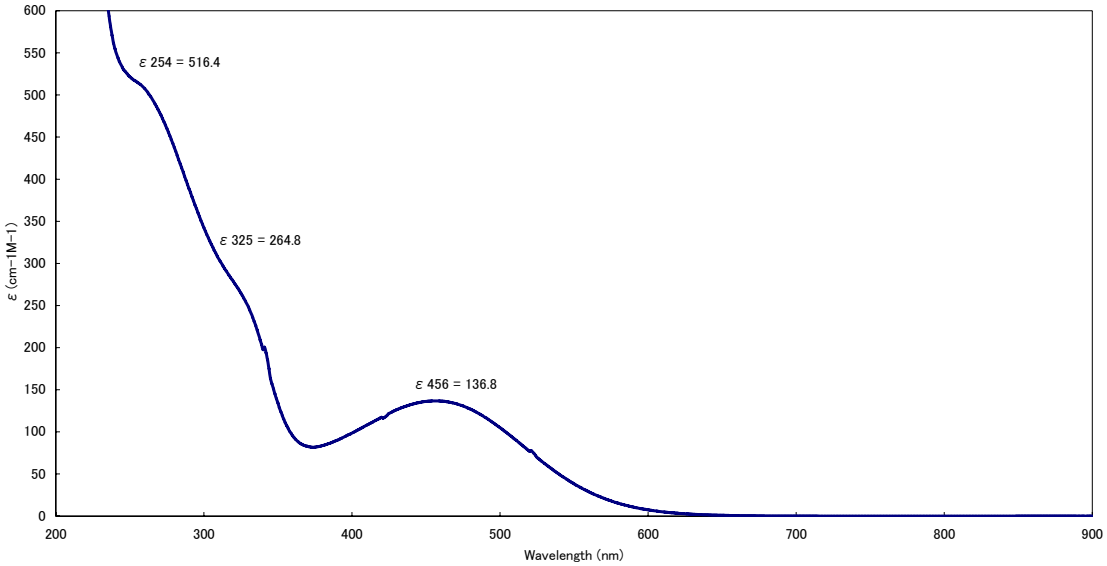

Fig. 5.6.2 UV-Vis spectrum of $[V(IV)O(N2Py3o)](ClO_4)_2$ in methanol at 25°C.

As expected for d^0 metal ions, there are no observable d-d bands in the visible region of the electronic absorption spectrum of the vanadium (V) oxo peroxo complex, while the UV region is dominated by a peak centered at 254nm, which is in assigned to the $\pi \rightarrow \pi^*$ transition of the pyridyl groups of the ligand.

The characteristic peak at 456 nm (ε=137) is assigned as a peroxo-vanadium charge-transfer transition. The transition is in the range typical for vanadium peroxo complexes[20,21,22].

5.7 Oxidation of the Vanadium (IV) Bispidine Complexes

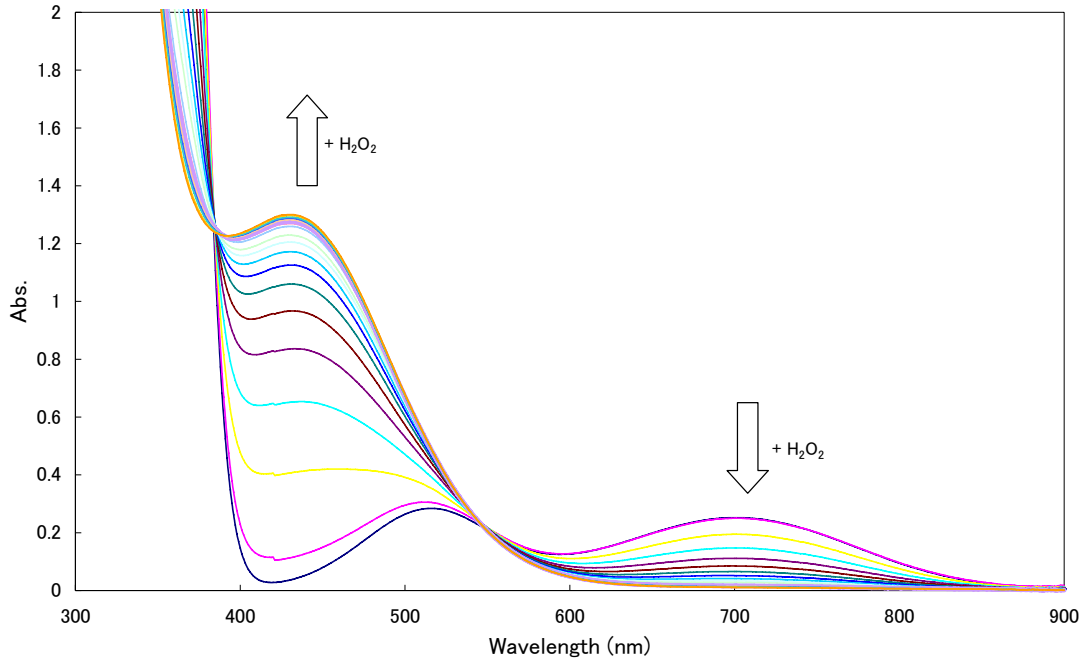

Fig. 5.7.1 Oxidation reaction of $[V(IV)=O(N2Py3o)]^{2+}$ with hydrogen peroxide in methanol at 25°C

The oxidation reaction of $[V(IV)=O(N2Py3o)]^{2+}$ complex was measured by UV-Vis spectroscopy. For the experiment, 11 mM of $[V(IV)=O(N2Py3o)](ClO_4)_2$ and 170 eq. of 30 % hydrogen peroxide were used. The measurement was carried out in dry methanol at 25°C. The spectra were recorded every 5 minutes. Two isosbestic points were observed at 390 nm and 560 nm which indicates there are only species with absorbance in the UV-Vis region in solution. According to the UV-Vis spectra the expected conversion occurred successfully, the two bands of the $[V(IV)=O(N2Py3o)]^{2+}$ complex (514 nm and 695 nm), shifted to a more intense single band at 429 nm. The color of the solution changed from light purple to orange.

The newly formed band at 456 nm is assigned to a hydroperoxo to V(V) charge transfer transition (Fig. 5.7.2.)

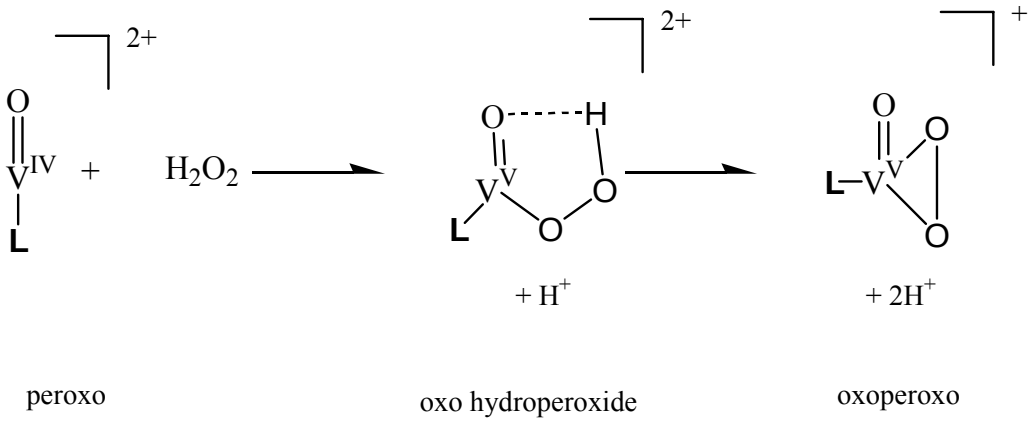

Fig. 5.7.2 Oxidation scheme of $[V(IV)=O\ (N2Py3o)]^{2+}$ with hydrogenperoxide

Further, the peak which appears at 429 nm shifted to 456 nm after 1 day (see Chapter 5.6.2). It probably indicates that the peak at 429 nm probably corresponds to the oxo-hydroperoxo V(V) complex as intermediate as shown Fig. 5.7.2.

This indicates there is a fast reaction from the *oxo* V(IV) to an *oxo hydroperoxo* V(V) complex followed by a slow rearrangement to the *oxo peroxo* V(V) complex, which also involves substitution of a pyridyl groups (see Fig. 5.3.3)

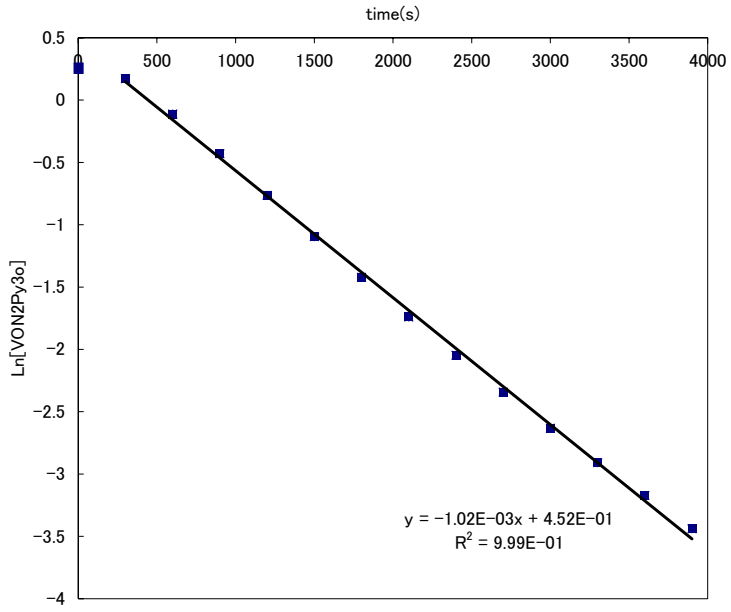

Fig. 5.7.3 ln[VON2Py3o] vs time(s) at 430 nm.

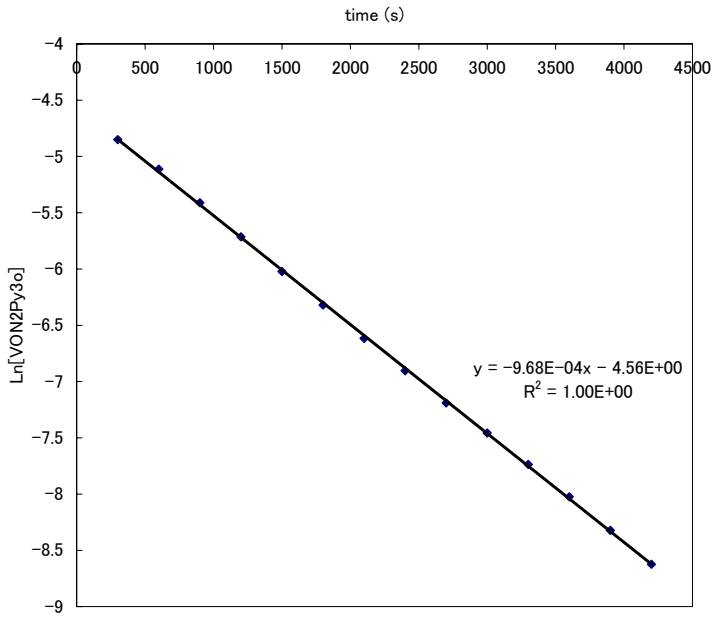

Fig. 5.7.4 ln[VON2Py3o] vs time(s) at 700 nm

A plot of the logarithm of time(s) vs. the concentration of $[V(IV)=O(N2Py3o)]^{2+}$ is shown in Fig. 5.7.3 and 5.7.4. The concentration of the $[V(IV)=O(N2Py3o)]^{2+}$ species was estimated by intensity of the peak at 430nm and 700nm, respectively.

$$-\frac{d[C]}{dt} = k[C] \qquad \textbf{(5.5)}$$

$$\int_{C_0}^{C_t} \frac{dC}{C} = -k\int_0^t dt \Leftrightarrow C_t = C_0 e^{-kt} \qquad \textbf{(5.6)}$$

$$\ln[C_t] = -kt + \ln[C_0] \qquad \textbf{(5.7)}$$

$$t_{1/2} = \frac{\ln 2}{k} \qquad \textbf{(5.8)}$$

It was observed that the reaction is first order due to the linearity of the plot in Fig. 5.7.4 after an initial reaction at approx. 300 seconds. The correlation coefficient of the linear region (R^2) is 0.999. From equation (5.7) and the slope, the rate constant was determined by linear fitting and the its value is presented in Fig. 5.7.4. The observed rate constant k_{obs} was estimated as $1.02*10^{-3}$ s^{-1}. The estimated half life is ($t_{1/2}$) 679.56 s from equation (5.8). The half-lives are generally independent of the initial concentration as shown in equation (5.8).

Further, from Fig. 5.7.4, the rate constant and half-life are estimated as $9.68*10^{-4}$ s^{-1} and 716.06 s, respectively. The results which are given at 430 and 700 nm are in good agreement, and this indicates that the absorption increases and decreases occur simultaneously, and are characteristic for the same reaction.

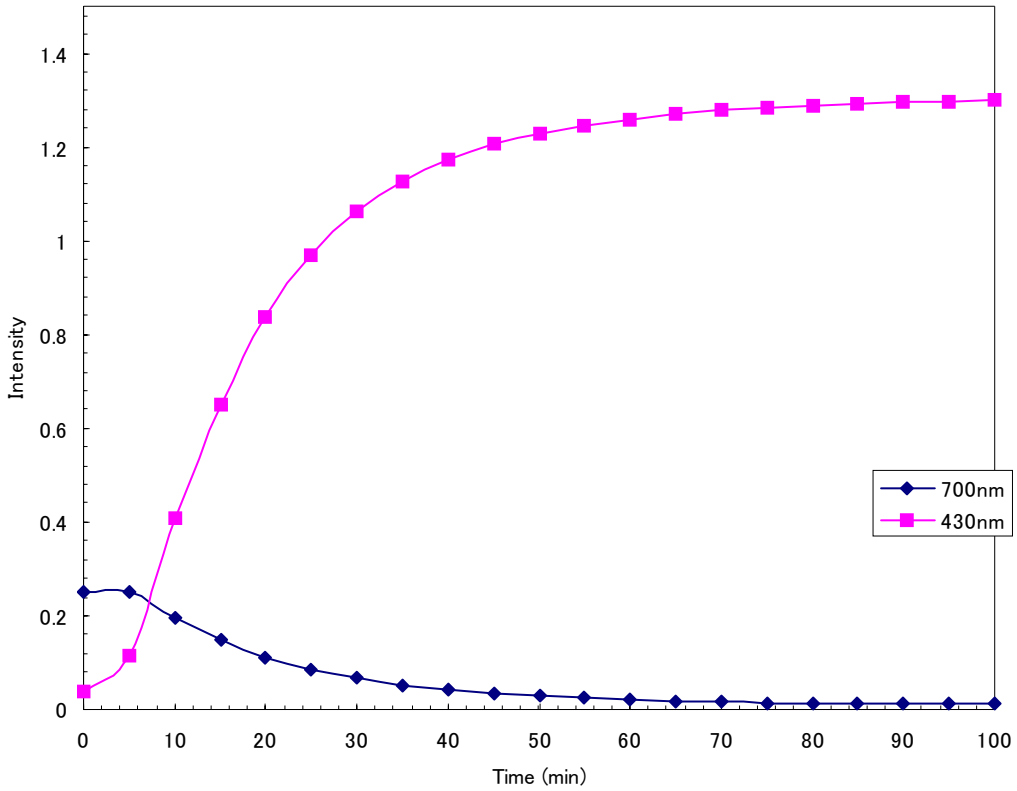

Fig. 5.7.5 Time dependence of the absorption intensities at 430 nm and 700 nm for [V(IV)=O(N2Py3o)]$(ClO_4)_2$.

The absorbance values at 430 and 700 nm are plotted as a function of the reaction time in Fig. 5.7.5. The intensity of the assigned hydroperoxide LMCT band and the d-d transition band increase or decrease in parallel. The first 5 min of the reaction shows a different behavior. The rate of product formation at the beginning is significantly slower, which might indicate that the reaction mechanism involves an intermediate which has to be formed first and which can take part in the reaction as catalyst, opening a faster pathway for the oxidative conversion. An autocatalytic mechanism can also be possible.

5.8 IR Spectra of $[V(IV)=O(N2Py3o)](ClO_4)_2$ and $[V(V)=O(O_2)(N2Py3o)]ClO_4$

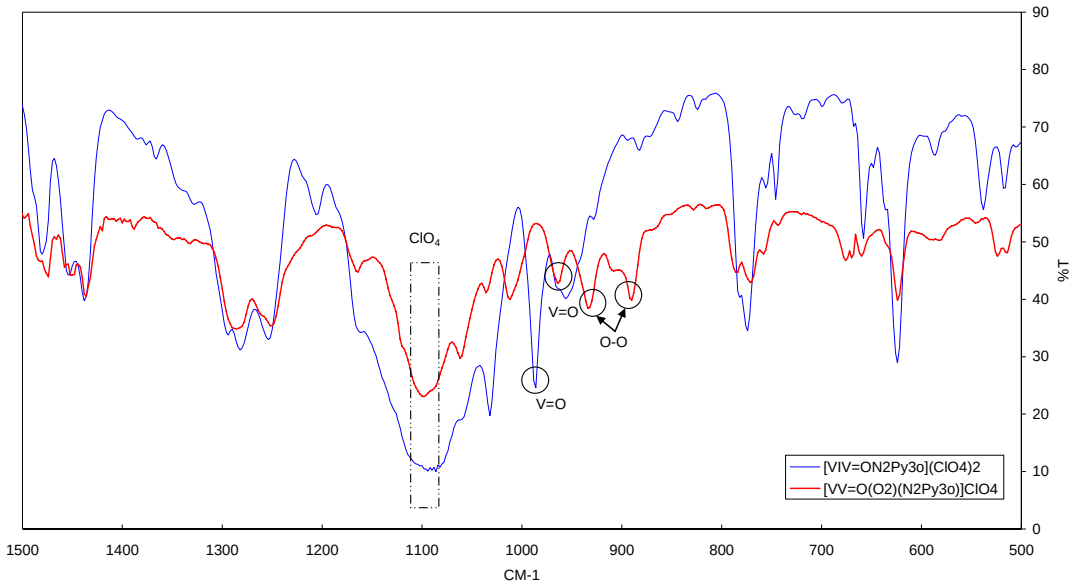

Fig. 5.8.1 Overlayof the IR-spectra of $[V(IV)=O(N2Py3o)](ClO_4)_2$ and $[V(V)=OO_2(N2Py3o)]ClO_4$, measured from KBr pellets

There is an absorption band at 986 cm^{-1} in $[V(IV)=O(N2Py3o)](ClO_4)_2$. For six-coordinate vanadyl (IV) complexes the frequency of the V=O stretching vibration is generally observed at ca. 950cm^{-1} while for five-coordinate vanadyl (IV) complexes it is found at ca. 980 cm^{-1} [23,24]. The peak at 986 cm^{-1} is therefore attributed to the V=O stretching vibration. The stretching vibration at 986cm^{-1} indicates rather a behavior typical for a 5-coordinate VO^{2+} complex, but the crystal structure of $[V(IV)=O(N2Py3o)](ClO_4)_2$ shows a 6-coordinate VO^{2+} complex.

The bond length of V-N7 of $[V(IV)=O(N2Py3o)](ClO_4)_2$ is 2.36Å, which is extremely long for V-N_{amine} bond (generally, bond lengths of V(IV)-N are in the range of ca.2.08-2.19Å). This might be a reason that the complex has a V=O stretching vibration

similar to five-coordinate vanadyl (IV) complexes.

Three absorptions were found at 890 cm^{-1}, 932 cm^{-1} and 962 cm^{-1} in the two IR spectrum of $[V(V)=OO_2(N2Py3o)]ClO_4$. The absorption at 962 cm^{-1} might be attributed to the V=O stretching vibration, two bands at 890 cm^{-1}, 932 cm^{-1} are tentatively assigned to the O-O stretching vibrations. For further confirmation isotope labeling experiments are needed.

Cramer et al.[25] have reported a relationship between the O-O stretching frequencies and the O-O bond length with a linear correlation as shown in Fig. 5.7. Generally , the compounds having an O-O bond length in the range of 1.4–1.5 Å and a ν_{OO} between 800 and 930 cm^{-1} are categorized as peroxides, whereas compounds with an O-O bond length of 1.2–1.3 Å and ν_{OO} between 1050 and 1200 cm^{-1} belong to the superoxide category[26,27,28].

The bond length of O-O in $[V(V)=O(O_2)(N2Py3o)]ClO_4$ is1.275Å. On the basis of the above categorization, this is in the range of superoxides and the O-O stretching frequencies should appear at ca.1250 cm^{-1}.

However the O-O stretching frequencies actually appeared at 890 cm^{-1} and 932 cm^{-1}.It is not consistent with the expectation, since no extra peaks were observed in the IR spectrum of the V(V)-peroxo complex in the range of 1250 cm^{-1} in comparison to the VO^{2+} complex.

The results of the XRD clearly show that the cationic part of the complex is +1, due to the stoichiometry, taking counter anions into consideration. Moreover, the mass spectrum shows a peak at 616.4 assigned to $[V(V)=O(O_{2)}(N2Py3o)]^{+}\cdot H_2O$ (616.52g/mol) with a +1 charge,. The possible combination is considered as either a $[V^{V}=O]^{3+}$ complex with a bound peroxide or a $[V^{IV}=O]^{2+}$complex with coordinated

superoxide ion. However the lack of a d-d band in the UV-vis spectrum indicates that the complex is undoubtedly formed between Vanadium (V) and peroxide. In spite of the above results, it was found that $[V(V)=O(O_2)(N2Py3o)]^+$ has an extremely short O-O bond distance of 1.275 Å. These results will need further detailed work (e.g., labeling studies of two ν_{OO} stretching mode and temperature dependent crystallography.

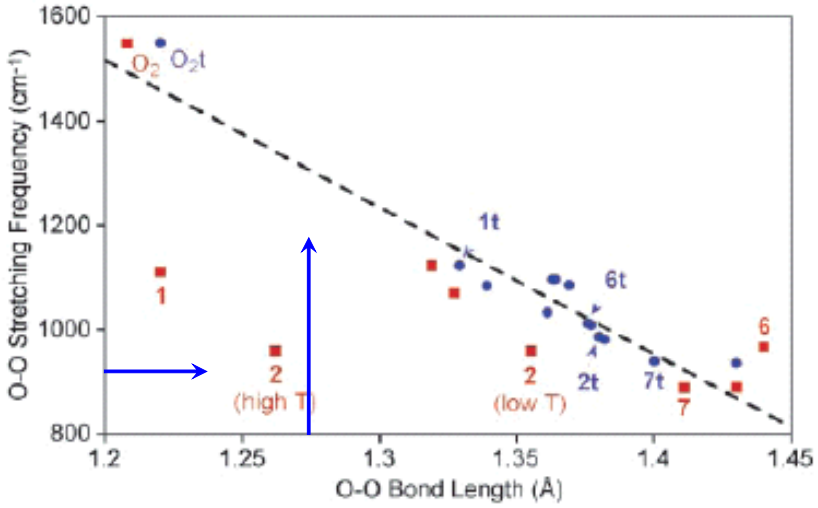

Fig. 5.8.2 Plot of O-O stretching frequencies (cm^{-1}) vs. O-O bond lengths (Å)[25]

5.9 NMR Spectrum of $[V(V)=O(O_2)(N2Py3o)]ClO_4$

The ^{1}H-NMR-spectrum of $[V(V)=O(O_2)(N2Py3o)]ClO_4$ was measured in d_6-DMSO at 300 K. The diamagnetism of the V(V) complex with N2Py3o was supported. The sharp single peaks observed at 5.59 ppm and 3.69 ppm are assigned to the H2/H4 CH protons and methoxy protons, respectively. These single peaks indicate a high level of symmetry in the entire vanadium complex, even with a side-on coordinating peroxo group and an uncoordinated pyridyl group. In the case of an asymmetrical complex, the peaks of the H2/H4 CH protons and the methoxy protons should be split.

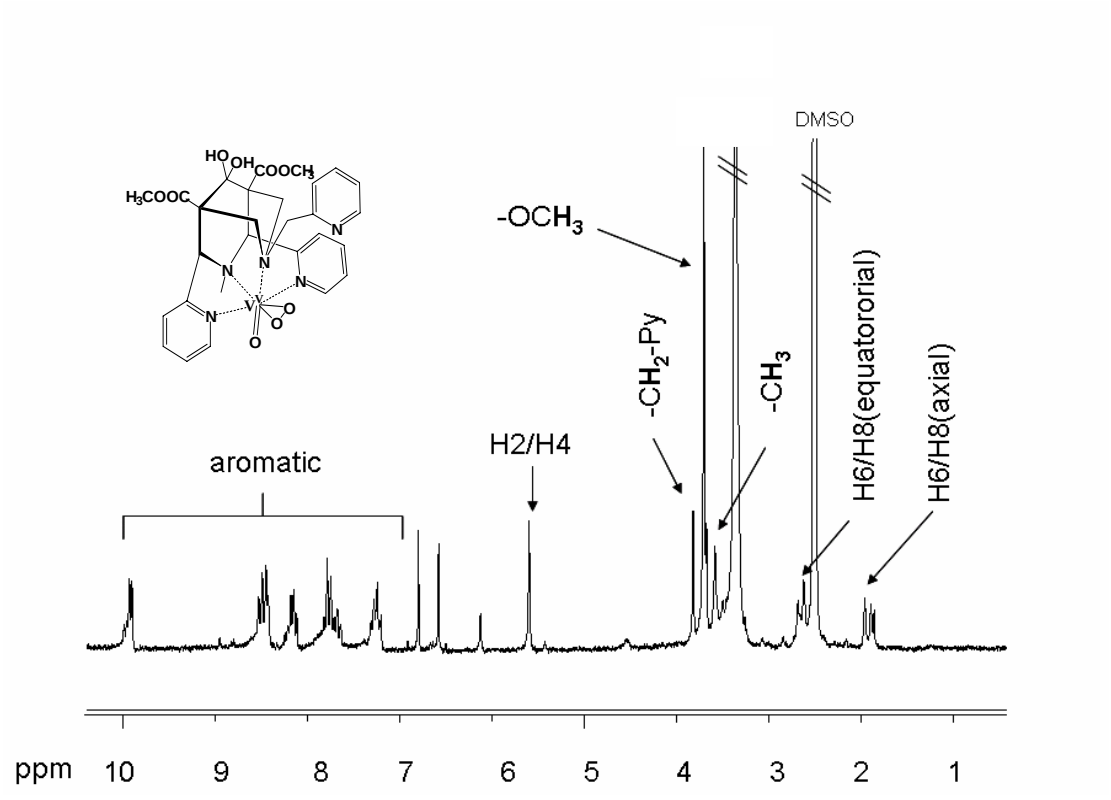

Fig. 5.9.1 ^{1}H-NMR spectrum of $[V(V)=O(O_2)(N2Py3o)]ClO_4$ (200MHz,d-DMSO)

References

[1] H. Sigel, A. Sigel, Eds. *Metal Ions in Biological Systems Vol.31: Vanadium and its Role in Life*,31, Marcel Dekker, Inc., New York,**1995**.

[2] A. Butler, J. V. Walker, *Chem. ReV.,* **1993**, *93*, 1937.

[3] D. Rehder, *Angew. Chem.*, **1991**, *30*, 148.

[4] N. D.Chasteen, *Ed. Vanadium in Biological Systems,* **1990**.

[5] A. Butler, M. J. Clague, G. E. Meister, *Chem. ReV.,* **1994**, *94*, 625.

[6] H. Mimoun, L. Saussine, E. Daire, M. Postel, J. Fischer, R. Weiss, *J. Am. Chem. Soc.,* **1983**, *105*, 3101.

[7] S. Kadota, I. G. Fantus, G. Deragon, H. J. Guyda, B. Hersh, B. I. Posner, *Biochim. Biophys. Res. Commun.,* **1985**, *147*, 259.

[8] A. Shaver, J. B. Ng, D. A. Hall, B. S.Lum, B. I. Posner, *Inorg.Chem.* **1993**, *32*, 3109.

[9] J. H. Mcneill, V. G. Yuen, H. R. Hoveyda, C. Orvig, *J. Med.Chem.* ,**1992**, *35*, 1489.

[10] P. Caravan, L. Gelmini, N. Glover, F. G. Herring, Li, H. J. H. McNeill, S. J. Rettig, I. A. Setyawati, Shuter, Y. E. Sun, S. Tracey, V. G. Yuen, C. Orvig, *J. Am. Chem. Soc*., **1995**, *117*, 127

[11] J. Selbin, *Cood.Chem.Rev.,***1966**, *1*, 293.

[12] H. Kelm, H. J. Krueger, *Angew. Chem.,* **2001**, *12*, 113.

[13] B. A. Goodman, J. B. Raynor, *Adv. Chem. Radiochem.*, **1970**, *13*, 135.

[14] W. Moffitt, J. Ballhausen, *Ann. Rev. Phys. Chem.,* **1956**, *7,* 107.

[15] C. J. Ballhausen, H. B. Gray. *Inorg. Chem.,***1962**, *1***,** 1**.**

[16] J. Hasselstroem, A.,Foehlisch, R.Denecke, *Phys. Rev. B.*, **2000**, *62,* 11192.

[17] P. H. Butler, Point Group Symmetry, Applications, Methods and Tables. (Plenum, new York, **1981**)

[18] L. E. Orgel, *J. Chem. Phys.*, **1955**, *23*, 1819.

[19] T. S. Piper, R. L. Carlin, *J. Chem. Phys.*, **1960**, *33*, 1208.

[20] G. J. Colpas, B. J. Hamstra, J. W. Kampf, V. L. Pecoraro, *J. Am. Chem. Soc.,* **1994**, *116*, 3627.

[21] G .J. Colpas, B. J. Hamstra, J. W. Kampf, V. L. Pecoraro, *J. Am. Chem. Soc.,* **1996**, *118*, 3469.

[22] H. Kelm, H-J. Krueger, *Inorg. Chem.,* **1996**, *35*, 3533.

[23] X. Li, M. S. Lah, V. L. Pecoraro, *Inorg. Chem.,* **1988**, *27*, 4657.

[24] J. A. Bonadies, C. J. Carrano, *J. Am. Chem. Soc.,* **1986**, *108*, 4088.

[25] C. J. Cramer, W. B. Tolman, K. H. Theopold, and A. L. Rheingold, *Proc. Natl. Acad. Sci. USA.*, **2003** , *100* , 3635.

[26] L. Vaska, *Acc. Chem. Res.* **, 1976,** *9* **,** 175.

[27] M. H. Dickman, M. T. Pope, *Chem. Rev.*, **1994**, *94***,** 569.

[28] J. J. Girerd, F. Banse, A. J. Simaan, *in Metal-Oxo and Metal-Pero*

6 SOD Assay of Bispidine Complexes

6.1 Introduction

Reactive oxygen species (ROS) such as the superoxide radical anion are considered to cause a number of diseases, such as atherosclerosis, cancer, and Alzheimer's disease.[1,2,3] Their toxic effects are amplified by pathological events including neutrophil activation, hyperoxia, metabolism of redox-active drugs, radiation exposure and ischemia/reperfusion.

Subsequently, the overproduced reactive oxygen species cause membrane damage, resulting from lipid peroxidation, and can also attack proteins and nucleic acids. Therefore, antioxidant enzymes are useful for the therapy of ROS-mediated injuries and diseases.

Superoxide dismutase (SOD) catalyzing the reduction from superoxide radical anion to H_2O_2 is the key enzyme for the protection from oxidative stress.

To achieve SOD activity, the redox potential of a complex is a very important factor. The redox potential of O_2/O_2^- and O_2^-/H_2O_2 are -0.33V and +0.89V, respectively. The redox potential of SOD falls into the range of $-0.3\ V \leqq E^0 \leqq +0.9\ V$, for example, E^0 of Fe-SOD is +0.26 V[4,5].

$$M^{n+} + O_2^- \longrightarrow M^{(n-1)+} + O_2$$

$$M^{(n-1)} + O_2^- + 2H^+ \longrightarrow M^{n+} + H_2O_2$$

Some of transition metal bispidine complexes may be considerable to be SOD mimics due to their redox properties. Tetradentate and pentadentate bispidine ligands with two tertiary amine and two/three pyridine donors enforce distorted octahedral geometry in their transition-metal complexes (in the case of Cu(II), 5-coordinate square pyramidal structures are common). Sites which are not occupied by ligand donor atoms, are free to coordinate substrates, and through their activation may lead to increasing reactivities. In this chapter the SOD activity of a series of Cu, Fe, Mn, Cr complexes with bispidine type ligands were investigated.

6.2 Compounds and Method of SOD Assay.

Fe(II), Mn(II), Cu(II) and Cr(III) complexes of four bispidine type ligands have been tested as SOD mimics. The activity was determined with the WST test (water soluble tetrazolium method). [6]

In this assay, the oxidation of WST by superoxide is measured spectrophotometrically at 450nm. The activity is reported as IC_{50} values, the catalyst concentration required to inhibit the WST formazan reduction by 50%.

In order to determine the SOD activity, several direct and indirect methods have been developed. Among these methods, an indirect method using nitroblue tetrazolium (NBT)[7] is commonly used due to its convenience and ease of use. However, there are several disadvantages to the NBT method, such as poor water solubility of the formazan dye and the interaction with the reduced form of xanthine oxidase. The WST-SOD assay method allows very conveniently the SOD peformance by highly water-soluble tetrazolium salt, WST-1 (2-(4- Iodophenyl)- 3-(4-nitrophenyl)-5-(2,4-disulfophenyl)- 2H-tetrazolium, monosodium salt) that produces a water-soluble formazan dye upon reduction with a superoxide anion.[8]

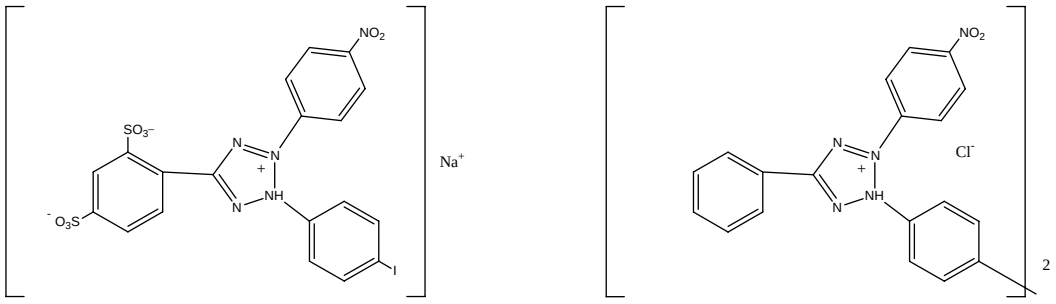

WST NBT

Fig. 6.1 Structure of tetrazolium ions

The rate of the reduction with O_2 is linearly related to the xanthine oxidase (XO) activity, and is inhibited by SOD, as shown in Fig. 6.2. The IC_{50} (50% inhibition activity of SOD mimics) can be determined by a colorimetric method.

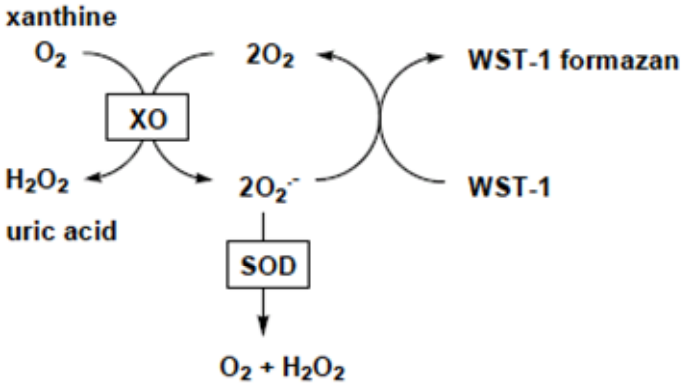

Fig. 6.2 Principle of WST-SOD assay method

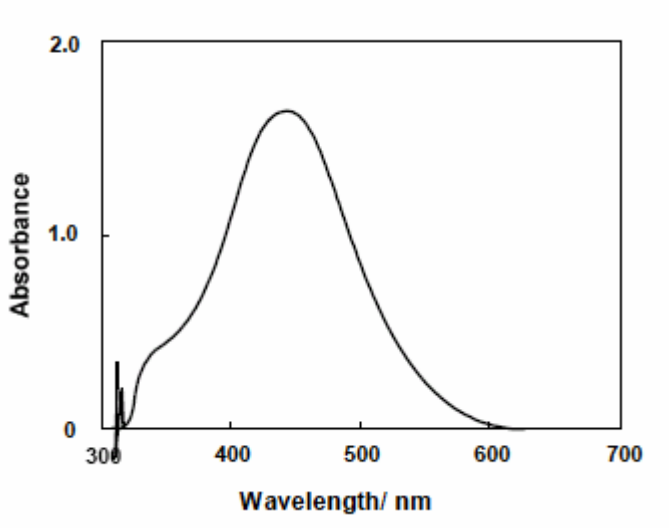

Fig. 6.3 Absorption spectrum of WST-1 formazan

6.3 Results and Discussion

The concentration-dependent inhibition curves (log[catalyst] vs. logIC_{50}) are approx. linear up to 95% inhibition.

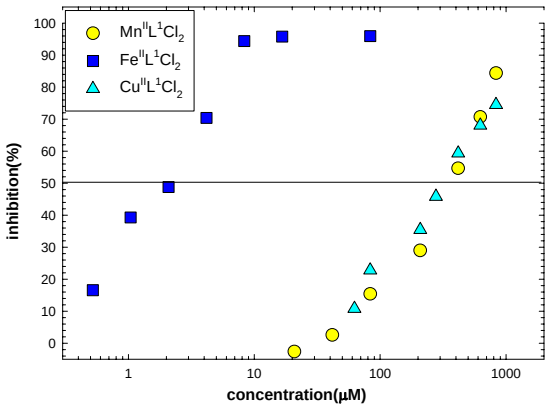

Fig. 6.4 Inhibition curves of Fe(II), Cu(II) and Mn(II) complexes of N2Py2

The Fe(II) complex with N2Py3o is the most active SOD mimic of our series. But it is less active than the Cu, Zn SOD enzyme by a factor of approx. 250.[9] The Fe(II) complexes are more active than the Mn(II) and Cu(II) compounds which have similar activity. (but Cu is somewhat less active) For Fe(II) the dinuclear compounds are less active than the mononuclear ones, which might be related to the redox potential and stoichiometry. A change of activity was observed when the anionic co-ligands were varied, but no clear trend could be found. Methylation of the α-C-atom of the pyridine donor changes the reactivity drastically.

For Cu(II) methylation increases the activity, this may be interpreted as a steric effect.

compounds	IC_{50} values (μM)
FeII(N2Py3o)SO4	1
FeII(N2Py3o)Cl2	2
FeII(N2Py2)Cl2	5
MnII(N4Py4)(CH3COO)2	6
MnII(N4Py4)(NO3)2	8
FeII(N2Py2)SO4	20
FeII(6-MeN2Py2)SO4	50
[FeII(N4Py4)]Cl2	60
[CuII(N2Py2)]Cl2	80
FeII(N2Py4)$(ClO_4)_2$	95
[CuII(N2Py3o)]Cl2	320
[MnII(N2Py3o)]Cl2	325
CuII(6-MeN2Py2)SO4	350
CuII(N2Py2)(CH3COO)2	1000
CuII(N2Py2)SO4	1000
CuII(N2Py2)(NO3)2	1000
Cr(N2Py2)Cl2PF6	no activity till 833 μM

Table 6.1 IC_{50} values of our complexes

Table 6.2 IC_{50} values vs redox potential vs $Ag/AgNO_3$

	IC_{50}	E^0
$[Fe^{II}(n2Py3o)SO_4]$	1	53
$[Fe^{II}(n2Py3o)Cl]Cl$	2	143
$[Fe^{II}(N2Py4)ClO_4]$	95	661

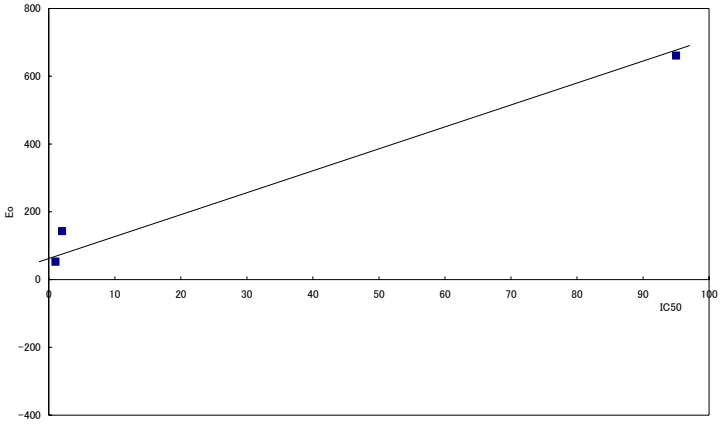

Fig. 6.5 Correlation of IC_{50} values and the redox potentials

The IC_{50} values are coorelated to the redox potentials. As mentioned in the introduction of this chapter, the necessary redox potential is in the range of -0.3V to +0.9V. The complexes with smaller redox potential show a higher SOD activity. There seems to be a linear correlation of the IC_{50} values and the redox potential.

References

[1] J. B. Mitchell, A. Samuni, M. C. Krishna, W. G. DeGraff, M. S. Ahn, U.Samuni, A. Russo, *Biochemistry*, **1990**, *29*, 2802.

[2] A. Samuni, D. Winkelsberg, A. Pinson, S. M. Hahn, J. B. Mitchell, A. Russo, *J. Clin. InVest.*, **1991**, *87*, 1526.

[3] J. R.Reddan, M. D. Sevilla, F. J.Giblin, V.Padgaonkar, D. Dziedzic, V. Leverenz, I. C.Misra, J. L.Peters, *Exp. Eye Res.*, **1993**, *56*, 543.

[4] J. J. Villafranca, F. J.Yost, I.Fridovich, *J. Biol. Chem.*, **1974,** *249*, 3532.

[5] J. J. Villafranca, *FEBS Lett.*, **1976,** *62*, 230.

[6] H. Ukeda, A. K. Sarker, D. Kawana , M. Sawamura, *Anal. Sci.*, **1999,*15***, 353 .

[7] C. Beauchamp, I. Fridovich, *Anal.Biochem.*, **1971**, *44*, 276.

[8] H. Ukeda, D. Kawana, S. Maeda and M. Sawamura, *Biosci. Biotechnol. Biochem.*, **1999**, ***63***, 485.

[9] H. Ukeda, D. Kawana, M. Sawamura, *Biosci. Biotechnol. Biochem.*, **1999**, *63*, 485.

7 Experimental

7.1 GENERAL

Materials

All commercially available chemicals were used without further purification. Solvents of technical quality were distilled prior to use.

Elemental analysis

Quantitativ analyses were carried out in the Microanalytical Laboratory of the Institute of Inorganic Chemistry (Heidelberg University). The code number of each measurement is reported together with the experimentally determined values.

Mass spectroscopy

Measurements were carried out on a Finnigan 8400 Mass-spectrometer. For FAB spectra nitrobenzyl alcohol was used as matrix. In the case of ESI, samples were dissolved in the appropriate solvent in 100µg/mL concentration.

IR spectroscopy

IR spectra were recorded from KBr pellets using a 16C type FT-IR spectrometer from Perkin Elmer.

NMR spectroscopy

The NMR spectra were recorded on a Bruker AS 200 spectrometer. The chemical shifts are given in ppm, with reference to TMS or the deuterated solvents. For the peak multiplicities the following abbreviations are used: s = singlet, d = doublet, dd = doublet of a doublet, t = triplet, dt = doublet of a triplet, m = multiplet. For the interpretation of the spectra the Win-NMR program was used.

Crystal structure determination

Intensity data were collected on a Syntex R3 or a Siemens-Stoe AED2 type diffractometer or a Bruker AXS SMART 1000 CCD area detector (MoKα radiation, λ = 0.71073 Å, ω- scan). The structures were solved by direct methods and refined by full matrix least-squares, based on F2 with all reflections using the SHELXTL program.

Hydrogen atoms were inserted in calculated positions or located in difference Fourier maps. Corrections for disordered solvent molecules and anions were applied using the SQUEEZE routine of the program system PLATON.

UV-Vis spectroscopy

UV-Vis spectra were recorded on a Varian Cary 1E or a JASCO V-570 spectrometer. For the measurements quartz cuvettes with 1 cm diameter were used.

Cyclic voltammetry

Cyclovoltammetric measurements were carried out by using a BAS100B electrochemical apparatus with BAS100W software. The working electrode was a glassy carbon electrode, a platinum wire was used as indicator electrode. The ionic strength was set to 0.1 M by using tetrabutylammonium-hexafluorophosphate. For potential measurements a $Ag/AgNO_3$ reference electrode was used. The scan rate was set to 100 mV/s.

EPR

EPR spectra were recorded on a Bruker Elexsys E 500 spectrometer.

SOD assay

A dojindo SOD assay kit-WST was used for all experiments.

7.2 Synthesis

7.2.1 Synthesis of $[V(IV)=O(N2Py3o)](ClO_4)_2 \cdot 2H_2O$

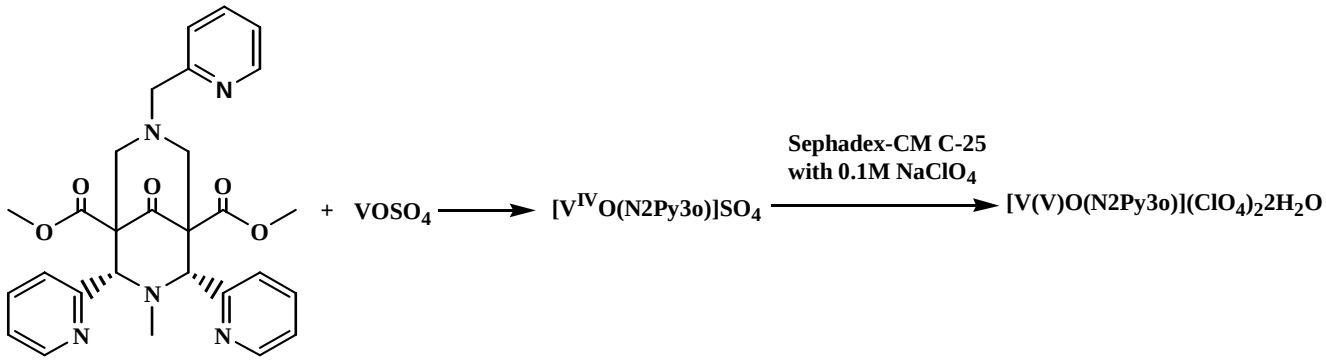

1.0g (1.94mmol) of N2Py3o was dissolved in 30 ml of methanol, subsequently 0.49g (1.94mmol) of $V(IV)OSO_4 \cdot 5H_2O$ was added ,dissolved in 5ml of methanol. After refluxing for ca.1 hour, the solution was evaporated to dryness and the product was separated on a Sephadex ® CM-C25 column with 0.1M $NaClO_4$. After partial, 0.83g (0.99mmol) of product was obtained by means of precipitation.

Yield : 51%

Elemental analysis

(16860)	calculated (%)	C	40.25	H	4.22	N	8.38
	observed (%)	C	40.65	H	4.11	N	8.43

ESI^+ MS : 599.3$[VO(N2Py3o)]^{2+}$ M=600.52

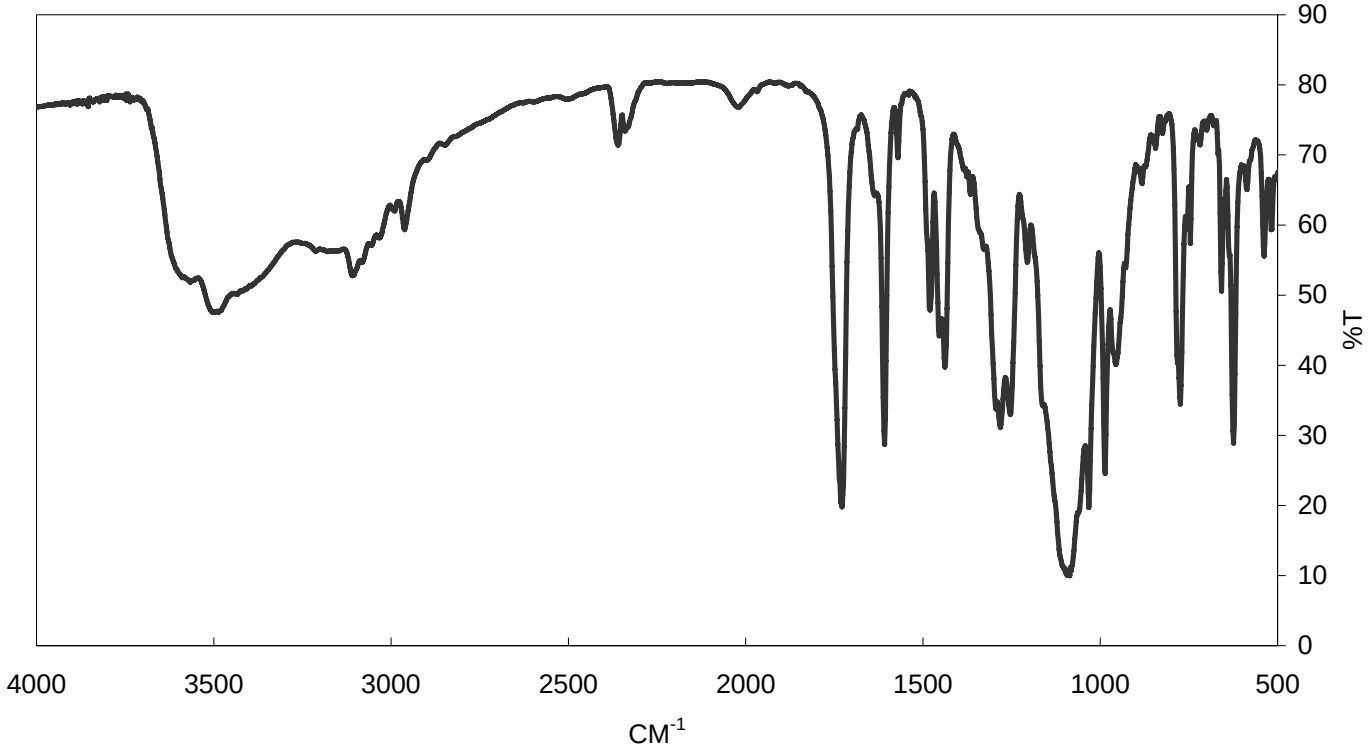

Fig. 7.2.1 Infrared spectrum of [V(IV)=O(N2Py3o)]$(ClO_4)_2 \cdot 2H_2O$ in KBr

IR[cm^{-1}] : 3484 (s,OH), 3092(w,OH), 2956(w), 1728(s), 1608(s),1479(m), 1437(w) , 1286(s), 1281(w), 1253(w) ,1205(w) 1098(s, ClO4), 1086(w), 986(w), 774(m) ,658(w) 624(s) ,538(w)

7.2.2 Synthesis of $[V(V)=O(O_2)(N2Py3o)]ClO_4 \cdot H_2O$

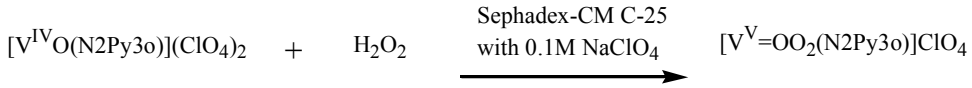

0.25g of $[V(V)O(N2Py3o)](ClO_4)_2 \cdot 3H_2O$ (0.30mmol) was dissolved in 30ml of methanol. Subsequently 300µl (10eq.)of 30% hydrogen peroxide was added to the solution. After 1day the product was purified on Sephadex ® CM-C25 eluent : 0.1M $NaClO_4$ aq.) After partial evaporation of the solvent, 0.11g (0.14mmol) of the product was obtained as a solid.

Yield:47%

Elemental analysis

(16858) calculated (%) C 44.84 H 4.44 N 9.34

observed (%) C 44.59 H 4.55 N 9.20

ESI^+ MS : 632.3$[V=OO_2(N2Py3o)]^+H_2O$ M=632.52

^{1}H-NMR (200MHz,DMSO) : σ=1.95(d, 2H, -C**H$_2$**-),σ=2.65(d, 2H,-C**H$_2$**-), σ=3.57(s, 3H, -NC**H$_3$**), σ=3.69(s, 6H,O-C**H**$_3$) ,σ=3.81(s, 2H,N-C**H2**-),σ=5.59(s, 2H,N-C**H**-),σ=5.59(s, 2H,N-C**H**^{2}-),σ=7.23-9.92 (m, 12H,Ar-**H**)

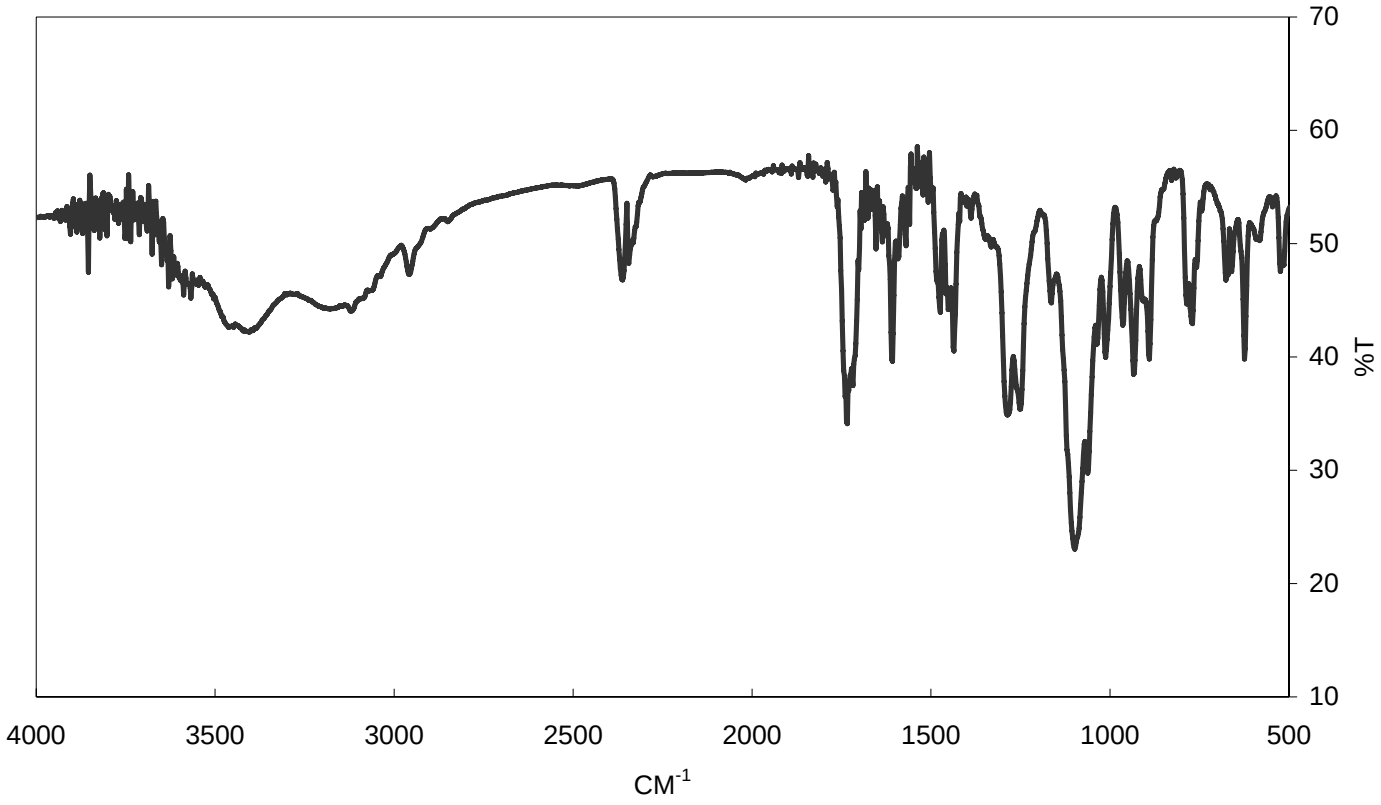

Fig. 7.2.2 Infrared spectra of $[V(V)=O(O_2)(N2Py3o)]ClO_4$ in KBr.

IR[cm^{-1}] : 3378 (s,OH), 2952(w), 1734(s), 1608(s),1475(m), 1450(w) ,1436(w) , 1286(s), 1250(s), 1164(w) , 1098(s, ClO4), 1061(w), 1035(w), 1012(m) ,963(w) 932(w) ,890(w) ,785(w) ,771(w) ,675(w) 623(m),523(m)

7.2.3 Synthesis of $[Co(III)(N2Py4)](ClO_4)_3$

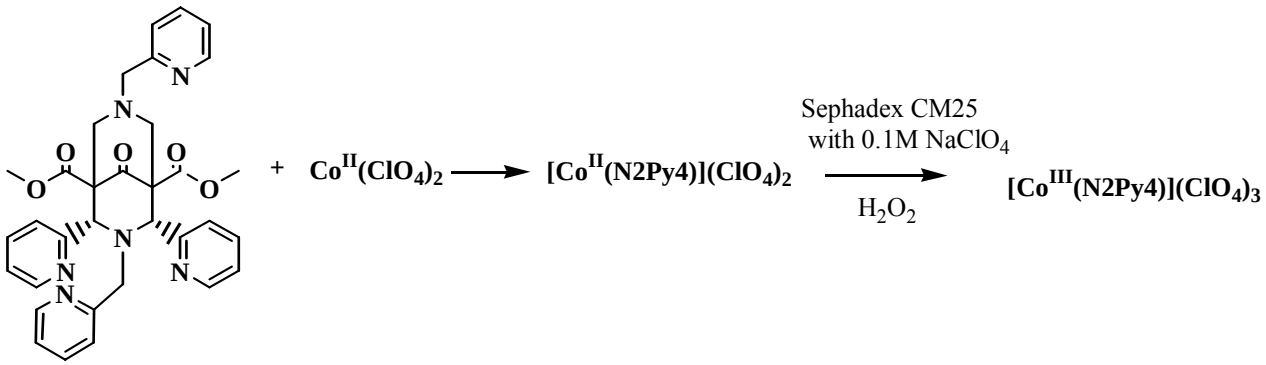

0.5g (0.84mmol) of N2Py4 was dissolved in 20 ml methanol and 0.31g (0.84mmol) of $Co(II)(ClO_4)_2 \cdot 6H_2O$ in 5ml methanol was added to the solution. After the stirring for ca.1 hr,the complex was precipitated and filtrated and dried. 0.52g (0.54mmol) of $[Co(II)N2Py4](ClO_4)_2$ was obtained.

0.3g of $[Co(II)N2Py4](ClO_4)_2$ was dissolved in 20ml of methanol and 17µl (3eq.) of 30% H_2O_2 aq. was added dropwise. After ca. 24 hours the product was isolated on Sephadex® CM25 with 0.1M $NaCl_{aq}$. The eluate was collected as a solid $[Co(III)(N2Py4)](ClO_4)_3$ evapolated and dried under vacuum.

^{1}H-NMR (200MHz,D2O) : σ=3.32(d, 2H, -C**H$_2$**-),σ=3.44(d, 2H,-C**H$_2$**-), σ=3.51(s, 2H, -N-C**H$_2$**-), σ=3.56(s, 2H,N-C**H$_2$**-),σ=3.69(s, 6H,-O-C**H**$_3$) , σ=5.83(s, 2H,N-C**H**-), σ=7.60-8.99 (m, 16H,Ar-**H**)

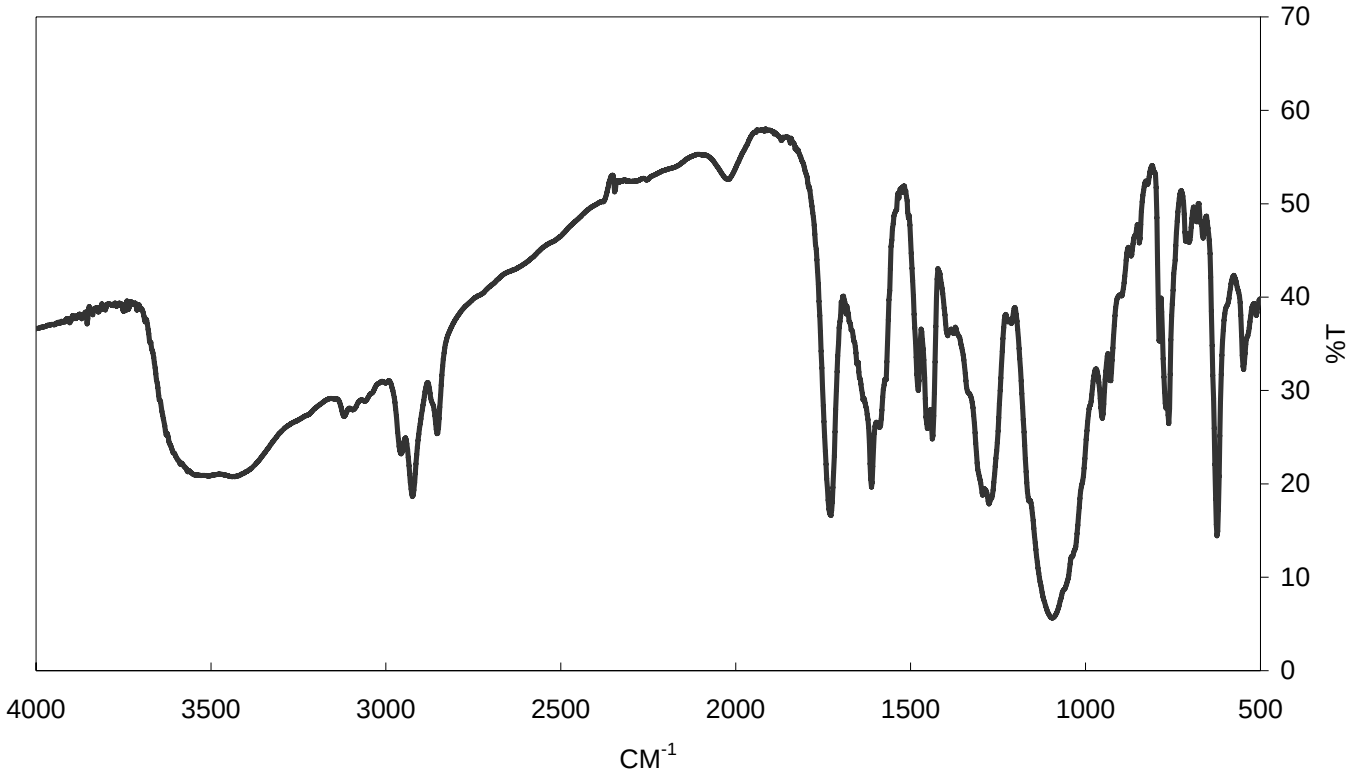

Fig. 7.2.4 Infrared spectrum of $[Co(III)(N2Py4)](ClO_4)_3$ in KBr

IR[cm^{-1}] : 3498 (s), 2920(m), 2848(m), 1724(s), 1614(s), 1476(m), 1440(m), 1436(m), 1264(s), 1082(s), 1038(m), 948(w), 926(w), 780(m), 762(m), 626(m), 546(w)

7.2.5 Synthesis of $[Co(III)(N2Py3o)Cl]Cl_2 \cdot 6H_2O$

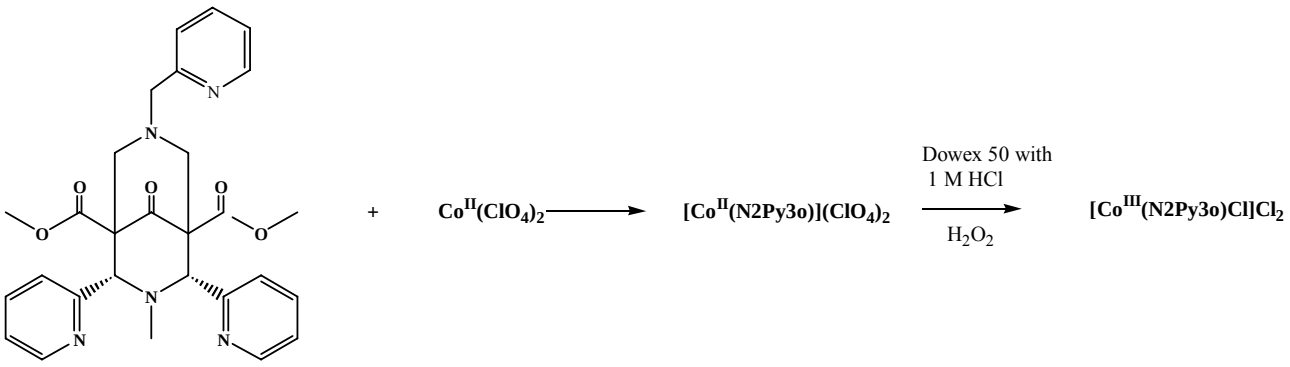

0.5g (0.97mmol) of N2Py3o was dissolved in 20 ml methanol and 0.35g (0.97mmol) of $Co(II)(ClO_4)_2 \cdot 6H_2O$ in 5ml methanol was added to the solution. After stirring for 1hr, the resulting product was precipitated, filtrated and dried. 0.42g (0.54mmol) of $[Co(II)(N2Py3O)(H_2O)](ClO_4)_2$ was obtained.

0.42g of $[Co(II)(N2Py3O)(H_2O)](ClO_4)_2$ was dissolved in 20ml of metanol, and 17µl (3eq.) of 30% hydrogen peroxide was added dropwise. After ca. 24 hours, the product was adsorbed onto Dowex® 50 and eluted with 1M HCl. The resulting product was evapolated and dried in vacuum.

Yield :0.21g (0.26mmol) (48.15%)

Elemental analysis

(16816)	calculated (%)	C	42.63	H	4.66	N	8.85
	observed (%)	C	42.59	H	5.24	N	8.88

ESI^+ MS : 313.9 $[Co(N2Py3o)Cl]^+H_2O$ M=2/627.96

^{1}H-NMR (200MHz,DMSO) : σ=2.60(d, 2H, -C**H$_2$**-),σ=2.75(s, 3H, -NC**H$_3$**), σ=3.05(d, 2H,-C**H$_2$**-),σ=3.75(s, 6H,O-C**H$_3$**) ,σ=4.80(s, 2H,N-C**H2**-),σ=5.28(s, 2H,N-C**H**-),σ=7.50-9.72 (m, 12H,Ar-**H**)

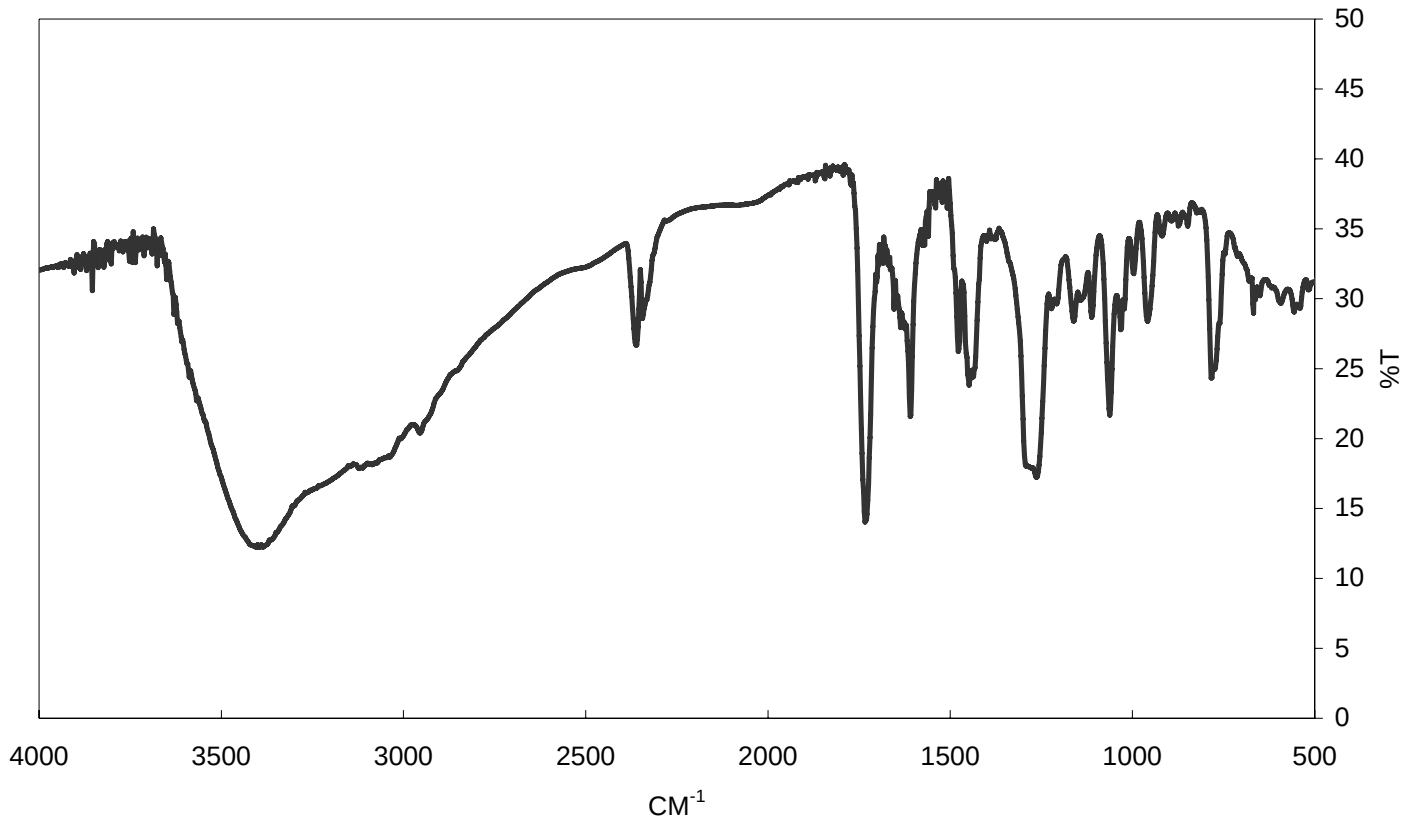

Fig. 7.2.5 Infrared spectra of $[Co(III)(N2Py3o)Cl]Cl_2$ in KBr

IR[cm^{-1}] : 3388 (s,), 2358(m), 1726(s), 1608(s),1474(w), 1436(m), 1262(s), 1156(w) , 1108(w), 1060(m), 1030(w), 950(w), 770(m)

7.2.6 Synthesis of [Co(III)(N2Py3u)Cl]Cl_2

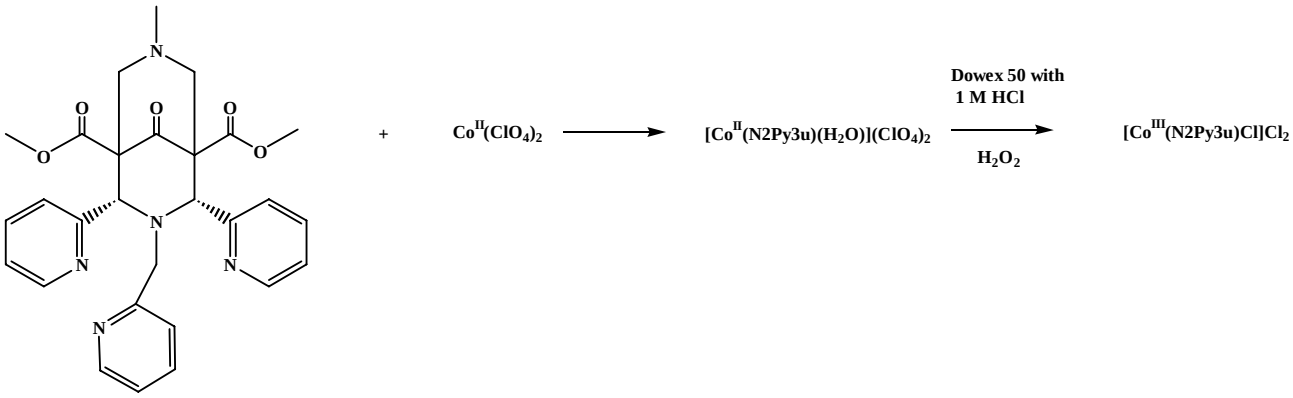

0.51g (0.989mmol) of N2Py3u was dissolved in 20 ml methanol and 0.36g (0.97mmol) of Co(II)$(ClO_4)_2 \cdot 6H_2O$ in 5ml methanol was added to the solution. After stirring for 1 hr, the resulting product was precipitated, filtrated and dried. 0.40g (0.54mmol) of [Co(II)(N2Py3u)(H2O)]$(ClO_4)_2$ was obtained.

0.40g (0.54mmol) of [Co(II)(N2Py3u)(H2O)]$(ClO_4)_2$ was dissolved into 20ml of metanol, and 17μl (3eq.) of 30% H_2O_2 aq. was added dropwise. After ca.24 hours, the product was isolated on Dowex ®50 with 1M HCl.

The resulting [Co(III)(N2Py3u)Cl]$Cl_2$was evapolated and dried up by vacuum pump. Single crystal suitable for XRD were obtained by diethyl ether diffusion into methanol solution.

ESI^+ MS : 296.4 $[Co(III)(N2Py3o)(OH)]^{2+}$ M=2/592.52=296.26

^{1}H-NMR (200MHz, D_2O) : σ=2.11(s, 3H, -NC**H$_3$**),σ=2.21(d, 2H, -C**H$_2$**-), σ=2.55(d, 2H, -C**H$_2$**-), σ=3.47(s, 6H, O-C**H$_3$**) ,σ=3.77(s, 2H,N-C**H2**-), σ=5.93(s, 2H, N-C**H**-),σ=7.15-9.26 (m, 12H, Ar-**H**)

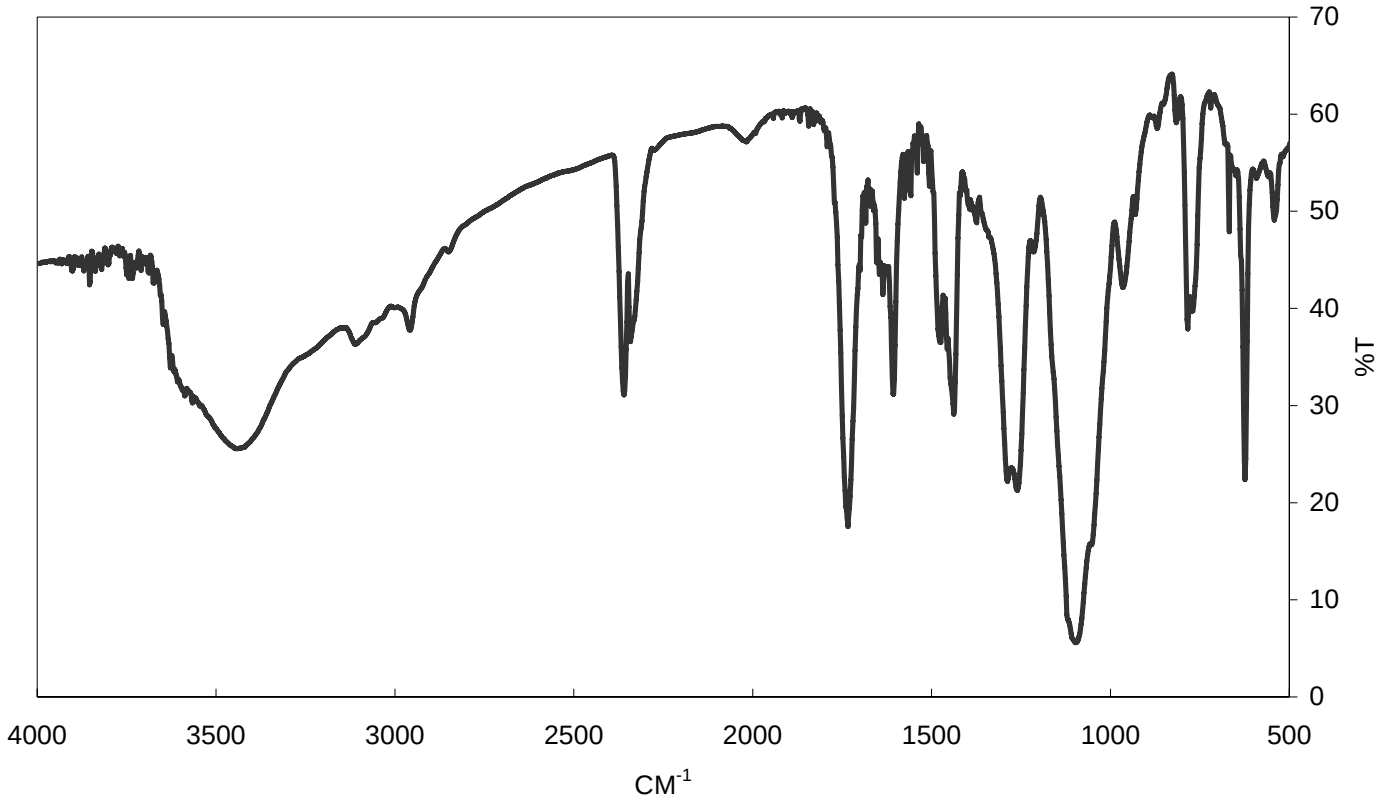

Fig. 7.2.6 Infrared spectra of [Co(III)(N2Py3u)Cl]Cl_2 in KBr

IR[cm^{-1}] : 3424(s,), 2358(m), 1732(s), 1606(s),1472(m), 1440(s), 1280(s), 1256(s) ,1086(s), 958(w), 774(m), 668(w), 622(w), 536(w)

7.2.7 Synthesis of $[Co(III)(N2Py2b)(CO_3)]\cdot PF_6$

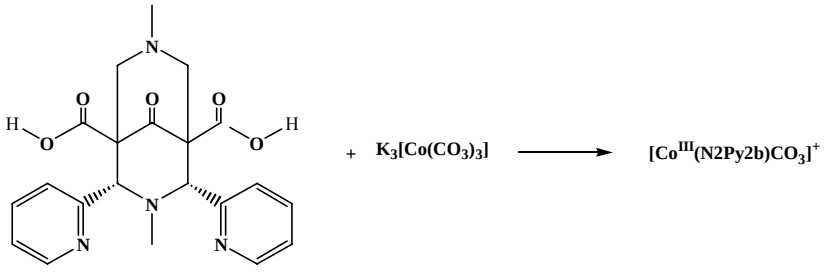

$K_3[CoCO_3]_3$ was prepared as according to published procedure:17.5g of (0.175mol) $KHCO_3$ was added to 17ml H_2O and the resulting slurry was kept cool in a freezing mixture of ice and NaCl. Separately 8g of $Co(II)Cl_2\,6H_2O$ (0.05mol) in 6ml of hot water and cooled on an ice bath After mixing with 10ml of 30% H_2O_2. The Co(II)-H_2O_2 mixture was added dropwise to the above slurry with stirring and filtrated. The clear filterate was cooled on an ice bath.

The resulting green solution was considered as approx. 1 mol/l Co^{3+}.

The Cobalt (III) bispidine complex was prepared: 1.0 g (2.28mmol) of N2Py2 was added to 20ml of methanol and an equivalences amount of green solution of $K_3[CoCO_3]_3$ was added.

After stirring in refluxing methanol for 20-30min, the resulting solution was isolated on Sephadex®CM25 with 0.1M $NaCl_{aq}$.

Elemental analysis

(15483)	calculated (%)	C 32.12	H	3.43	N	6.81
	observed (%)	C 32.54	H	3.48	N	7.00

$[Co(III)(N2Py2b)K_2(CO_3)]PF_6 3H_2O$

* methylester groups of N2Py2b are hydrolyzed

ESI$^+$ MS :567.2 $[Co(III)(N2Py2b)CO_3]^+$ M=567.46

:599.2 $[Co(III)(N2Py2b)CO_3]^+ H_2O$ M=599.50

^{1}H-NMR (200MHz,DMSO) : σ=1.80(d, 2H, -C**H$_2$**-),σ=2.51(d, 2H,-C**H$_2$**-), σ=2.51 (s, 3H, -NC**H$_3$**),σ=3.50(s, 3H, -NC**H$_3$**), σ=5.25(s, 2H,N-C**H**-),σ=7.85-8.85 (m, 8H,Ar-**H**

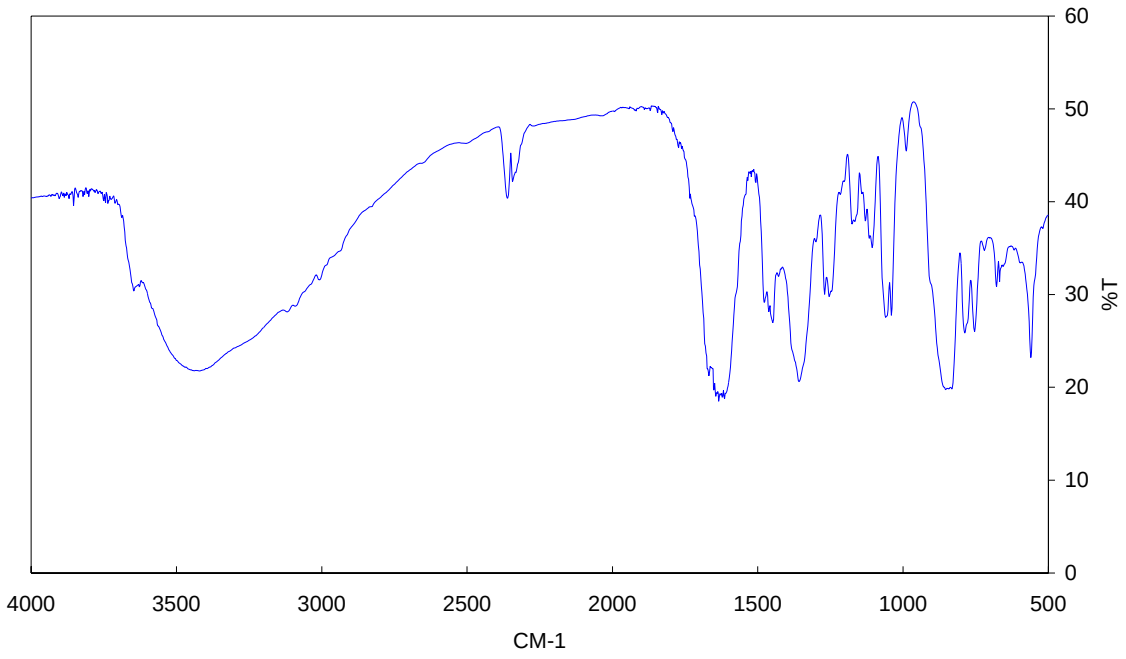

Fig. 7.2.7 Infrared spectra of $[Co(III)(N2Py2b)\ CO_3]\cdot PF_6$ in KBr

IR[cm^{-1}] : 3430 (s,), 2356(m), 1618(s), 1450(m), 1352(s), 1266(m), 1244(m) ,1158(w) ,1102(w), 1052(m), 1038(m), 986(w), 840(s), 782(m), 750(m), 562(m),

7.2.8 Synthesis of $[Co(III)(N2Py2a)]Cl_2 \cdot ClO_4]$

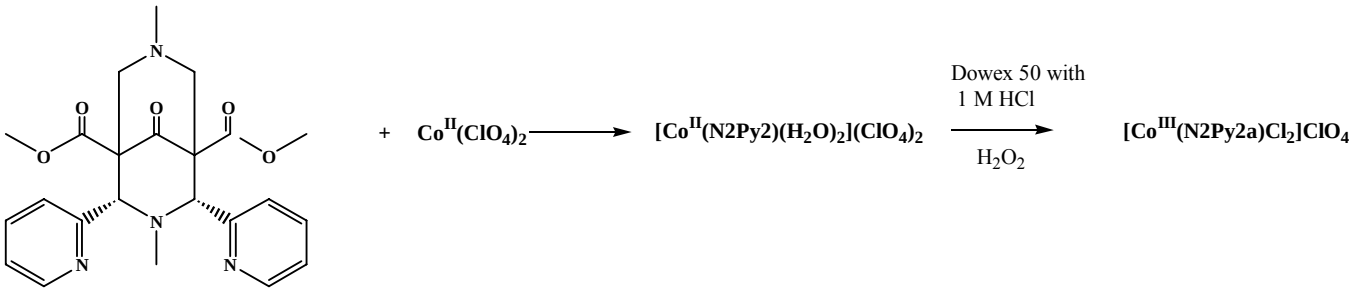

0.5g (1.14mmol) of N2Py2 was dissolved in 20 ml of methanol and 0.35g (0.97mmol) of $Co(II)(ClO_4)_2 \cdot 6H_2O$ in 5ml methanol was added to the solution. After stirring for 1hr, the resulting compound was precipitated, filtrated and dried. 0.42g (0.54mmol) of $[Co(II)(N2Py2)(H_2O)_2](ClO_4)_2$ was yielded.

0.42g of $[Co(II)(N2Py2)(H_2O)_2](ClO_4)_2$ was dissolved in 20ml methanol and 17μl (3eq.) of 30%$H_2O_{2\ aq}$ was added dropwise. After 1 day, the product was separated on Dowex® 50 with 1M HCl. The resulting product $[Co(III)(N2Py2a)Cl_2]ClO_4$ was evaporated and dried in vacuum.

Yield : 0.21g(0.26mmol) (48.15%)

Elemental analysis

(16816)	calculated (%)	C	42.63	H	4.66	N	8.85
	observed (%)	C	42.59	H	5.24	N	8.88

* methyl group at N7 on N2Py2a are substituted to H.

ESI^+ MS :553.3 $[Co(III)(N2Py2a)Cl_2]^+$ M=553.3

: 571.3 $[Co(III)(N2Py2a)Cl_2]^+ H_2O$ M=571.3

^{1}H-NMR (200MHz,DMSO) : σ=2.25(d, 2H, -C**H$_2$**-),σ=2.80(d, 2H,-C**H$_2$**-),

σ=3.55(s, 6H,O-C**H$_3$**) ,σ=3.95 (s, 3H, -NC**H$_3$**),

σ=5.25(s, 2H,N-C**H**-),σ=7.25-9.25 (m, 8H,Ar-**H**)

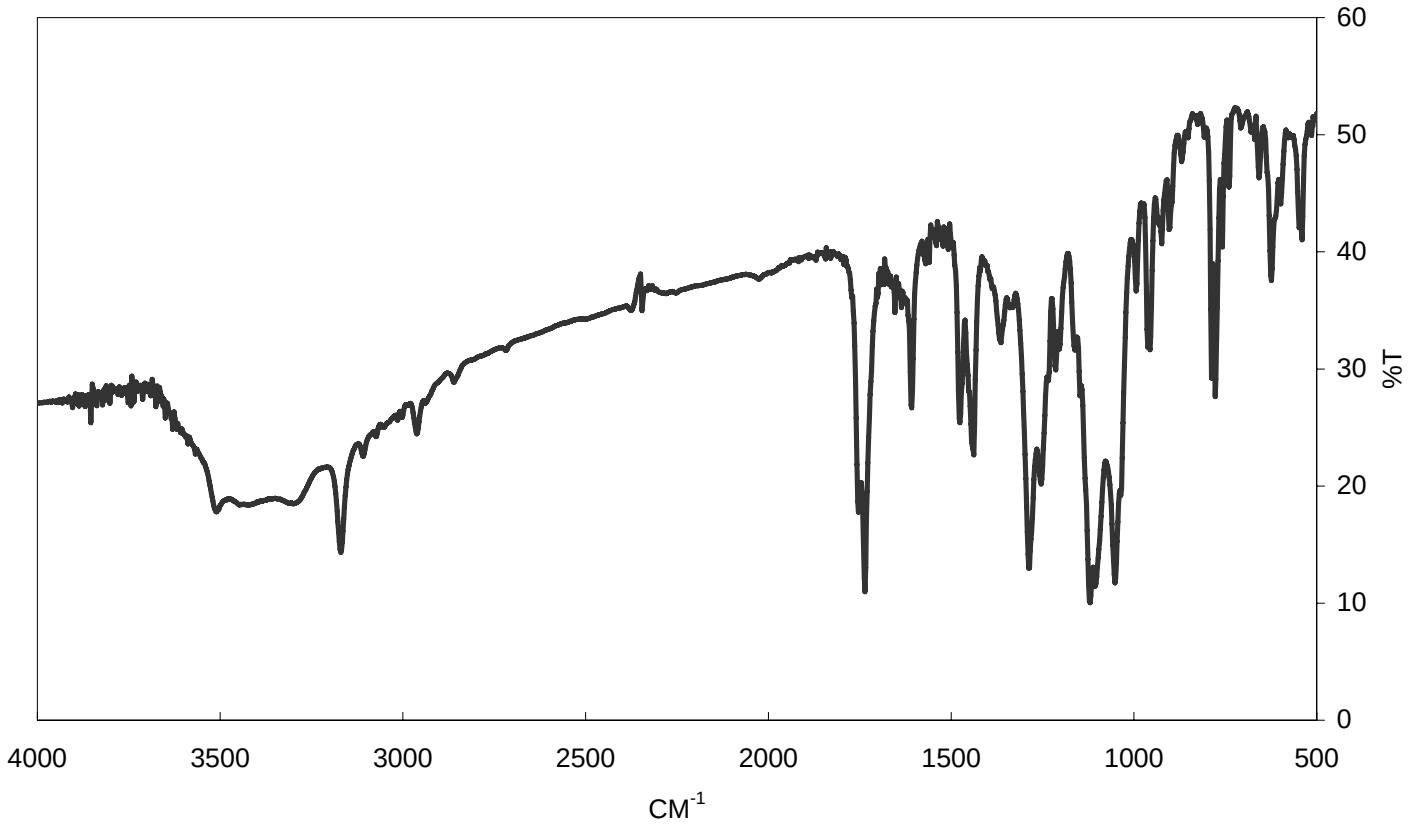

Fig. 7.2.8 Infrared spectrum of [Co(III)(N2Py2a)Cl_2]ClO_4 in KBr

IR[cm^{-1}] : 3168 (s,), 2958(w), 1756(m), 1738(s), 1608(s),1476(s), 1438(w) , 1364(s), 1286(s), 1252(m) ,1214(w) ,1108(s), 1108(s), 1102(s), 1050(s), 954(m), 924(w), 902(w) ,788(m) ,778(m) ,758(m), 740(w), 624(w)

7.3 Determination of Protonation Constants and Stability Constantnts

Potentiometric titrations of the ligands in the absence (to determine ligand acidity constants) and in the presence of metal ions (to determine complex stability constants) were performed on 25 cm^3 samples,with metal ion concentration of 0.5 x 10^{-3} – 1.0 x 10^{-3} mol dm^{-3}. For the measurements 4:5 and 2:1 metal / ligand ratios were used, as solvent H_2O or dioxane/H_2O = 2:3 systems were applied. For all ligands, except for N2Py4, 40 vol% aqueous dioxane was used for the titration due to low solubility at higher pH region. The experiments with ligand N2Py4 were carried out in both H_2O and 40 vol% aqueous dioxane.

The measurements were carried out by using a pH meter equipped with a 6.0202.100 combined electrode (Metrohm) and a 665 Dosimat automatic burette (Metrohm), containing a carbonate free 0.1M stock solution of sodium hydroxide.

For each measurements 120-240 titration points were recorded from the acidic region to start with the probably highest possible protonation degree. During the titration, nitrogen was bubbled through the sample solutions to ensure both the absence of oxygen and carbon dioxide and to stir the solutions. All pH measurements were carried out at constant ionic strength (μ = 0.1mol dm^{-3} KCl) and constant temperature (T = 298K). The overall stability constants were calculated by using the program Hyperquad2000[1].

References

[1] P. Gans, A. Sabatini, A. Vacca, *Talanta.*, **1996**, *43*, 1739.

Acknowledgement

First, I would like to sincerely acknowledge my supervisor **Prof. Dr. Peter Comba** for the interesting themes and his kind and patient.

I would also like to thank to **Prof. Dr. G. Linti, Prof. Dr. H. Wadepohl and Dr. H. Pritzkow** for the XRD analysis.

I would also like to thank to all members of AK Comba, especially, **Tarnai Mate, Lòpez de Laorden Carlos, Prikhod`ko Alexander, Schatz Erik, Zhang Xiangming, Kyaw Naing, Yang Kim, Torcaru Laura, Daubinet André, Müller Vera, Rohwer Heidi, Bautz Jochen, Kerscher Marion, Martin Bodo, Jakob Maik, Rosana Elena Ferrari Zijlstra, Seibold Björn, Stelzer Karin and von Schoenebeck-Schilli Marlies.**

I also appreciate former supervisors in Japan **Prof. Dr. Katsutoshi Inoue, Prof. Dr. Kazuharu Yoshizuka** and **Prof. Dr. Keisuke Oto.**

I would also like to thank to my parents, brothers, my girl friend Junko Aoki and friends in Japan and Germany.

I also appreciate the financial support from DAAD.